Nanomagnetics

2003 J. Phys.: Condens. Matter 15 R841

(http://iopscience.iop.org/0953-8984/15/20/202)

INSTITUTE OF PHYSICS PUBLISHING JOURNAL OF PHYSICS: CONDENSED MATTER

J. Phys.: Condens. Matter **15** (2003) R841–R896 PII: S0953-8984(03)35571-7

TOPICAL REVIEW

Nanomagnetics

R Skomski

Department of Physics and Astronomy and Center for Materials Research and Analysis, University of Nebraska, Lincoln, NE 68588, USA

Received 17 January 2003
Published 12 May 2003
Online at stacks.iop.org/JPhysCM/15/R841

Abstract

Magnetic nanostructures, such as dots and dot arrays, nanowires, multilayers and nanojunctions, are reviewed and compared with bulk magnets. The emphasis is on the involved physics, but some applications are also outlined, including permanent magnets, soft magnets, magnetic recording media, sensors, and structures and materials for spin electronics. The considered structural length scales range from a few interatomic distances to about one micrometre, bridging the gap between atomic-scale magnetism and the macroscopic magnetism of extended bulk and thin-film magnets. This leads to a rich variety of physical phenomena, differently affecting intrinsic and extrinsic magnetic properties. Some specific phenomena discussed in this review are exchange-spring magnetism, random-anisotropy scaling, narrow-wall and constricted-wall phenomena, Curie temperature changes due to nanostructuring and nanoscale magnetization dynamics.

Contents

1. Introduction

Thousands of years of human curiosity have led to the discovery of magnetism, and for many centuries magnetism has stimulated progress in science and technology. For a long time, the focus had been on macroscopic magnetism, as exemplified by the compass needle, by the geomagnetic field and by the ability of electromagnets and permanent magnets to do mechanical work. Atomic-scale magnetic phenomena, such as quantum-mechanical exchange [1–4], crystal–field interaction [5] and relativistic spin–orbit coupling [6, 7], were discovered in the first half of the last century and are now exploited, for example, in advanced permanent–magnet intermetallics such as $SmCo_5$ and $Nd_2Fe_{14}B$ [8]. However, only in recent decades it became clear that solid-state magnetism is, to a large extent, a nanostructural phenomenon. The scientific and technological importance of magnetic nanostructures has three main reasons:

(i) there is an overwhelming variety of structures with interesting physical properties, ranging from naturally occurring nanomagnets and comparatively easy-to-produce bulk nanocomposites to demanding artificial nanostructures,
(ii) the involvement of nanoscale effects in the explanation and improvement of the properties of advanced magnetic materials, and
(iii) nanomagnetism has opened the door for completely new technologies.

A naturally occurring *biomagnetic* phenomenon is magnetite (Fe_3O_4) nanoparticles precipitated in bacteria, molluscs, insects and higher animals. Magnetostatic bacteria live in dark environments and contain chains of 40–100 nm magnetite particles used for vertical orientation [9]. Similar magnetite particles have been found in the brains of bees, pigeons and tuna, and it is being investigated whether and how the particles serve as field sensors for migration [10]. Magnetite and other oxide particles are also responsible for *rock magnetism*, exploited for example in archaeomagnetic dating and for monitoring changes in the Earth's magnetic field [11, 12]. Due to dilution and incomplete saturation, the thermoremanent magnetism of oxide particles in volcanic rocks is between 0.0001 and 1 μT, as compared to the geomagnetic field of the order of 100 μT. Typical particle sizes, varying between less than 1 and 100 μm, are at the upper end of the structures of interest here, but the magnetization dynamics in these particles is a nanoscale phenomenon. Smaller oxide particle sizes, less than 10 nm,

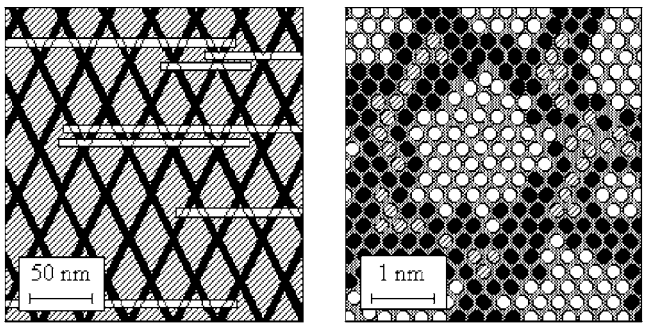

Figure 1. Two schematic bulk nanostructures: (a) sintered Sm–Co and (b) magnetic clusters (white) embedded in a matrix. The two structures are very different from the point of view of size, geometry, origin and functionality. The Sm–Co magnets, consisting of a rhombohedral Sm_2Co_{17}-type main phase (grey), a Cu-rich $SmCo_5$-type grain-boundary phase (black) and a Zr-rich hexagonal Sm_2Co_{17}-type platelet phase (white), are produced by a complicated annealing process and widely used in permanent magnets [8, 26]. Nanostructures such as that shown in (b) can be produced, for example, by mechanical alloying and are used as permanent magnets [27], soft magnets [24] and magnetoresistive materials [28, 29].

are observed in gels having the nominal composition $FeO(OH)\cdot nH_2O$ [13]. Fine particles are also encountered in superparamagnetic systems [14], ferrofluids [15] and meteorites [16].

The further improvement of current magnetic materials heavily relies on nanostructuring. This refers not only to materials such as permanent magnets, soft magnets and recording media but also to emerging areas such as spin electronics. An example of improving the performance of magnetic materials by nanostructuring is hard–soft permanent-magnet composites [8, 17–22]. As analysed in [19], atomic-scale magnetism does not support substantial improvements of permanent magnets beyond existing intermetallics such as $SmCo_5$, Sm_2Co_{17} and $Nd_2Fe_{14}B$, but adding a soft phase to a hard phase in a suitable nanostructure *improves* the permanent-magnet performance beyond that of the hard phase. This 'metamaterials' approach exemplifies the materials-by-design strategy and makes it possible to produce materials not encountered in nature. Other nanoscale effects are exploited in soft magnetic nanostructures, for example in $Fe_{73.5}Si_{13.5}B_9Cu_1Nb_3$ [23–25], where soft magnetic Fe_3Si grains are embedded in an amorphous matrix. Figure 1 shows two structures of interest in this context.

A fascinating approach is artificial nanostructuring to create completely new materials and technologies. One area is the ever-progressing miniaturization in computer technology, as epitomized by the use of nanostructured media for ultra-high density magnetic recording [30–39]. A related area is spin electronics [40, 41], and various types of nanostructures, such as multilayers and nanojunctions, are being investigated in this context. One problem of current interest is spin injection into nonferromagnetic materials [42, 43] and magnetic semiconductors [44, 45], whereas the use of spin degrees of freedom in quantum computing [46, 47] remains a challenge to future research. Another area is magnetoresistive sensors exploiting magnetoresistance effects in metallic thin films [48–51], granular systems [28, 29, 52] and magnetic oxides [41, 53–55]. Some other present or future applications are nanoparticle ferrofluids for cancer treatment, guided by a magnet and delivering high local doses of drugs or radiation [56], micro-electromechanical systems (MEMS) and other nanodevices, and nanoscale magnetic-force nanotips made from PtCo [57, 58].

From a theoretical point of view, nanostructural phenomena are often described by differential equations of the type $\nabla^2\phi - \kappa^2\phi = f(\boldsymbol{r})$, where κ^{-1} is an interaction length. This

must be contrasted to the inhomogeneous Laplace (or Poisson) equation $\nabla^2\phi = f(\boldsymbol{r})$ which implies long-range interactions and describes, for example, electrostatic and magnetostatic phenomena. The interaction length reflects competition between different atomic energy contributions. When the competition is between the electrons' kinetic energy (hopping) and electrostatic energies (Coulomb interaction and exchange), then κ^{-1} scales as k_F or a_0. However, when the main competition involves relativistic interactions, then the interaction length increases to $l_0 = a_0/\alpha$, where $\alpha = 4\pi\varepsilon_0 e^2/\hbar c \approx 1/137$ is Sommerfeld's fine-structure constant [8, 59]. An example is the competition between magnetocrystalline anisotropy and exchange, because the spin–orbit coupling necessary to create anisotropy is a higher-order relativistic correction to the leading electrostatic contributions. Length scales of the order of $l_0 = 7.52$ nm are indeed encountered in many nanomagnetic problems [8, 21, 59], indicating that nanomagnetism goes beyond a 'mixture' of atomic and macroscopic physics.

A related question concerns the transition from nanoscale to macroscopic behaviour. How many atoms are necessary to make a nanostructure indistinguishable from a bulk magnet? As we will analyse below, the answer to this reduced-dimensionality problem depends not only on the geometry of the structure but also on whether one considers intrinsic or extrinsic magnetic properties. *Intrinsic* properties, such as the spontaneous magnetization M_s, the first uniaxial anisotropy constant K_1 and the exchange stiffness A, refer to the atomic origin of magnetism. As a rule, intrinsic properties are realized on length scales of at most a few interatomic distances and tend to approach their bulk values on a length scale of less than 1 nm, although there are exceptions to this rule [8, 60]. *Extrinsic* properties, such as the remanence M_r and the coercivity H_c, are nonequilibrium properties—related to magnetic hysteresis—and exhibit a pronounced real-structure dependence [8, 61–63]. For example, the coercivity of technical iron doubles by adding 0.01 wt% nitrogen [63]. Such small concentrations have little effect on the intrinsic properties but lead to inhomogeneous lattice strains on a scale of many interatomic distances, affecting the propagation of magnetic domain walls and explaining the observed coercivity increase. Magnetic nanostructures exhibit a particularly rich extrinsic behaviour, including phenomena such as random-anisotropy scaling [64], remanence enhancement [17], micromagnetic localization [65], bulging-type nucleation modes [66] and a variety of grain-boundary [67] and exchange-coupling effects [68, 69].

This review deals with the physics of magnetic nanostructures. Section 2 is devoted to the geometrical aspect of nanomagnetism, introducing various types of nanostructures, section 3 focuses on the relation between atomic physics and nanomagnetism and section 4 investigates nanoscale phenomena in a narrower sense. Section 5 discusses zero- and finite-temperature dynamic effects, section 6 summarizes this work and draws some tentative conclusions. Finally, the appendix summarizes some information on materials of interest in nanomagnetism.

2. Magnetic nanostructures

Advanced magnetic nanostructures are characterized by a fascinating diversity of geometries, ranging from complex bulk structures (figure 1) to a broad variety of low-dimensional systems. Figure 2 shows some examples. This section introduces typical geometries of interest in nanomagnetism and outlines their key features; the division into subsections is somewhat arbitrary, because many structures fit into two or more categories.

2.1. Particles and clusters

Various types of small magnetic particles exist in nature (section 1) or are produced artificially. Fine-particle systems, such as Fe in Al_2O_3 with particle diameters of the order of 5 nm, have been investigated over many decades [70]. So-called 'elongated single-domain (ESD)

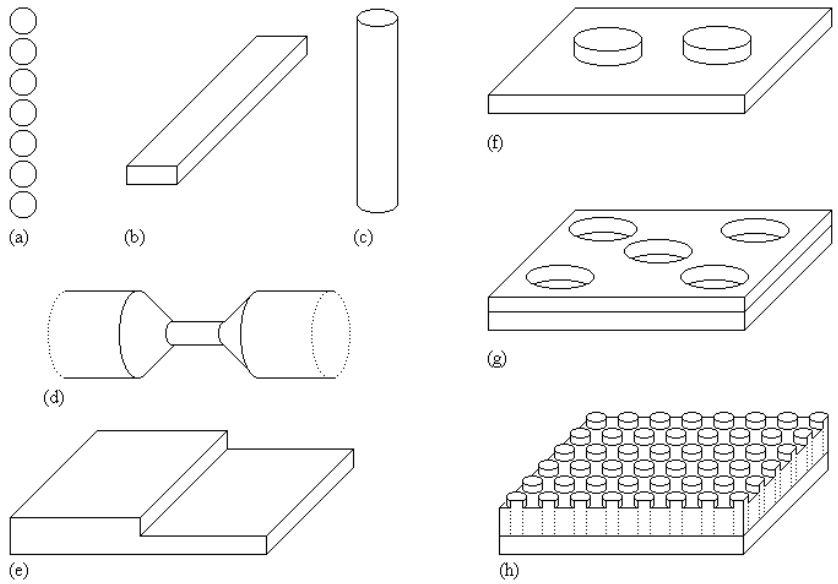

Figure 2. Typical nanostructure geometries: (a) chain of fine particles, (b) striped nanowire, (c) cylindrical nanowire, (d) nanojunction, (e) vicinal surface step, (f) nanodots, (g) antidots and (h) particulate medium.

particles' [71] are used, for example, in magnetic recording. The properties of particles are also of interest for the investigation of nanowires (section 2.4), dot arrays (section 2.3) and thin-film (section 2.2) and bulk (section 2.5) composites. A crude criterion for the survival of the individuality of dots, particles and clusters in complex nanostructures is the strength of the exchange and magnetostatic interparticle interactions (section 4.7).

Interesting applications of small particles are stable colloidal suspensions known as *ferrofluids* [15, 72]. A variety of materials can be used, such as Fe_3O_4, $BaFe_{12}O_{19}$, Fe, Co and Ni, and a typical particle size is 10 nm. Most ferrofluids are based on hydrocarbons or other organic liquids, whereas water-based ferrofluids are more difficult to produce. They are used as liquids in bearings and to monitor magnetic fields and domain configurations.

Very small nanoparticles are also known as *clusters*. Their production by various techniques and typical structural properties have been reviewed by Sellmyer *et al* [39]. In both free and embedded clusters, nanoparticle effects are particularly important. First, the large surface-to-volume ratio of clusters leads to a comparatively strong diameter dependence of the intrinsic properties such as anisotropy [73] and magnetization [74]. Second, clusters tend to be superparamagnetic [14, 75], particularly at high temperatures (section 5.3).

The ground-state domain configuration and the mechanism of magnetization reversal in small magnetic particles [75–80] depend on the particle size. At the macroscopic end of the range there are, e.g., arrays of (110) Fe dots on sapphire, having a thickness of about 50 nm and lateral dimensions of the order of 1 μm [78]. Such dots are characterized by flux closure [78, 81]. In contrast, clusters are single-domain magnets (section 4.2) and their reversal starts by coherent rotation (section 4.3).

2.2. Thin films and multilayers

Many magnetic thin films and multilayers [51, 82–87] can be considered as nanostructures, but since thin-film magnetism has developed into a separate branch of condensed matter

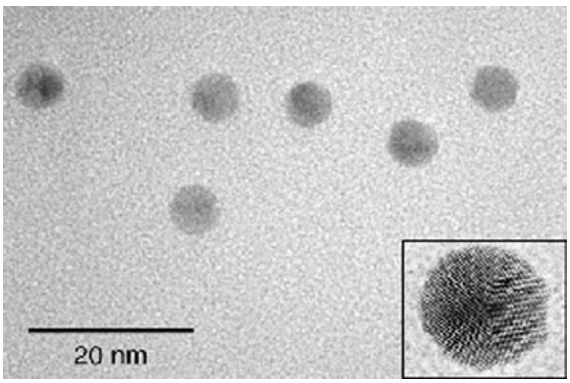

Figure 3. An example of high resolution TEM from 5.6 nm Co clusters produced in our system. (Courtesy D J Sellmyer.)

physics, a comprehensive introduction to these structures goes beyond the scope of this work. Nanostructured thin films with intermediate or high coercivities [20, 21, 88, 89] have been studied in the context of permanent magnetism and magnetic recording.

Thin-film structures exhibit a number of interesting properties. Examples are anisotropies of ideal and vicinal surfaces and of interfaces [84, 90, 91], moment modifications at surfaces and interfaces [92, 93], thickness-dependent domain-wall and coercive phenomena [59, 82, 86, 94], interlayer exchange coupling [48–50] and finite-temperature magnetic ordering [95]. Two specific examples are the nanoscale exchange-coupling or 'exchange-spring' effects in multilayers [18, 19, 88, 96–99] and the pinning of domain walls in sesquilayer iron–tungsten thin films [86].

2.3. Particle arrays and functional components

Two-dimensional arrays of nanoparticles are interesting scientific model systems with many present or future applications. In particular, advanced magnetic recording media can be characterized as a complex array of magnetic particles, and interest in dot arrays [30, 75, 100–104] has been sparked by the search for ever-increasing storage densities in magnetic recording. In very small dots, quantum-mechanical effects are no longer negligible and there are phenomena such as quantum-well states. Quantum-dot effects are of interest in quantum computing and spin electronics [51, 105].

There are many methods for producing nanoparticle arrays [38, 51, 106]. A traditional, though somewhat cumbersome, method to produce periodic arrays of nanoscale magnetic particles, dots and wires is nanolithography [107, 108]. Other examples are molecular-beam epitaxy [109], the use of STMs [110], chemical vapour deposition [101] and e-beam nanolithography [107, 108]. The call for well-characterized large-area arrays of nanoparticles has stimulated the search for advanced production methods such as laser-interference lithography (LIL), where laser-intensity maxima effect a local decomposition of a nonferromagnetic material into ferromagnetic islands [103]. Another development is the use of ion beams [34, 111], for example focused ion-beam (FIB) milling [111], to create small particles and particle arrays with well-defined properties.

Most easily produced and investigated are submicron dots made from iron-series transition metals, such as Ni [101], but it is also possible to use intermetallics, such as permalloy [81, 112], and to reduce the dot size to less than 100 nm. The arrays may be square or hexagonal, or

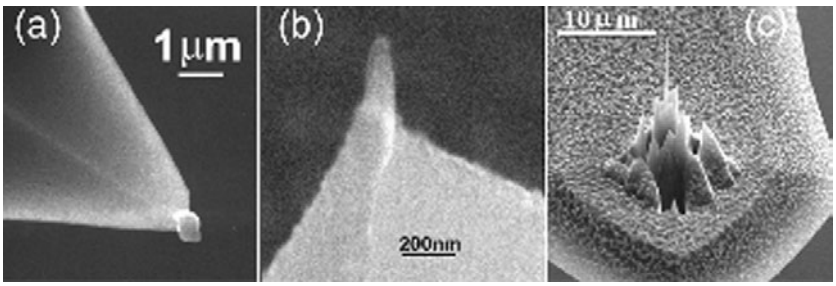

Figure 4. Advanced MFM tips made by (a) ion milling, (b) electron beam deposition, (c) FIB milling. (Courtesy S-H Liou.)

the dots may form other structures such as corrals. Among the investigated phenomena are the properties of individual dots and interdot interactions [46, 112, 113]. A related class of nanostructures is *antidots*, that is, holes in a film rather than dots on a film [109, 114, 115]. Antidots exhibit interesting resistive and magnetoresistive properties [114], but magnetic domains in antidots have been studied too [115]. Potential applications include magnetic recording, sensors, magnetic and quantum computing, micron- and submicron-size mechanical devices, short-wavelength optics and spin electronics. In section 4 we will discuss some magnetic properties of dots and dot arrays.

Other functional structures are, for example, nanojunctions [40, 116], spin valves (section 5.5) and tips for magnetic-force microscopy (MFM tips). Figure 4 shows three MFM tips made by various techniques [57]. Some properties of nanojunctions and spin valves will be discussed in sections 4.4 and 5.5.

2.4. Nanowires

There is a smooth transition from elongated dots and thin-film patches [117, 118] to nanowires [38, 119–121]. Magnetic nanowires are scientifically interesting and have potential applications in many areas of advanced nanotechnology, including patterned magnetic media, magnetic devices and materials for microwave applications. Thin-film nanowires, such as in figure 2(b), are comparatively easily obtained by depositing magnetic materials on vicinal surfaces [51, 117] and by exploiting structural anisotropies of the substrate [86]. They can be produced with thicknesses down to one or two monolayers. Electrodeposition of magnetic materials into porous alumina may be used to produce regular wire arrays [38, 119, 121]. Other ways of fabricating cylindrical nanowires include the deposition into molecular sieves [38, 122–125], track-etched polymer membranes [126, 127] and mica templates [128].

By electrodeposition into porous anodic alumina [124, 129, 130] it is now possible to produce Fe, Co and Ni wires with diameters ranging from 4 to 200 nm, depending on the anodization conditions, and lengths of up to about 1 μm [38, 106, 119, 121, 131–135]. Typically, the nanowires form nearly hexagonal columnar arrays with variable centre-to-centre spacings of the order of 50 nm [38, 121, 131, 135]. The resulting materials are of interest as magnetic recording media [132, 136], for optical and microwave applications [137, 138] and as electroluminescent display devices [139]. Aside from the above-mentioned iron-series transition-metal elements, there is interest in depositing alloys and multilayers, such as Fe/Pt, into porous templates [38, 140, 141]. On the other hand, magnetoresistive effects have been investigated in electrodeposited Co–Cu alloy nanowires [142] and Co–Ni–Cu/Cu multilayered nanowires [143].

Much of the early work on magnetic nanowire arrays was concerned with exploratory issues, such as establishing an easy axis for typical preparation conditions, the essential involvement of shape anisotropy, as opposed to magnetocrystalline anisotropy, and the description of magnetostatic interactions between wires (see, e.g., [38, 127, 135, 144] and references therein). More recently, attention has shifted towards the understanding of magnetization processes [145–147]. On a nanometre scale, interatomic exchange is no longer negligible compared to magnetostatic interactions. This leads to a transition from curling-type to quasi-coherent nucleation (section 4.3). For Fe, Co and Ni, the corresponding diameters are about 11, 15 and 25 nm, respectively, irrespective of the critical single-domain radius [8]. Furthermore, in section 4.6 we will see that the reversal behaviour is affected by the deposition-dependent polycrystallinity [38] of typical transition-metal nanowires [148]. Some other interesting phenomena are magnetic-mode localization (section 4.7), as evident, e.g., from experimental activation volumes (section 5.3), spin waves (section 5.2) and current-induced magnetization reversal [149].

2.5. Nanocomposites and other bulk materials

Embedded *clusters*, *granular materials* and other bulk nanostructures are of great importance in nanoscience. The structural correlation lengths of typical nanocomposite materials range from about 1 nm in x-ray amorphous structures to several 100 nm in submicron structures and can be probed, for example, by small-angle neutron scattering (SANS) [150] and electron microscopy [21]. Magnetic glasses [13, 151] and atomic-scale defect structures are beyond the scope of nanomagnetics, but they are of indirect interest as limiting cases and because nanomagnetic phenomena have their quantum-mechanical origin in atomic-scale magnetism.

Structures similar to figure 1(b) can be produced by methods such as mechanical alloying [152] and chemical reactions [27, 153]. Depending on grain size and microchemistry, they are used, for example, as permanent magnets (Nd–Fe–B), soft magnets (Fe–Cu–Nb–Si–B) and magnetoresistive materials (Co–Ag). There are two types of exchange-coupled permanent magnets: isotropic magnets [17, 154–158], which exhibit random anisotropy and remanence enhancement (section 4.6), and oriented hard–soft composites [19, 21, 88], which utilize exchange coupling of a soft phase with a high magnetization to a hard skeleton. Closely related systems with many potential applications are magnetic clusters deposited in a matrix. For example, the narrow size distribution of 10–20% makes this material interesting as a granular media for magnetic recording [39]. A well-known *soft magnetic* nanocomposite is the 'Yoshizawa' alloy $Fe_{73.5}Si_{13.5}B_9Cu_1Nb_3$ [23, 159], which consists of iron–silicon grains embedded in an amorphous matrix. The Fe–Si nanocrystallites, which provide most of the magnetization, crystallize in the cubic DO_3 structure and have a composition close to Fe_3Si.

Nanoscale composites must be distinguished from amorphous metals (magnetic glasses) and spin glasses, whose exchange and anisotropy disorder is on an atomic scale [13, 151, 160–162]. However, the boundary is smooth and spin glasses and amorphous materials exhibit various nanostructural phenomena. On the other hand, spin-glass-like phenomena are observed in some nanostructures. For example, interacting particles give rise to spin-glass-like (cluster-glass) dynamics [70, 163] and isotropic nanostructures can be considered as random-anisotropy magnets [164].

3. Atomic-scale effects

Intrinsic magnetic properties, such as magnetization and anisotropy, are determined on an atomic scale. For example, the magnetization of α-Fe, $\mu_0 M_s = 2.15$ T, is associated with the body-centred cubic structure of elemental iron. However, some intrinsic effects are realized

on a length scale of several interatomic distances. Examples are Ruderman–Kittel–Kasuya–Yosida (RKKY) interactions between localized moments embedded in a Pauli paramagnetic matrix and the disproportionally strong contribution of surface and interface atoms to the magnetic anisotropy of nanostructures.

3.1. Magnetic moment

The magnetic moment m of solids nearly exclusively originates from the electrons in partly filled inner electron shells of transition-metal atoms. Of particular importance are the iron-series transition-metal or 3d elements Fe, Co and Ni and the rare-earth or 4f elements, such as Nd, Sm, Gd and Dy. Palladium series (4d), platinum series (5d) and actinide (5f) atoms have a magnetic moment in suitable crystalline environments. There are two sources of the atomic magnetic moment: currents associated with the orbital motion of the electrons and the electron spin. The magnetic moment of iron-series transition-metal atoms in metals (Fe, Co, Ni, YCo_5) and nonmetals (Fe_3O_4, NiO) is largely given by the *spin* and the moment, measured in μ_B, is equal to the number of unpaired spins. For example, Fe^{2+} (ferrous iron) has four unoccupied 3d $\downarrow$ orbitals, so that the moment per ion is 4 μ_B. The orbital moment is very small, typically of the order of 0.1 μ_B, because the orbital motion of the electrons is quenched by the crystal field [8, 165, 166]. In contrast, rare-earth moments are given by Hund's rules, which predict the spin and orbital moment as a function of the number of inner-shell electrons [165].

The moment per atom is largely determined by intra-atomic exchange. Exchange is an electrostatic many-body effect, caused by $1/|\boldsymbol{r} - \boldsymbol{r}'|$ Coulomb interactions between electrons located at $\boldsymbol{r}$ and $\boldsymbol{r}'$. Physically, $\downarrow\uparrow$ electron pairs in an atomic orbital are allowed by the Pauli principle but are unfavourable from the point of view of Coulomb repulsion. In the case of parallel spin alignment, $\uparrow\uparrow$, the two electrons are in different orbitals, which is electrostatically favourable, but the corresponding gain in Coulomb energy competes against an increase in one-electron energies. (Only *one* electron benefits from the low ground-state energy—the second electron must occupy an excited one-electron level.) The magnetic moments of insulating transition-metal oxides and rare-earth metals are located on well-defined atomic sites. However, in Fe, Co and Ni, as well as in many alloys, the moment is delocalized or *itinerant*. Itinerant ferromagnetism is characterized by non-integer moments and explained in terms of the metallic band structure [167–170]. Nonmagnetic metals (Pauli paramagnets) have two equally populated $\uparrow$ and $\downarrow$ subbands; an applied magnetic field may transfer a few electrons from the $\downarrow$ band to the $\uparrow$ band, but the corresponding spin polarization is very small, of the order of 0.1%. Itinerant ferromagnetism is realized by narrow bands, where the intra-atomic exchange is stronger than the bandwidth-related gain in single-electron hybridization (Stoner criterion).

Atomic magnetic moments are affected by several nanoscale mechanisms. First, nonmagnetic atoms may become spin-polarized by neighbouring ferromagnetic atoms. A semiquantitative description of these effects is provided by the Landau–Ginzburg type [171] expression

$$-A_2\nabla^2 M + A_0 M = H_{ex}(\boldsymbol{r}). \tag{3.1}$$

Here $M(\boldsymbol{r})$ is the induced magnetization (moment per unit volume), H_{ex} is the intra-atomic exchange field and A_0 and A_2 describe the electronic properties of the system. Essentially, $\chi(k, T) = 1/(A_0 + k^2 A_2)$ is the wavevector-dependent exchange-enhanced spin susceptibility, which is known for a variety of systems [172]. Equation (3.1) predicts an exponential decay of the magnetization with a decay length of $1/\kappa = (A_2/A_0)^{1/2}$. In simple metals, κ scales as the Fermi wavevector ($\kappa \sim k_F$) and ferromagnetism is difficult to induce. However, exchange enhanced Pauli paramagnets, such as Pd and Pt, are very close to satisfying the Stoner criterion,

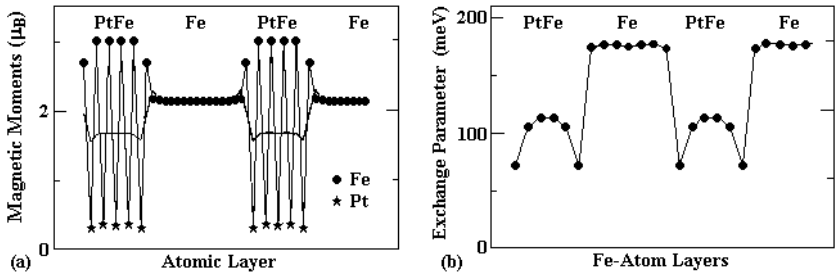

Figure 5. Intrinsic properties of multilayered Pt–Fe structures (after [169]).

so that A_0 and κ are small [8, 172]. A similar A_0 reduction is encountered in semiconductors [44] and in semimetals such as Sb, where the decay length is of the order of 1 nm [173].

Nanoscale moment modifications are important at surfaces and interfaces [173, 174], but they do not extend very far into the bulk. By definition, Bloch wavefunctions extend to infinity, but nanoscale finite-size effects yield only small corrections to the metallic moment. This can be seen, for example, from real-space approaches based on the moment's theorem [8, 175–178]. When only nearest neighbours are taken into account, these methods yield the correct bandwidth but ignore details of the band structure, such as peaks in the density of states. Increasing the number of neighbours improves the resolution of the density of states and makes it possible to distinguish between bulk sites and sites close to surfaces. Figure 5 shows the modification of the moment and of the effective interatomic exchange in multilayered Fe–Pt magnets, as obtained from first-principle electronic-structure calculations [169].

As a rule, nanoscale intrinsic phenomena are caused by small differences between atomic interaction energies. In terms of (3.1), this occurs when $A_0 \approx 0$ due to competing hopping and intra-atomic exchange energies. A loosely related phenomenon, observed for example in rare-earth elements and alloys, is noncollinear spin structures [13]. Helimagnetic rare-earth noncollinearity is characterized by k vectors depending on the ratio of the nearest- and next-nearest-neighbour exchange (section 3.2), and k may be, in principle, a very small fraction of k_F. Even more complicated spin arrangements are possible in disordered magnets with competing interatomic exchange interactions (spin glasses) and at surfaces and interfaces. Furthermore, surface states [51, 178] modify the magnetic moment of surface atoms [51, 174]. Another type of noncollinearity is caused by spin–orbit coupling. The orbit of an electron, and therefore its crystal-field interaction, depend on the spin direction, so that electrons on sites without inversion symmetry can minimize the crystal-field energy by forming a slightly noncollinear spin structure. In spin glasses, this is known as Dzyaloshinskii–Moriya interaction [151], but the same effect occurs in other low-symmetry structures [179].

Noncollinear states must not be confused with micromagnetic structures, such as domains and domain walls (section 4.2). For example, small particles may exhibit some noncollinearity due to competing exchange, particularly at the surface, but an applied magnetic field merely changes the direction of the net magnetization, leaving the atomic-scale noncollinear correlations $\langle \boldsymbol{M}(\boldsymbol{r}_i) \cdot \boldsymbol{M}(\boldsymbol{r}_j) \rangle$ unchanged. By contrast, micromagnetic magnetization processes, such as domain-wall motion, change the relative magnetization directions of well-separated spins in comparatively small magnetic fields.

3.2. Magnetization and magnetic order

In a strict sense, ferromagnetism is limited to infinite magnets, because thermal excitations in finite magnets cause the net moment to fluctuate between opposite directions. In

practice, it is difficult to distinguish the magnetism of particles larger than about 1 nm from true ferromagnetism, because interatomic exchange ensures well-developed ferromagnetic correlations inside the particles. Similar arguments apply to other nanostructures, such as wires [117]. The interatomic exchange ensures not only zero- and finite-temperature magnetic order and exchange stiffness (section 4.2) but also finite-temperature magnetocrystalline anisotropy (section 3.3).

Compared to the intra-atomic Hund's rules exchange, which is always positive, the sign of the interatomic exchange constant J is difficult to predict. In ferromagnets, such as Fe, Co and $Nd_2Fe_{14}B$, J is positive, and at zero temperature all spins are parallel. Ferrimagnets, such as Fe_3O_4 and $BaFe_{12}O_{19}$, and antiferromagnets, such as cobaltous oxide (CoO) and MnF_2, involve negative exchange constants and are characterized by two (or more) sublattices with opposite moments [165, 180]. Sublattice formation may be spontaneous, as in typical antiferromagnets, or linked to the atomic composition, as in ferrimagnets.

Oxides are often antiferromagnets, but when the interatomic hopping integral is zero by symmetry, as in CrO_2, then the direct exchange gives rise to ferromagnetism (Goodenough–Kanamori rules) [8]. A widely used phenomenological approach to discuss interatomic exchange is the *Heisenberg* interaction $-J\hat{\boldsymbol{S}}_1 \cdot \hat{\boldsymbol{S}}_2$ between neighbouring atomic spins $\hat{\boldsymbol{S}}_1$ and $\hat{\boldsymbol{S}}_2$. One example is the RKKY interaction $J \sim \cos(2k_F R)/R^3$ between atomic moments embedded in a free-electron gas of Fermi wavevector k_F [181]. For magnetic nanoparticles embedded in a nonmagnetic metallic matrix, the oscillating character of the RKKY interaction does not mean that it averages to zero, but the net increase with increasing particle size is comparatively weak, and for particles larger than about 1 nm the net RKKY interaction is less pronounced than the magnetostatic interaction [182, 183].

In ferromagnets, the competition between interatomic exchange and thermal disorder leads to the vanishing of the spontaneous magnetization at a well-defined sharp Curie temperature T_C. The total interatomic exchange per atom does not exceed about 0.1 eV, corresponding to $T_C \approx 1000$ K. This is much smaller than the intra-atomic exchange, which is of the order of 1 eV, so that atomic moments at T_C remain close to their zero-temperature values[1] and typical magnetization processes in solids are caused by magnetization rotations. On the other hand, the ratio $\mu_B/k_B = 0.672\ \mathrm{K\ T^{-1}}$ means that magnetostatic fields in solids, of the order of 1 T, are of little consequence to the problem of room-temperature magnetic order. To determine the spontaneous magnetization $M_s(T)$ it is sufficient to know the partition function $Z = \Sigma_\mu \exp(-E_\mu/k_B T)$, but the number of configurations μ increases exponentially with the size of the magnet, and only in a few cases do there exist exact solutions [184]. On a mean-field level, the magnetization is derived from the Hamiltonian $-\mu_B H_{ex} S_z$, where $H_{ex} \sim J$ is the average exchange field and $S_z = -S, \ldots, S-1, S$. The partition function is a sum over all values of S_z, and taking into account that H_{ex} is proportional to $M_s(T)$ then yields a self-consistent mean-field equation for M_s. Below the Curie temperature $T_C \sim J$, the mean-field equation has two ferromagnetic solutions $\pm M_s(T)$, whereas above T_C the magnetization is zero. The mean-field model is easily generalized to two or more sublattices; for N sublattices (or N non-equivalent atomic sites) it yields N coupled algebraic equations [60, 185].

The mean-field model does not work very well at low temperatures, where M_s is determined by spin waves (section 5.2), and close to T_C, where long-range critical fluctuations interfere [184, 186, 187]. The mean-field approach leads, for example, to the physically unreasonable prediction of ferromagnetism in one dimension [186, 187]. In terms of expansions of the type (3.1), critical phenomena are described by diverging correlation lengths

[1] There are a few exceptions, such as very weak itinerant ferromagnets (for example $ZrZn_2$) and low-spin high-spin transition in fcc iron.

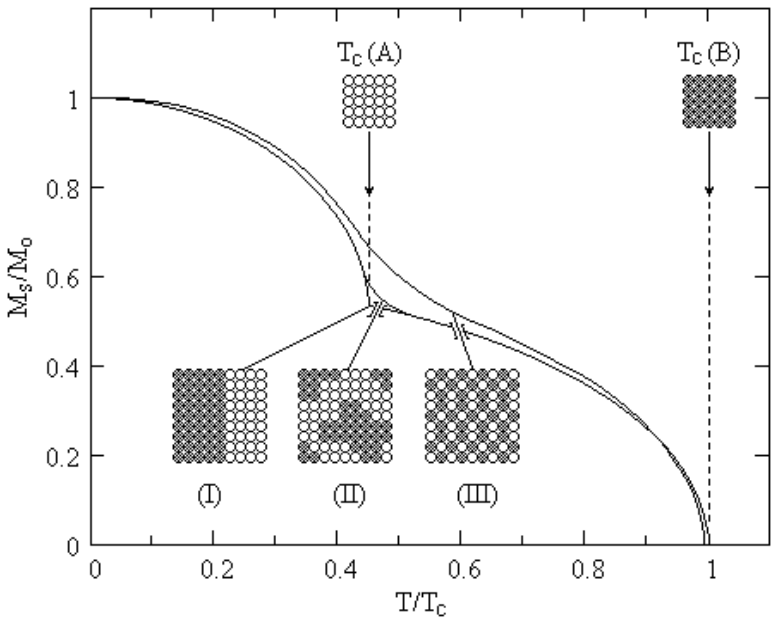

Figure 6. Spontaneous magnetization of inhomogeneous magnets: (I) macroscopic mixture, (II) nanostructure and (III) alloy. In alloys and nanostructures, there is only one Curie temperature, although the $M_s(T)$ curves of nanostructures exhibit a two-phase-like inflection whose curvature may be difficult to resolve experimentally.

$\xi \approx 1/\kappa$. They scale as $\xi \sim 1/|T - T_C|^{\nu}$, where ν is a critical exponent [188]. Critical exponents depend on the dimensionality of the magnet [95, 117, 184, 187, 189], and in nanostructures there exist various finite-size [128, 190–193] and surface [95, 173, 194, 195] corrections.

An interesting problem is the Curie temperature of composite nanostructures [60, 191, 196–199]. Using a super-cell mean-field approach, Ma and Tsai [196] estimated that the Curie temperature of an equiatomic multilayer reaches about 80% of the maximum Curie temperature for layer periodicities of four monolayers. In other words, two layers of a magnetic material are sufficient to realize about 80% of the bulk T_C. In disordered nanostructures, the mean-field Curie temperature is obtained by diagonalizing a multi-sublattice interaction matrix [60]. Disordered two-phase nanostructures have a single common Curie temperature close to the Curie temperature of the phase with the strongest exchange coupling. Figure 6 illustrates this point by showing $M_s(T)$ curves for different nanostructures. A loosely related intrinsic proximity mechanism has been proposed to explain the existence of ferromagnetic carbon in a meteorite [16].

When the grain size is larger than a few interatomic distances then the $M_s(T)$ curve of an inhomogeneous ferromagnet is difficult to distinguish from a mixture of macroscopic phases. The reason is that the perturbations decay as $\exp(-R/\xi)$ and ξ is very small, except for the immediate vicinity of T_C [60]. This example shows that intrinsic properties are realized on fairly small length scales, even if the range of critical fluctuations goes to infinity. It also explains why many two-phase nanostructures, such as the multilayers investigated in [200], mimic the coexistence of two independent magnetizations. An alternative but equivalent explanation is that exchange-energy differences associated with long-range fluctuations are quite small and cannot compete against nanoscale local features. A different approach is to

parametrize the effect of a region with reduced Curie temperature in terms of an effective exchange stiffness. This approach has led to the concept of exchange-field penetration active over distances of the order of 5 nm [201], giving rise to an appreciable Curie temperature enhancement [202]. However, these large values cannot be understood in terms of two-phase nanostructures [60] and probably reflect imperfections such as impurities and percolating bridges.

3.3. Anisotropy

The energy of a magnetic solid depends on the orientation of the magnetization with respect to the crystal axes, which is known as magnetic anisotropy. Permanent magnets need a high magnetic anisotropy in order to keep the magnetization in a desired direction. Soft magnets are characterized by a very low anisotropy, whereas materials with intermediate anisotropies are used as magnetic recording media. In terms of the magnetization angles ϕ and θ, the simplest anisotropy-energy expression for a magnet of volume V is $E_a = K_1 V \sin^2\theta$. This anisotropy is known as lowest-order (or second-order) *uniaxial* anisotropy and K_1 is the first uniaxial anisotropy constant. It is often convenient to express anisotropies in terms of anisotropy fields. For example, the expression $E_a = K_1 V \sin^2\theta$ yields $H_a = 2K_1/\mu_0 M_s$.

For magnets of low symmetry (orthorhombic, monoclinic and triclinic), the lowest-order anisotropy energy is

$$E_a = K_1 V \sin^2\theta + K_1' V \sin^2\theta \cos(2\phi) \tag{3.2}$$

where K_1 and K_1' are, in general, of comparable magnitude. This expression must also be used for magnets having a low-symmetry shape, such as ellipsoids with three unequal principal axes, for a variety of surface anisotropies, such as that of bcc (011) surfaces [86], and for nanoparticles with random surfaces. For arbitrary easy axis directions $\boldsymbol{n}$, as encountered for example in polycrystalline materials, the expression $K_1 \sin^2\theta$ must be replaced by $-K_1(\boldsymbol{n}\cdot\boldsymbol{s})^2$.

Higher-order anisotropy expressions contain, in general, both uniaxial and in-plane terms. For example,

$$\frac{E_a}{V} = K_1 \sin^2\theta + K_2 \sin^4\theta + K_2' \sin^4\theta \cos 4\phi \tag{3.3}$$

contains second- and fourth-order terms and describes tetragonal, hexagonal, rhombohedral and cubic crystals. Hexagonal and rhombohedral crystals are characterized by $K_2' = 0$, whereas in the tetragonal case K_2 and K_2' are of the same order of magnitude. In cubic crystals, K_1, K_2 and K_2' are all of higher order, and only two of these three constants are independent [8]. A common expression for cubic anisotropy is

$$\frac{E_a}{V} = K_1(s_x^2 s_y^2 + s_y^2 s_z^2 + s_x^2 s_z^2) + K_2^{(c)} s_x^2 s_y^2 s_z^2 \tag{3.4}$$

where $K_2^{(c)} \neq K_2$ is the second cubic anisotropy constant [8]. For some other anisotropy expressions see, for example, [8, 203, 204].

Competing anisotropies give rise to spin structures such as easy-cone magnetism, where the magnetization forms an angle $\theta_c = \arcsin(|K_1|/2K_2)$ with the c axis. Since the temperature dependences of K_1 and K_2 are generally different (K_2 is often negligible at high temperatures), the preferential magnetization direction may change as a function of temperature (spin-reorientation transition). A similar film-thickness-dependent transition is observed in films where surface and bulk anisotropy contributions compete.

Figure 7 illustrates the physical origin of coercivity. Small ellipsoidal particles exhibit shape anisotropy

$$K_{1,sh} = \frac{\mu_0}{4}(1 - 3D)M_s^2 \tag{3.5}$$

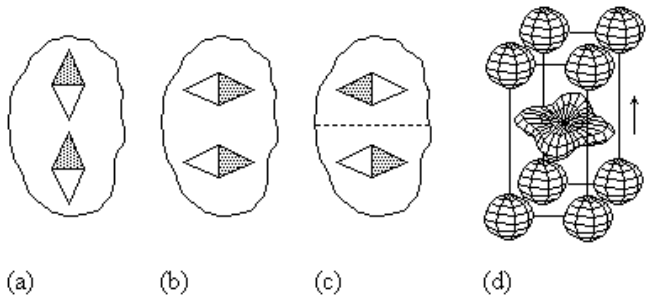

Figure 7. Physical origin of magnetic anisotropy: (a–c) compass-needle analogy of shape anisotropy and (d) magnetocrystalline anisotropy. From the point of view of magnetostatic interaction, (a) is more favourable than (b), so that the easy magnetization direction of a small elongated particle is parallel to the long axis. In a macroscopic magnet this mechanism is ineffective, because domain formation (c) interferes. The arrow in (d) shows the spin direction of the central atom.

where $D = D_z$ is the ellipsoid's demagnetizing factor ($D = 0$ for long cylinders, $D = 1/3$ for spheres and $D = 1$ for plates) [205]. Shape anisotropy is important in magnetic nanostructures made from soft magnetic materials, for example in Fe, Co and Ni particles [8, 206] and in nanowires [38, 135, 144, 148]. In large particles, shape anisotropy is destroyed by internal flux closure [59] (section 4.2). The anisotropy of most materials is of magnetocrystalline origin, reflecting the competition between electrostatic crystal-field interaction and spin–orbit coupling [6]. The crystal field reflects the local symmetry of the crystal or surface and acts on the orbits of the inner-shell d and f electrons. For example, figure 7(d) shows the charge density of a magnetic central atom in a tetragonal environment. Due to the crystal field, which contains both electrostatic and hopping contributions [207], the electron orbits depend on the anisotropic crystalline environment.

The magnitude of the magnetocrystalline anisotropy depends on the ratio of crystal-field energy and spin–orbit coupling. As a relativistic phenomenon, spin–orbit coupling is most pronounced for inner-shell electrons in heavy elements, such as rare-earth 4f electrons. This leads to a rigid coupling between spin and orbital moment, and the magnetocrystalline anisotropy is given by the comparatively small electrostatic interaction of the unquenched 4f charge clouds [208] with the crystal field [8, 203, 209]. However, the absence of quenching means that typical rare-earth single-ion anisotropies are much larger than 3d anisotropies [8, 209, 210]. This is exploited in advanced permanent magnets, where it leads to very high coercivities, such as 4.4 T in $Sm_3Fe_{17}N_3$-based magnets [8, 211].

In 3d atoms, the spin–orbit coupling $\lambda \approx 50$ meV is much smaller than the crystal-field energy $E_0 \geqslant 1$ eV, and the magnetic anisotropy is a perturbative effect. For uniaxial symmetry, the anisotropy is of the order of λ^2/E_0, whereas the anisotropy of cubic materials scales as λ^4/E_0^3. In 3d oxides, E_0 reflects the electrostatic crystal-field splitting [6], whereas in itinerant magnets it is roughly equal to the d-band width [7]. Typical second- and fourth-order transition-metal anisotropies are of the order of 2 and 0.02 MJ m^{-3}, respectively. A manifestation of magnetocrystalline anisotropy is magnetoelastic anisotropy, where the crystal field is changed by mechanical strain. For example, cubic magnets subjected to uniaxial stress exhibit uniaxial anisotropy. The magnetoelastic contribution to the first anisotropy constant is equal to $3\lambda_s\sigma/2$, where σ is the uniaxial stress and λ_s is the saturation magnetostriction. Experimental room-temperature values of λ_s are -7×10^{-6} for iron, -33×10^{-6} for nickel, 40×10^{-6} for Fe_3O_4, -1560×10^{-6} for $SmFe_2$ and 75×10^{-6} for FeCo. These contributions are important, for example, in strained polycrystalline or amorphous films [206, 212].

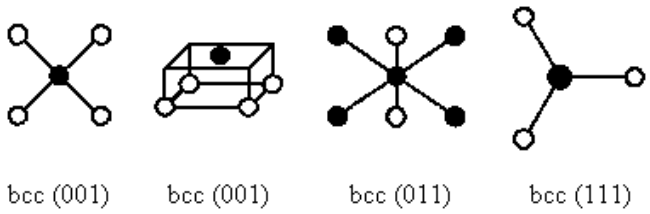

Figure 8. Surface anisotropy. The anisotropy contribution of surface (black) and subsurface (white) atoms depends on the local environment. Lowest-order biaxial anisotropy is realized for bcc (011) but not for bcc (001) and bcc (111).

To realize second-order anisotropy, the atomic environment of the transition-metal atoms must have a sufficiently low symmetry [86, 90–92, 213]. Figure 8 illustrates that this is often, but not always, the case for surface atoms. Magnetic *surface anisotropy*, first analysed by Néel [90], is important in complicated structures and morphologies such as ultrathin transition-metal films [84], multilayers [214], rough surfaces [213], small particles [73] and surface steps [215]. In a variety of cases it has been possible to calculate surface anisotropies from first principles [92, 214, 216–219]. The same is true for some other low geometries, such as Fe wires embedded in Cu [220] and freestanding monatomic Co wires [221]. An interesting point is that surface anisotropies easily dominate the bulk anisotropy of cubic materials. From the tables in the appendix we see that bulk anisotropies are about two orders of magnitude smaller than lowest-order anisotropies. Due to the comparatively large number N_s of surface atoms of small particles, the surface contribution dominates the bulk anisotropy in particles smaller than about 3 nm, even if one takes into account that the net surface anisotropy is not necessarily linear in N_s but tends to scale as $N_s^{1/2}$ due to random-anisotropy effects (section 4.6).

Magnetocrystalline anisotropy is characterized by a pronounced temperature dependence [8, 26, 203, 222–224]. For example, in an intermediate temperature range the leading rare-earth anisotropy contribution of permanent magnet intermetallics, such as $SmCo_5$ and $Nd_2Fe_{14}B$, scales as $1/T^2$ [225]. The main reason is that typical anisotropy energies per atom are quite small, E_a/k_BT ranging from less than 0.1 to a few K. The realization of room-temperature anisotropy requires the support of the interatomic exchange field, which suppresses the switching of individual atomic spins into states with reduced anisotropy contributions [8, 222, 226].

4. Mesoscopic magnetism

The atomic-scale effects investigated in section 3 determine a magnet's intrinsic properties, such as the spontaneous magnetization M_s, the first uniaxial anisotropy constant K_1 and the exchange stiffness A. To some extent, these quantities are modified by nanoscale effects, but most corrections are rather unimportant on length scales larger than about 1 nm, and to a good approximation the intrinsic properties can be considered as local parameters. For example, $M_s(\boldsymbol{r})$ and $K_1(\boldsymbol{r})$ reflect the local chemistry and the unit vector $\boldsymbol{n}(\boldsymbol{r})$ of the easy magnetization direction corresponds to the local c-axis orientation of the crystallites.

Why is knowledge of the local intrinsic properties not sufficient for an unambiguous determination of the spin state? The reason is that $M_s = |\boldsymbol{M}|$ is supported by quite large intra-atomic energy differences, whereas *rotations* of the magnetization vector are quite easy to realize because they do not change M_s. It is this rotation of the magnetization that determines the magnet's hysteresis loop and its extrinsic properties. Zeeman and self-interaction magnetic fields, interatomic exchange and magnetic anisotropy all contribute to the rotation, which

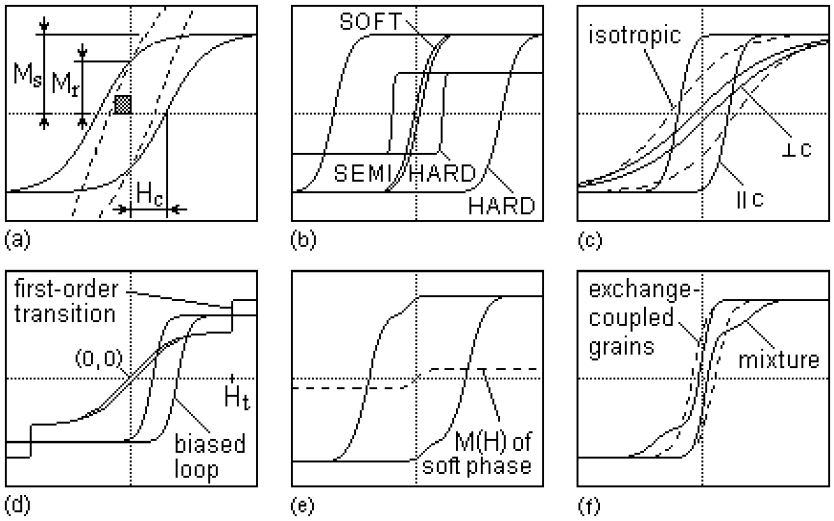

Figure 9. Hysteresis loops: (a) basic extrinsic quantities derived from an M–H loop (full) and the corresponding B–H loop (broken), (b) hysteresis loops of hard, semihard and soft magnets, (c) loops measured parallel and perpendicular to an easy c axis, (d) an exchange-biased loop and a loop exhibiting a first-order transition, (e) and (f) two-phase loops. The isotropic loop in (c) corresponds to a randomly oriented ensemble of particles. Ideally, the perpendicular curves shown in (c) are rectangular, but structural disorder encountered in practice leads to a smoothing of the loops. All loops shown in this figure are schematic and exist in many variations and combinations.

occurs on a mesoscopic scale and is known as micromagnetism [227], although nanomagnetism would be a better name to characterize the length scales involved.

Magnetic nanostructures exhibit a particularly rich extrinsic behaviour, including effects such as random-anisotropy scaling [64], remanence enhancement [17], micromagnetic localization [65], bulging-type nucleation modes [66] and a variety of grain-boundary [228] and exchange-coupling effects [68, 69]. Even traditional 'microstructured' magnets exploit nanometre-scale features for performance optimization[2]. For example, the best room-temperature permanent magnets are now made from Nd–Fe–B [229–231], but as-cast samples with the correct stoichiometry exhibit a disappointingly low coercivity unless the grain-boundary structure is optimized by a specific heat treatment.

4.1. Phenomenology of hysteresis

The most important micromagnetic phenomenon is magnetic *hysteresis*, which refers to the dependence of the magnetization as a function of the external magnetic field (figure 9). Hysteresis is a complex nonlinear, nonequilibrium and nonlocal phenomenon, reflecting the existence of anisotropy-related metastable energy minima separated by field-dependent energy barriers. On an atomic scale, the barriers are easily overcome by thermal fluctuations, but on nanoscale or macroscopic length scales the excitations are usually too weak to overcome the barriers. The determination of the local magnetization $\boldsymbol{M}(\boldsymbol{r})$, from which the hysteresis loop is obtained by averaging, is further complicated by the influence of the magnet's *real structure* (defect structure, morphology, metallurgical 'microstructure').

An extrinsic property of crucial importance in permanent magnetism is the *energy product* $(\mathrm{BH})_{max}$ [8, 206]. Physically, it is twice the magnetostatic energy per magnet volume

[2] The prefix 'micro' originates from the greek word $\mu\iota\kappa\rho\varsigma$, meaning 'small' but not implying any well-defined length scale.

stored outside the magnet, but in practice it is determined from the B–H hysteresis loop, where it is equal to the grey area in figure 9(a). The energy product of hard magnetic steel is about 1 kJ m^{-3}, whereas advanced $Nd_2Fe_{14}B$ [229] magnets have room-temperature energy products of about 451 kJ m^{-3} [231]. This means that a compact Nd–Fe–B magnet of less than 3 g is now able to replace a 1 kg horseshoe magnet—a feature of major importance for advanced consumer electronics, car design and computer technology. However, the outlook for discovering new ternary phases with significantly improved permanent magnetic properties has been poor [8, 19] and nanostructuring has developed into a major tool for further improvements (sections 4.4 and 4.5).

Figure 9(f) indicates that nanostructuring has a pronounced influence on the hysteresis. This is exploited in the soft magnetic random-anisotropy nanostructures introduced in section 2.5, in permanent magnets, in magnetic-recording media and in materials for sensors. For example, adding a soft material with a high magnetization, such as $Fe_{65}Co_{35}$ ($\mu_0 M_s = 2.43$ T), to an oriented hard magnet *enhances* the permanent energy product if the grain size of the soft regions is sufficiently small [19]. The reason is that the energy product increases with coercivity H_c (figure 9) but can never exceed the value $\mu_0 M_r^2/4 \leqslant \mu_0 M_s^2/4$. In the case of ideal rectangular hysteresis loops, this upper limit is reached for $H_c = M_s/2$, and even in real magnets there is little energy-product improvement on making H_c much larger than $H_c/2$. Adding the soft phase enhances the magnetization, while the surplus anisotropy of advanced hard magnetic intermetallic phases, such as $SmCo_5$, $Nd_2Fe_{14}B$ and PtCo, ensures a sufficient coercivity (section 4.4).

The development of exchange-coupled permanent magnets has, in fact, several starting points. Coehoorn *et al* [17] developed remanence-enhanced isotropic Nd–Fe–B materials; this research has its scientific roots in earlier random-field [232] and random-anisotropy [64, 233] theories. A second starting point is the investigation of magnetic multilayers [18, 19, 96], which is now widely associated with Kneller's concept of exchange-spring magnetism. Third, attempts to predict the nucleation-field coercivities $H_c = H_N$ for three-dimensional two-phase nanostructures have given rise to a quantitative analysis of the permanent-magnet performance of oriented two-phase nanostructures of arbitrary geometry [19, 234]. Frequently considered experimental structures are multilayers consisting of two different phases [18–20, 22, 68, 96–99, 235] and granular materials [7–9, 21, 23, 28, 29, 57, 66, 154, 155, 234, 236, 237].

A key theoretical problem is to derive magnetization curves by simulating [238–241] or modelling the magnet's nanostructure. Only in a few cases is it possible to obtain exact coercivity results. Examples are the coherent-rotation or Stoner–Wohlfarth model (section 4.3) and the nucleation field in aligned hard–soft nanocomposites. Much progress has been made in the field of numerical simulation [239, 240], although the size of the simulated structures is limited to about $100 \times 100 \times 100$ lattice points, and the explanation and prediction of real magnets has remained a demanding task. This is due to the nonlinear, nonlocal and nonequilibrium character of the involved magnetization processes and to the multiscale nature [237, 242] of the structures. However, it has been known for decades that neither the coercivity nor the loop shapes of real materials are reproduced by Stoner–Wohlfarth theory. For example, the coercivity of optimized permanent magnets is only 20–40% of the anisotropy field. The main reason is imperfections affecting nanoscale magnetization processes.

4.2. Micromagnetic background

To determine hysteresis loops it is necessary to trace the local magnetization $\boldsymbol{M}(\boldsymbol{r})$ as a function of the applied field. Usually, this is done on a continuum level [8, 192, 227]. Narrow-wall phenomena, which have been studied for example in rare-earth cobalt permanent magnets [243]

and at grain boundaries [67, 237, 244], involve individual atoms and atomic planes and lead to comparatively small corrections to the extrinsic behaviour (section 4.5). The starting point is the energy functional

$$E = \int \left\{ A\left[\nabla\left(\frac{\boldsymbol{M}}{M_s}\right)\right]^2 - K_1\frac{(\boldsymbol{n}\cdot\boldsymbol{M})^2}{M_s^2} - \mu_0\boldsymbol{M}\cdot\boldsymbol{H} - \frac{\mu_0}{2}\boldsymbol{M}\cdot\boldsymbol{H}_d(\boldsymbol{M})\right\}\mathrm{d}V \tag{4.1}$$

where $\boldsymbol{n}(\boldsymbol{r})$ is the unit vector of the local anisotropy direction, $\boldsymbol{H}$ is the external or Zeeman field and

$$\boldsymbol{H}_d(\boldsymbol{r}) = \frac{1}{4\pi}\int \frac{3(\boldsymbol{r}-\boldsymbol{r}')(\boldsymbol{r}-\boldsymbol{r}')\cdot\boldsymbol{M}(\boldsymbol{r}') - |\boldsymbol{r}-\boldsymbol{r}'|^2\boldsymbol{M}(\boldsymbol{r}')}{|\boldsymbol{r}-\boldsymbol{r}'|^5}\,\mathrm{d}V' \tag{4.2}$$

is the magnetostatic self-interaction field[3]. Equation (4.1) is also known as the micromagnetic *free* energy, indicating that A, K_1, $\boldsymbol{n}$ and M_s are temperature-dependent equilibrium quantities which can, in principle, be determined from an atomic scale partition function.

The ∇ term in (4.1) means that the exchange is treated on a continuum level. A more general approach is to use an exchange-interaction kernel of the type $J(|\boldsymbol{r}-\boldsymbol{r}'|) = J(R)$, but for small k vectors the Fourier-transformed interaction integral $\int J^*(k)\sin(kR)R\,\mathrm{d}R$ can be expanded into powers of k. Comparing the quadratic term with $-Ak^2$ yields the exchange stiffness A as a functional of $J(R)$. For example, RKKY interactions are diagonal in k-space and are proportional to the Lindhard screening function $F(x) = 1 - x^2/3 + \mathrm{O}(x^4)$, where $x = k/2k_F$ [172, 181]. Aside from short-wavelength magnetization variations, where k is comparable to k_F, (4.1) ignores exchange contributions anisotropic with respect to the 'bond' direction $\boldsymbol{k}/k$ and with respect to the magnetization direction $\boldsymbol{M}/M_s$. The first type of exchange anisotropy occurs, for example, in intermetallics consisting of atomic layers, such as PtCo and $SmCo_5$, and then means that intraplanar exchange is different from interplanar exchange. The second type of exchange anisotropy is a spin–orbit effect and yields a small anisotropic contribution to the finite-temperature magnetization.

Dimensional analysis of (4.1) yields two fundamental *length scales*, namely the wall-width parameter

$$\delta_0 = \sqrt{\frac{A}{K_1}} \tag{4.3}$$

and the exchange length

$$l_{ex} = \sqrt{\frac{A}{\mu_0 M_s^2}}. \tag{4.4}$$

Simplifying somewhat, the *wall-width parameter* determines the thickness of the domain wall separating magnetic domains of different magnetization directions [56, 61, 62, 245] and the spatial response of the magnetization to local perturbations [237]. The wall-width parameter varies from about 1 nm in extremely hard materials to several 100 nm in very soft materials. The *exchange length* is the length below which atomic exchange interactions dominate typical magnetostatic fields. It determines, for example, the transition from coherent rotation to curling (section 4.3) and the grain size below which the hysteresis loops of two-phase magnets look single-phase-like (figure 9). Since typical ferromagnets have magnetizations of the order of 1 T and exchange stiffnesses of the order of 10 pJ m^{-1}, l_{ex} is between 1 and 2 nm for a broad range of materials. In practice, most lengths derived from l_{ex} carry a factor of 5 [8], so that

[3] This field differs by $\boldsymbol{M}/3$ from the internal magnetostatic field obtained from Maxwell's equations. However, magnetic fields couple as $\boldsymbol{M}\cdot\boldsymbol{H}$ to the magnetization, so that any term proportional to $\boldsymbol{M}\cdot\boldsymbol{M} = M_s^2$ amounts to a physically irrelevant shift of the zero-point energy [8].

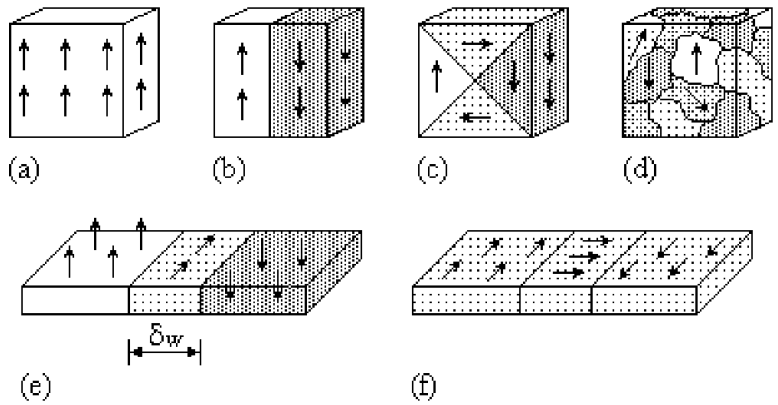

Figure 10. Micromagnetic spin configurations: (a) single-domain state, as observed in very small particles, (b) two-domain configuration, as encountered in fairly small particles with uniaxial anisotropy, (c) flux closure in cubic magnets, (d) complicated domain structure in a polycrystalline magnet, (e) Bloch wall in a thin film with perpendicular anisotropy and (f) Néel wall in a thin film with in-plane anisotropy. In macroscopic magnets, the thickness δ_w of the domain walls separating the domains is much smaller than the domain size, but in nanostructures the distinction between domains and domain walls often fades.

experimental exchange-length scales are close to 10 nm. From an atomic point of view, the order of magnitude of l_{ex} is $a_0/\alpha = 7.52$ nm, where a_0 is the Bohr length and $\alpha \approx 1/137$ is Sommerfeld's fine-structure constant [59]. Physically, the involvement of the fine-structure constant reflects the higher-order relativistic character of the anisotropy.

The magnetostatic self-interaction term in (4.1) favours *magnetic domains* with partial or complete flux closure [108, 192, 206, 246–248]. As indicated in figure 10, domains are separated by comparatively thin *domain walls* [61, 62, 247]. Essentially, the thickness of the walls is determined by the competition between exchange, which favours smooth walls, and anisotropy, which favours narrow transition regions. Examination of (4.3) and (4.4) leads to the conclusion that the wall with δ_w is proportional to δ_0. For a 180° Bloch wall in a bulk magnet, $\delta_w = \pi\delta_0$, but many thin-film walls, such as the Néel wall shown in figure 10(f), involve magnetic charges, and δ_w depends on l_0 too. Note that the Bloch wall width is also written as δ_B, to distinguish it from other wall types. Sometimes δ_B is interpreted as an exchange length determining the effective range of exchange interactions. If this was a valid consideration, then ideally soft materials, where $K_1 = 0$ and $\delta_B = \infty$, would realize exchange coupling on a truly macroscopic scale, without giving rise to two-phase inflections in the hysteresis loops.

Domain formation is favourable from the point of view of magnetostatic self-interaction, but there are no ground-state domains if the gain in magnetostatic energy is smaller than the domain-wall energy. Substituting the Bloch-wall magnetization [82, 247]

$$M_z(x) = -M_s \tanh(x\sqrt{K_1/A}) \tag{4.5}$$

into (4.1) and performing the integration yields the domain-wall energy $\gamma = 4\sqrt{AK_1}$. For a sphere containing two semisphere domains of opposite magnetization, the wall energy is therefore $4\pi\sqrt{AK_1}R^2$. The gain in magnetostatic energy is roughly equal to half the single-domain energy, that is, to $\mu_0 M_s^2 V/12$ [245]. Domain formation is therefore favourable for spheres whose radius is larger than the *critical single-domain radius*:

$$R_{SD} = \frac{36\sqrt{AK_1}}{\mu_0 M_s^2}. \tag{4.6}$$

In very hard magnets, R_{SD} exceeds 1 μm. However, the critical single-domain size and domain size in multi-domain structures are strongly geometry-dependent [59, 245, 248]. For example, the domain size (stripe width) in films with perpendicular anisotropy D_d is easily estimated by comparing the stray-field energy $\mu_0 M_s^2 D_d L^2$, where L^2 is the film area, with the wall energy $\gamma b L(L/D_d)$, where b is the film thickness [245]. Minimizing the total energy with respect to D_d yields $D_d \approx (\gamma b/\mu_0 M_s^2)^{1/2}$. In other words, the domain size exhibits a square-root dependence on the film thickness.

Equation (4.6) describes spherical magnets whose size is larger than the domain-wall width δ_B. However, the radius of soft magnetic nanoparticles is often smaller than δ_B and inhomogeneous magnetization states then extend throughout the particle, $\nabla M \sim M_s/R$. The corresponding magnetostatic and exchange energies scale as $\mu_0 D M_s^2 R^3$ and AR, respectively, and a strongly nonuniform ground state is realized when R is much larger than $\sqrt{A/\mu_0 D M_s^2} = D^{-1/2} l_{ex}$. In plate-like thin-film dots, the relevant demagnetizing factor D is proportional to the ratio of film thickness to dot diameter. It can be shown that this scaling law is valid for $\mu_0 D M_s^2 \gg K_1$. In the opposite limit, $\mu_0 D M_s^2 \ll K_1$, the expressions depend on the easy axis direction and involve R_{SD}.

It is important to note that the critical single-domain radius is an *equilibrium* property, involving the comparison of the energies of single- and multi-domain states but independent of the energy barriers separating the states. It determines, for example, the virgin state after thermal demagnetization. In contrast, hysteresis is a *non*-equilibrium phenomenon caused by energy barriers. Furthermore, equilibrium domains are qualitatively different from the nonuniform (incoherent) magnetization states occurring during magnetization reversal (sections 4.3 and 4.4). The onset of nonuniform (incoherent) reversal in perfect ellipsoids of revolution is governed by the exchange length (4.4). This quantity is anisotropy-independent and, in hard magnets, much smaller than R_{SD}. The popular but incorrect equating of single-domain magnetism and coherent rotation, as epitomized by the unfortunate term 'ESD particle' (section 2.1), has its origin in the focus on soft and semi-hard magnets in the first half of the 20th century.

4.3. Fundamental magnetization processes

The most intriguing aspect of hysteresis is the coercive force or *coercivity*, figure 9(a). It describes the stability of the remanent state and gives rise to the classification of magnets into hard magnetic materials (permanent magnets), semihard materials (storage media) and soft magnetic materials. A widely used phenomenological coercivity expression [249]

$$H_c = \alpha_K \frac{2K_1}{\mu_0 M_s} - D_{eff} M_s - \Delta H(T, \eta) \tag{4.7}$$

where α_K is the real-structure-dependent Kronmüller parameter [250, 251], D_{eff} is a magnetostatic interaction parameter and ΔH is a fluctuation-field correction due to thermal activation [8, 249, 252]. The comparatively small ΔH term, which will be discussed in section 5.3, means that the coercivity depends on the sweep rate $\eta = \mathrm{d}H/\mathrm{d}t$ of the external field.

A key problem of coercivity theory is to determine H_c from the magnet's real structures. In small particles, the exchange is sufficiently strong to ensure that $\boldsymbol{M}(\boldsymbol{r})$ is constant throughout the magnet, that is, $\nabla \boldsymbol{M}$ in (4.1) is zero. Depending on the context, this regime is called *coherent rotation*, uniform rotation or Stoner–Wohlfarth reversal [227, 253, 254]. For uniaxial ellipsoids of revolution having the symmetry axis parallel to the external field $\boldsymbol{H} = H\boldsymbol{e}_z$, the energy (4.1) then becomes

$$\frac{E}{V} = K_1 \sin^2\theta + \frac{\mu_0}{2}(1 - 3D) M_s^2 \sin^2\theta - \mu_0 M_s H \cos\theta \tag{4.8}$$

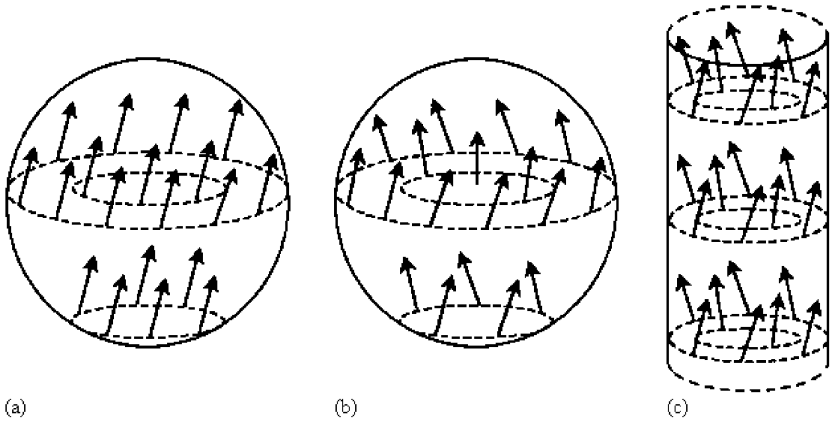

Figure 11. Nucleation modes in homogeneous magnets: (a) coherent rotation in a sphere, (b) curling in a sphere and (c) curling in a cylinder. The arrows show the local magnetization $\boldsymbol{M} = M_z \boldsymbol{e}_z + \boldsymbol{m}$, where $\boldsymbol{e}_z$ is parallel to the axis of revolution of the ellipsoid (cylinder).

where D is the demagnetizing factor introduced in section 3.3 and θ is the angle between $\boldsymbol{M}$ and $\boldsymbol{e}_z$. The coercive field, at which the magnetization jumps from $M = M_z = M_s$ to $M = -M_s$ is obtained by stability analysis. Expanding (4.8) into small powers of θ yields

$$\frac{E}{V} = \left(K_1 + \frac{\mu_0}{2}(1 - 3D)M_s^2 + \frac{\mu_0}{2} M_s H \right) \theta^2. \tag{4.9}$$

The energy minimum associated with $\theta = 0$ vanishes when the reverse field reaches the coercive field

$$H_c = \frac{2K_1}{\mu_0 M_s} + \frac{1}{2}(1 - 3D)M_s. \tag{4.10}$$

The Stoner–Wohlfarth model, as epitomized by this equation, works fairly well for very small particles, where $\nabla \boldsymbol{M} = 0$ is a good approximation. It is frequently applied to ensembles of noninteracting and randomly oriented small particles, where a generalization of (4.8) yields the coercivity $H_c = 0.48 H_a$ and the remanence $M_r = 0.5 M_s$. However, in most real magnets the Stoner–Wohlfarth model significantly overestimates the coercivity, because flux closure effects and structural imperfections lead to $\nabla \boldsymbol{M} \neq 0$ [8, 254] and because intergranular interaction effects are ignored in (4.8).

The Stoner–Wohlfarth coercivity (4.10) is a simple example of a *nucleation* field, H_N. In micromagnetism, the term 'nucleation' refers to the instability of the remanent state in a reverse magnetic field $H_z = -H_N$. It does not necessarily imply localization effects [8, 192], although localized nucleation is frequently encountered in practice (section 4.7). In small particles the nucleation mode is uniform (coherent), in contrast to the incoherent and often localized modes realized in large particles. Figure 11 illustrates the geometrical meaning of the incoherent *curling* mode, which is realized in large but perfect ellipsoids of revolution. Curling is favourable from the point of view of magnetostatic self-interaction, because the vortex-like mode yields some flux closure, but it costs some exchange energy, because $\nabla \boldsymbol{M} \neq 0$. The derivation of the curling mode involves the exchange term in (4.1). After some calculation [8, 192, 227, 254] one obtains the nucleation field (coercivity):

$$H_N = \frac{2K_1}{\mu_0 M_s} - D M_s + \frac{c(D) A}{\mu_0 M_s R^2}. \tag{4.11}$$

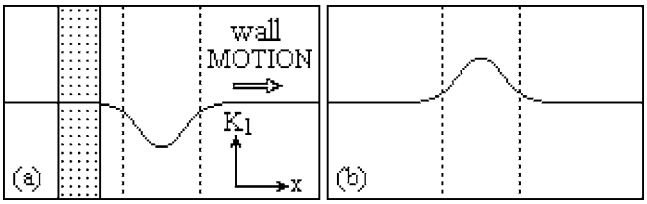

Figure 12. Domain-wall pinning: (a) attractive pinning and (b) repulsive pinning.

Here the radius R refers to the two degenerate axes of the ellipsoid, $c = 8.666$ for spheres ($D = 1/3$) and $c = 6.678$ for needles ($D = 0$). In (4.14), the magnetostatic contribution, $-DM_s$, is always negative, in contrast to the term $(1 - 3D)M_s/2$ in (4.10). This means that there is no shape anisotropy in large magnets, although the exchange term in (4.11) partly compensates for the absence of shape anisotropy in a proper sense [66]. Coherent rotation and curling modes in misaligned magnets are discussed in [255].

Comparison of (4.10) and (4.11) yields a transition from coherent rotation to curling at a coherence radius R_{coh}. For $R < R_{coh}$, the exchange energy dominates and the nucleation is realized by coherent rotation, whereas for $R > R_{coh}$ the nucleation behaviour is dominated by flux closure and realized by curling. For spheres one obtains $R_{coh} = 5.099 l_{ex}$, where l_{ex} is defined in (4.4) and tabulated for some materials in the appendix. In 'wires' ($D = 0$), the coherence radius $R_{coh} = 3.655 l_{ex}$ [8, 192, 227]. These radii are typically of the order of 5–10 nm. In thin films with perpendicular anisotropy ($D \approx 0$), curling occurs when the cross section of the films exceeds some value scaling as l_{ex}^2 [59]. The involvement of the exchange length can also be deduced from dimensional arguments, as outlined in section 4.2. Note that R_{coh} is anisotropy-independent, in contrast to the critical single-domain radius R_{SD}. Since $R_{coh} \ll R_{SD}$ in hard magnets, there is a broad region $R_{coh} \approx 10$ nm and $R_{SD} \approx 1\ \mu$m, where single-domain particles demagnetize incoherently.

A key distinction in micromagnetism is between nucleation and domain-wall *pinning*. Nucleation-controlled magnets are, ideally, defect- and domain-free and the coercivity is essentially given by the nucleation field. In contrast, pinning-type magnets contain pronounced inhomogeneities, which ensure coercivity by impeding the motion of the domain walls. Pinning determines, for example, the coercivity of iron and steel magnets [63, 206, 246], where the pinning force is associated with macroscopic mechanical strain. Pinning at nanoscale grain-boundary features is exploited, for example, in industrial Sm–Co–Cu–Zr magnets, which consist of regions of a main phase (essentially Sm_2Co_{17}) separated by a pinning grain-boundary phase (copper-rich $SmCo_5$) [8, 26, 68, 256, 257]. Figure 12 illustrates the difference between two pinning mechanisms, repulsive and attractive pinning. Repulsive pinning involves inhomogeneities whose anisotropy is higher than that of the main phase. Since high anisotropies yield high domain-wall energies $4(AK_1)^{1/2}$, the penetration of the wall into the high-anisotropy regions is energetically unfavourable. By comparison, attractive pinning means the capturing of a wall in a low-anisotropy region.

The pinning energy barrier is, to a fair approximation, proportional to the anisotropy difference, and by changing the chemical composition or, for some compositions, the temperature [258] it is possible to adjust the anisotropy and to tune the pinning behaviour. This is exploited in the development of permanent magnets for high-temperature applications [226, 258–263]. One example is high-temperature Sm–Co–Cu–Ti alloys having coercivities above 1.2 T (12 kOe) at 500 °C [258]. Note that the temperature dependence of the coercivity is dominated by the intrinsic mechanism, whereas thermally activated jumps

over energy barriers yield only a small sweep rate and magnetic-viscosity corrections to the coercivity (section 5.3).

A simple planar-wall pinning expression is $H_c = (\mathrm{d}\gamma(x)/\mathrm{d}x)/(2\,\mu_0 M_s)$, where $\gamma(x)$ is the average wall energy as a function of the wall position [246]. For a small planar inhomogeneity characterized by the anisotropy $K = K_1 + \Delta K$ and the thickness b the above coercivity reduces to [246]

$$H_N = H_a \frac{\pi_b}{3\sqrt{3}\delta_B} \frac{|\Delta K|}{K} \tag{4.12}$$

where $\delta_B = \pi(A/K)^{1/2}$ is the Bloch-wall width of the main phase and $H_a = 2K/\mu_0 M_s$. A rather straightforward way to discuss arbitrary K_1 and A profiles is to use a variation principle [258]. For small inhomogeneity amplitudes, this method yields exact results. Ignoring the exchange-stiffness variation, the energy of a one-dimensional wall of arbitrary width and profile is

$$E_w(x) = \int K_1(x)\left(1 - \tanh^2\left(\frac{\pi}{\delta_B}(\xi - x)\right)\right)\mathrm{d}\xi \tag{4.13}$$

where x denotes the wall position.

The pinning caused by a very few large defects, as illustrated in figure 12, is known as strong pinning. In contrast, pinning involving a large number of small pinning centres, such as atomic defects, is called *weak pinning*. In the case of weak pinning [264], the wall energy is averaged over a distance of the order of δ_B, so that the density of pinning centres determines the pinning strength. Some aspects of weak pinning will be discussed in section 4.6. Other types of pinning are, e.g., pinning at surface defects [248] and pinning caused by sesquilayer film-thickness modulation [86].

4.4. Nucleation in nanocomposites and multilayers

For perfect and aligned ellipsoids of revolution, (4.10) and (4.11) are *exact* results, which makes it tempting to use the nucleation field H_N as an estimate for the coercivity of real magnets. However, the condition of perfection is quite stringent, because a single nanoscale inhomogeneity may initiate the magnetization reversal of a macroscopic magnet. This localized nucleation leads to strong reduction of H_N and solves Brown's paradox [227, 265], according to which observed coercivities are often much smaller than predicted by (4.10)–(4.11).

To determine the nucleation field from (4.1), we write the local magnetization as

$$\boldsymbol{M}(r) = M_s\left(\sqrt{1 - m^2}\,\boldsymbol{e}_z + \boldsymbol{m}(\boldsymbol{r})\right) \tag{4.14}$$

where $\boldsymbol{m}$ is the perpendicular magnetization component ($|\boldsymbol{m}| = \sin\theta$). Taking into account that $\boldsymbol{n} = \boldsymbol{e}_z$ for aligned magnets, inserting (4.14) into (4.1) and expanding the result in powers of $\boldsymbol{m}$ yields the quadratic free-energy expression

$$E = \int [A(\nabla \boldsymbol{m})^2 + K_{eff}(\boldsymbol{r})\boldsymbol{m}^2 - \tfrac{1}{2}\mu_0 M_s H \boldsymbol{m}^2]\,\mathrm{d}\boldsymbol{r}. \tag{4.15}$$

In a strict sense, the effective local anisotropy $K_{eff}(\boldsymbol{r})$ is a complicated real-structure-dependent tensor[4]. However, in lowest order the tensor character of K_{eff} amounts to removing the degeneracy of $\boldsymbol{m}$ with respect to m_x and m_y [19] and one can treat K_{eff} as a scalar. This approach is exact for coherent rotation and curling, where $K_{eff} = K_1 + \mu_0(1 - 3D)M_s^2/4$ and

[4] In k space, the structure of this term is $\boldsymbol{k} \otimes \boldsymbol{k}/k^2$, compared to the diagonal expression Ak^2 describing exchange. A physical interpretation of the projection $\boldsymbol{k} \otimes \boldsymbol{k}$ in terms of Maxwell's equations is that a planar magnetization inhomogeneity changes the perpendicular field component (parallel to $\boldsymbol{k}$) but leaves the in-plane component unchanged.

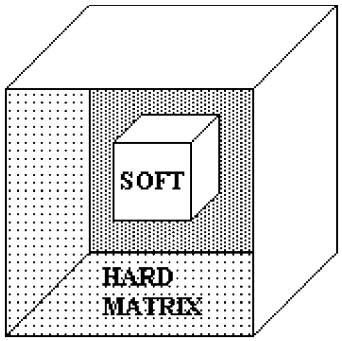

Figure 13. Soft-magnetic cube embedded in a very hard single-crystalline matrix ($K_1 \gg \mu_0 M_s^2$).

$K_1 - \mu_0 D M_s^2/2$, respectively, and a good approximation for magnets where magnetostatic effects can be treated on a mean-field level [113].

Eigenmode analysis of (4.15) yields the differential equation

$$A\nabla^2 m - \left(K_{eff}(\boldsymbol{r}) + \frac{\mu_0}{2} M_s H\right) m = 0 \tag{4.16}$$

where we have assumed that A is constant throughout the magnet. In terms of (4.16), imperfections appear as a modification of the local anisotropy $K_{eff}(\boldsymbol{r})$ and lead to a nucleation field and coercivity reduction [19, 65, 66, 234].

To solve the nucleation problem we note that (4.16) has the same structure as the single-particle Schrödinger equation

$$-\frac{\hbar^2}{2m}\nabla^2\psi + (V_1(\boldsymbol{r}) - E)\psi = 0. \tag{4.17}$$

This analogy makes it possible to use ideas known from quantum mechanics to solve micromagnetic problems. In particular, the nucleation field and the nucleation mode are analogous to the ground-state energy and the ground-state wavefunction, respectively [19].

A simple example is a soft magnetic cube of volume L^3 embedded in a very hard matrix (figure 13). The corresponding wavefunctions are particle-in-a-box states for an infinite potential well:

$$\Psi(x, y, z) = \Psi_0 \sin\left(\frac{\pi n_x x}{L}\right) \sin\left(\frac{\pi n_y y}{L}\right) \sin\left(\frac{\pi n_z z}{L}\right) \tag{4.18}$$

and the ground-state energy is $3\pi^2\hbar^2/2mL^2$. Using this energy and comparing (4.16) and (4.17) we obtain the nucleation field

$$H_N = \frac{6\pi^2 A}{\mu_0 M_s L^2} \tag{4.19}$$

where M_s is the spontaneous magnetization of the soft phase. This result can also be written as

$$H_N = H_a \frac{3\delta_B^2 M_h}{L^2 M_s} \tag{4.20}$$

where $H_a = 2K_1/\mu_0 M_h$ is the anisotropy field of the hard phase, M_h is the magnetization of the hard phase and $\delta_B = \pi(A/K_1)^{1/2}$ is the Bloch wall width of the hard phase. In the past, nucleation fields have been obtained for several cases: spherical particles in an

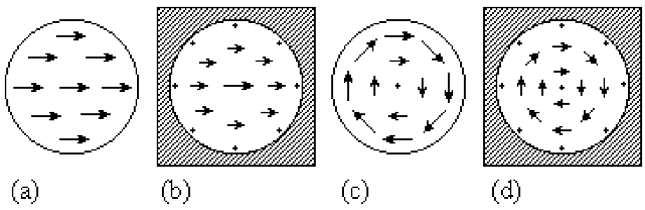

Figure 14. Nucleation modes in spheres surrounded by a hard magnetic shell: (a) coherent rotation, (b) bulging, (c) curling and (d) clamped curling. The figures are top views on the equator plane and the arrows show $\boldsymbol{m}(\boldsymbol{r})$ for the core phase (white) and in the hard magnetic environment (grey) $\boldsymbol{m}(\boldsymbol{r}) \approx 0$. In both cases, the radial dependence of $\boldsymbol{m}$ is given by spherical Bessel functions [66].

infinitely hard matrix [234], small inclusions in a matrix of arbitrary anisotropy and exchange stiffness [19, 66], various types of multilayers [19, 96] and some core-shell and nanowire configurations [66, 113, 145].

From (4.19) and (4.20) we see that H_N increases with decreasing inclusion size L. However, the small-inclusion divergence predicted by (4.19) and (4.20) is not realized in practice, because the anisotropy field H_a of the hard phase provides a cut-off. Extrapolating (4.20) to $H_N \approx H_a$ shows that the nucleation field reaches the anisotropy field when the size or radius of the soft inclusion becomes comparable to the Bloch wall width of the hard phase [18, 19, 234]. Since the Bloch wall width of typical permanent magnets is of the order of 5 nm, soft regions should be smaller than about 10 nm to ensure complete exchange coupling. However, this value depends to some extent on the geometry of the nanostructure; it is smallest for spheres but somewhat larger for multilayers. When the size of inhomogeneities is smaller than about 10 nm, then one can replace the local anisotropy $K_1(\boldsymbol{r})$ and the local magnetization $M_s(\boldsymbol{r})$ by volume averages [8, 19]. The quantum-mechanical analogue of this limit is the virtual-crystal approximation, where the potential $V(\boldsymbol{r})$ is averaged over atomic disorder.

The weaker requirement, that the switching field of the soft phase is comparable to the required coercivity, rather than comparable to the anisotropy field of the hard phase, leads to somewhat larger critical sizes, scaling as $R_{coh} \sim l_{ex}$ [66]. The same length scale determines the critical grain size above which the hysteresis loops of magnets consisting of hard and soft phases exhibit an inflection-type superposition of single-phase loops [68, 98, 266]. Figure 9(f) shows examples of these loops for the small-inclusion plateau regime (broken curve) and the large-inclusion exchange-spring regime (full curve). In contrast to the domain-wall width of the hard phase, that of the soft phase is irrelevant to the problem (section 4.2).

The nucleation modes for soft inclusions in a very hard matrix are *clamped*, that is, $m(\boldsymbol{r}) = 0$ at the hard–soft interface [66]. Figure 14 compares the clamped modes for spherical inclusions with the free-surface modes of isolated particles. The 'quasi-coherent' or 'bulging' mode shown in figure 14(b) has the angular symmetry of the coherent-rotation mode but is incoherent due to its radial variation. Bulging and clamped curling are realized for small and large inclusion diameters, respectively [66]. Similar localized modes exist in some inhomogeneous wire and thin-film geometries [65, 66, 113].

Two-phase nanostructuring is of practical interest in permanent magnetism (section 4.1). As briefly outlined in section 4.1, the hard phase acts as a skeleton to ensure a coercivity of the order of $H_c/2$, whereas adding the soft magnetic high-magnetization phase enhances M_s and M_r [19]. For suitable combinations of hard and soft phases, the upper limit to the energy products exceeds 1000 kJ m^{-3} [8, 19]. This limit is essentially independent of the shape of the soft and hard regions so long as the size of the soft regions remains sufficiently small. Various

combinations of soft magnetic phases with $SmCo_5$ [20, 22, 235], $Nd_2Fe_{14}B$ [88] and PtFe [21] have been investigated, but the development of the required well-textured and fine-grained nanostructure has remained a demanding task. Experimentally, the theoretical predictions have been realized in a Pt–Fe composite, whose energy product of 420 kJ m^{-3} (53 MGOe) exceeds that of hard magnetic PtFe and nearly reaches that of Nd–Fe–B [21], in spite of the only moderate magnetization of the involved PtFe and $PtFe_3$ phases. Note that the structures described by (4.16) are aligned. Texture effects, which dominate in isotropic magnets, are considered in section 4.6.

The energy-product enhancement discussed in this section exploits the nanoscale character of the competition between exchange and anisotropy. As discussed in section 3.2, it is not possible to enhance the finite-temperature magnetization of a phase having a low bulk Curie temperature by exchange-coupling it to a phase having a high bulk Curie temperature [60].

4.5. Grain boundaries and nanojunctions

The spin structure at grain boundaries and nanojunctions is a nanoscale phenomenon of great importance in permanent magnetism, magnetic recording, soft magnetism and spin electronics. In permanent magnets, it is often necessary to maximize [8, 19] or minimize the intergranular exchange, depending on the desired reversal mechanism (section 4.4 and 4.6). Strong intergranular exchange reduces the coercivity of isotropic soft magnetic nanostructures but is undesired in magnetic recording, where it negatively affects the storage density [32, 267], and the resistance of spin-electronic structures depends on the local magnetization at interfaces and at junctions [67, 237, 244, 268, 269]. From a theoretical point of view, the micromagnetics of granular interfaces and constrained domain walls was first investigated in the context of polycrystalline rare-earth transition-metal intermetallics [67], although various earlier papers, e.g. [19, 96, 243, 270], anticipate much of the involved physics.

For simplicity, we restrict ourselves to the linear case, which is realized, for example, in weakly textured systems. Applying the present approach to large angles introduces corrections, such as a wall-width enhancement by a factor $\pi/2$, but the essential physics of the following paragraphs remains unchanged. First we use (4.14) and the corresponding equation for the local easy axis as $\boldsymbol{n}(\boldsymbol{r}) = \sqrt{1 - a^2(\boldsymbol{r})}\boldsymbol{e}_z + \boldsymbol{a}(\boldsymbol{r})$, where $\boldsymbol{a}(\boldsymbol{r})$ are the transverse vector components of $\boldsymbol{n}$. Series expansion then yields $\boldsymbol{M} = M_s(1 - m^2/2)\boldsymbol{e}_z + M_s\boldsymbol{m}$ and $\boldsymbol{n} = (1 - a^2/2)\boldsymbol{e}_z + \boldsymbol{a}$. With $\boldsymbol{H} = H\boldsymbol{e}_z$ and (4.1) leads to

$$E = \int \left[A(\nabla \boldsymbol{m})^2 + K_1(\boldsymbol{m} - \boldsymbol{a})^2 + \tfrac{1}{2}\mu_0 M_s H \boldsymbol{m}^2\right] \mathrm{d}\boldsymbol{r}. \tag{4.21}$$

In this equation, which is an extension of (4.15), we have incorporated the magnetostatic self-interaction into K_1 and H. To minimize E with respect to $\boldsymbol{m}(\boldsymbol{r})$ we exploit that the minimum of any functional $F = \int \eta \, \mathrm{d}V$ is characterized by the functional derivative $\delta F/\delta \boldsymbol{m}(\boldsymbol{r}) = 0$. Explicitly,

$$\frac{\delta F}{\delta \boldsymbol{m}(\boldsymbol{r})} = -\nabla\left(\frac{\partial \eta}{\partial \nabla \boldsymbol{m}(\boldsymbol{r})}\right) + \frac{\partial \eta}{\partial \boldsymbol{m}(\boldsymbol{r})} \tag{4.22}$$

so that [67]

$$-\nabla(A\nabla \boldsymbol{m}) + \left(K_1 + \tfrac{1}{2}M_s H\right)\boldsymbol{m} = K_1 \boldsymbol{a}(\boldsymbol{r}). \tag{4.23}$$

This equation means that the polycrystalline easy axis disorder $\boldsymbol{a}(\boldsymbol{r})$ acts as a random inhomogeneity.

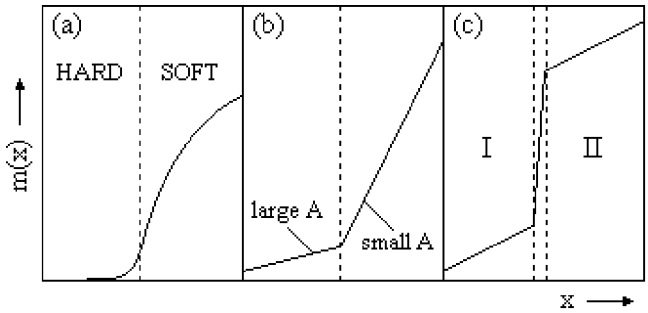

Figure 15. Boundary conditions and exchange: (a) hard–soft interface with common A, (b) interface between two ferromagnetic phases with different A and (c) quasi-discontinuous magnetization due to strongly reduced exchange between grains I and II. Note that the perpendicular magnetization component $m(x)$ can be interpreted as a magnetization angle.

The term $\nabla(A\nabla \boldsymbol{m})$ reflects due to local character of exchange stiffness $A(\boldsymbol{r})$ [19]. For sharp phase boundaries, the exchange term reduces to the boundary condition

$$\left(A(x)\frac{\partial m}{\partial x}\right)\bigg|_{x_0-\varepsilon} = \left(A(x)\frac{\partial m}{\partial x}\right)\bigg|_{x_0+\varepsilon}. \tag{4.24}$$

Figure 15 illustrates the physical meaning of this boundary condition. A jump in $A(x)$ leaves the magnetization continuous but yields a change in the slope of the perpendicular magnetization component $m(x)$. The solutions of (4.23) are exponentially decaying in the adjacent grains and nearly linear in the interface region [67, 237, 244].

When the exchange stiffness in the grain-boundary region is much lower than that of the two adjacent phases, then one encounters a *quasi-discontinuity* of the magnetization, as shown in figure 15(c). Experimentally, reduced interface exchange reflects real-structure features such as impurity atoms diluting the interatomic exchange, oxide layers covering the grains and interface amorphization. For $H = 0$, the relative strength of the quasi-discontinuity

$$\Delta = \frac{1}{1 + 2A'\delta_B/\pi AD} \tag{4.25}$$

where D is the thickness of the interface region. Zero exchange in the grain-boundary region ($A' = 0$) yields an ideal magnetization jump, $\Delta = 1$, as expected for complete decoupling. For $D = 0$, (4.25) reduces to the trivial prediction of a vanishing quasi-discontinuity ($\Delta = 0$). In the intermediate regime, the large ratio δ_B/D tends to suppress the influence of the reduced interface exchange. In a *layer-resolved* analysis, the ∇ operator in (4.21) and (4.23) must be replaced by magnetization-angle differences, but a comparison with the continuum solution [237, 244] reveals only minor corrections due to the discrete nature of the layers. However, the layer-resolved anisotropies and exchange constants may deviate from the respective bulk values.

Using the integral $\int(\nabla M)^2\,\mathrm{d}x \approx M_s^2\int(\nabla \boldsymbol{m})^2\,\mathrm{d}x$ as a crude measure to gauge the spin-dependent scattering ability of an interface we find that the scattering is maximized for interface thicknesses of the order of $D = \delta_0 A'/A$. Smaller thicknesses lead to a reduction of the quasi-discontinuity and make the scattering more bulk-like. Compared to Bloch wall scattering, where $\int(\nabla \boldsymbol{m})^2\,\mathrm{d}x \approx 1/\delta_0$, the maximum scattering is enhanced by a factor A/A', so that optimized exchange-decoupled grains would yield very large scattering. Unfortunately, strong reductions of A' are likely to negatively affect the spin injection through the boundary region, thereby reducing the magnetoresistance. Another way of enhancing the scattering is using very hard materials, where δ_0 is small, but this requires large fields to switch the magnetization direction [237].

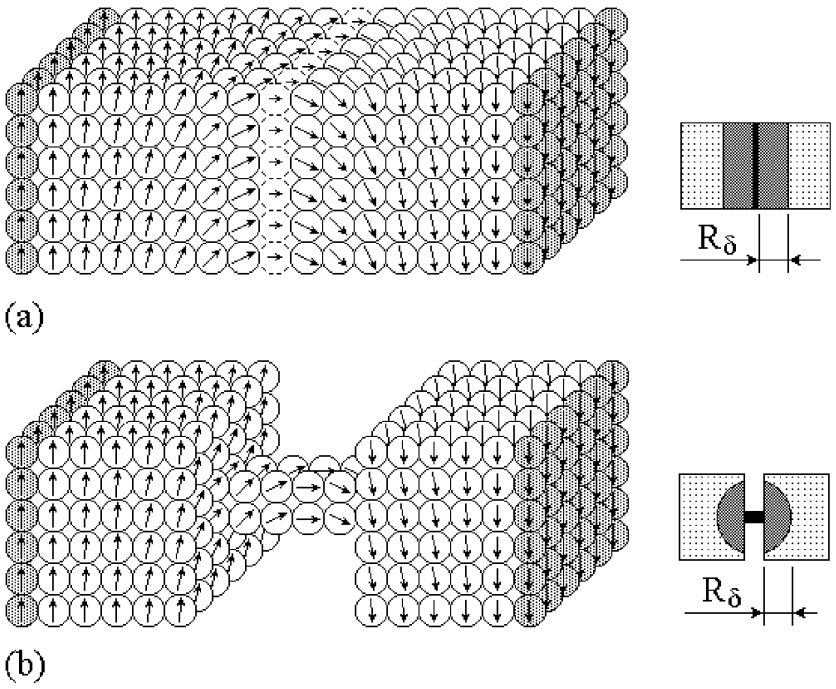

Figure 16. Exchange effects at interfaces: (a) planar interface and (b) contact junction [67, 237].

Varying the relative alignment of the grains and evaluating the energy (4.21) as a function of the misalignment vector $\boldsymbol{a}$ yields an *effective exchange* between grains. The effective exchange corresponding to (4.25) is [244]

$$J_{eff} = S_0\sqrt{AK_1}\,\frac{1}{1+\pi DA/2\delta_B A'} \tag{4.26}$$

where S_0 is the interface area. From this equation we see that the effective exchange can never be larger than the value $S_0(AK_1)^{1/2}$, which scales as Bloch wall energy of a perfect magnetic crystal (section 4.2). This result must be contrasted to the popular assumption [267] that $J_{eff} \approx S_0A'/a$, which assigns a bond of strength $J' \approx A'/a$ to each of the $N \approx S_0/a^2$ adjacent pairs of atoms and overestimates the effective exchange, particularly in soft magnets. Solutions similar to (4.26) have also been obtained for hard–soft interfaces [67], where most of the energy is stored in the soft phase.

The one-dimensional character of the structural features considered above means that the solutions of (4.23) are piecewise exponential, proportional to $\exp(\pm x/\delta_0(x))$. To tackle the problem for arbitrary geometries and dimensions, it is convenient to rewrite (4.23) as a linear operator equation, $\mathsf{Q}\boldsymbol{m} = \boldsymbol{a}$. The formal solution of this equation is $\boldsymbol{m} = \mathsf{G}\boldsymbol{a}$ or, in real space, $\boldsymbol{m}(\boldsymbol{r}) = \int \mathsf{G}(\boldsymbol{r},\boldsymbol{r}')\ \boldsymbol{a}(\boldsymbol{r}')\,\mathrm{d}V'$, where $\mathsf{G} = \mathsf{Q}^{-1}$ is the propagator (Green function) of the micromagnetic problem [67]. $\mathsf{G}(r)$ is proportional to $K_{d/2-1}(r/r_\delta)$, where K_m is Macdonald's modified Bessel function of order m and r_δ is the interaction length of the problem [271]. In the absence of magnetic fields, $r_\delta \approx \delta_0 = \delta_B/\pi$. For one-dimensional problems, $\mathsf{G}(r)$ is exponential, whereas three-dimensional problems are described by $K_{1/2}(r/r_\delta) \sim \exp(-r/r_\delta)/r$. Figure 16 illustrates the meaning of G for two examples. In figure 16(b), the semi-infinite character of the connected ferromagnetic bodies does not affect $\mathsf{G}(r)$ very much, because (4.24) implies that $\partial\boldsymbol{m}/\partial\boldsymbol{r}_\perp = 0$ at free surfaces. Note that r_δ

does not depend on the strength of the inhomogeneities: varying the exchange in the interface region in (a) or the size or coupling strength of the junction in (b) affects the *amplitude* of the perturbation but leaves its range r_δ unchanged. This complicates the determination of the spin structure at nanojunctions and similar features from first principles, because the perturbed regions tend to contain thousands or even millions of atoms and because the energy differences involved are very small.

4.6. Textured magnets and random-anisotropy behaviour

A broad variety of magnetic materials are characterized by completely or partially random easy axes. Completely random easy axes, $\langle \boldsymbol{n}(\boldsymbol{r})\rangle = 0$, are encountered in isotropic nanostructures and in many amorphous magnets [13, 162, 164, 272]. Partial easy axis randomness or texture is found, for example, in partially oriented polycrystalline magnets [21] and in strained amorphous magnets [159]. Random anisotropy and texture effects are of great scientific and technological importance. In the 1970s it became clear that random anisotropy structures exhibit scientifically and technologically interesting properties, and the control and exploitation of random anisotropy effects has become a major issue in permanent magnetism [8, 17, 157], magnetic recording [32, 244, 273] and soft magnetism [25, 274].

Atomic-scale random anisotropy effects have first been discussed in the context of spin glasses [13, 151, 160, 272], although there is a clear distinction between canonical random exchange spin glasses and random anisotropy magnets [13, 151]. Interatomic exchange in random anisotropy magnets favours ferromagnetic spin alignment, competing against the randomness and yielding interesting spin correlation effects. The same is true for random field magnets, which were investigated first [232]. The coercivity and remanence of atomic random anisotropy magnets was investigated in the late 1970s [233, 275, 276], whereas Chudnovsky *et al* [64] investigated random anisotropy effects in polycrystalline materials. From a technological point of view, texture tends to deteriorate magnetization, hysteresis-loop shape and coercivity. The coercivity reduction is undesired in permanent magnets and recording media but exploited to reduce losses in soft magnets. Furthermore, the negative effect of texture on the magnetization is partly compensated by exchange. However, intergranular exchange may reverse this effect, which is known as remanence enhancement.

In permanent magnets, perfect c-axis alignment is difficult to realize and most nanostructures, including those investigated in [21], exhibit some degree of polycrystalline texture. The starting point for the description of weak texture is (4.23). Neglecting the comparatively weak influence of exchange inhomogeneities [19], the term $\nabla(A\nabla\boldsymbol{m})$ in (2.23) becomes $A\nabla^2\boldsymbol{m}$. Since the spatial average $\langle\boldsymbol{a}\rangle$ of the easy-axis fluctuations vanishes, $\langle\boldsymbol{m}\rangle = 0$, we have to consider the average $\langle\boldsymbol{m}(\boldsymbol{r})\cdot\boldsymbol{m}(\boldsymbol{r}')\rangle$. In particular, choosing $\boldsymbol{r} = \boldsymbol{r}'$ yields the average magnetization $\langle M_z\rangle = M_s(1 - \langle\boldsymbol{m}^2\rangle/2)$, whereas for $\boldsymbol{r} \neq \boldsymbol{r}'$ the average describes spatial magnetization correlations. Putting $\mathsf{Q} = \mathsf{Q}_0 + \delta\mathsf{Q}$, where $\mathsf{Q}_0 = \mathsf{G}_0^{-1}$ is an easy-to-invert operator and $\delta\mathsf{Q}$ is a small perturbation, yields the series expansion $\mathsf{G} = \mathsf{G}_0 - \mathsf{G}_0\delta\mathsf{Q}\mathsf{G}_0 \pm \cdots$. In lowest-order perturbation theory, $\langle\boldsymbol{m}(\boldsymbol{r})\cdot\boldsymbol{m}(\boldsymbol{r}')\rangle = \langle\mathsf{G}_0\boldsymbol{a}(\boldsymbol{r})\mathsf{G}_0\boldsymbol{a}(\boldsymbol{r}')\rangle$ [67, 266]. In the limit of strong coupling, the magnetization curves obey $M_s - M_z(H) \sim (H_c - H)^{(d-4)/2}$ [228]. The opposite limit of weakly coupled large grains yields

$$\langle\boldsymbol{m}^2\rangle = \frac{4K_1^2}{(2K_1 + \mu_0 M_0 H)^2}\langle\boldsymbol{a}^2\rangle + \frac{8K_1^2 A}{(2K_1 + \mu_0 M_0 H)^3}\langle\boldsymbol{a}\cdot\nabla^2\boldsymbol{a}\rangle. \tag{4.27}$$

Exploiting that $\boldsymbol{a}\cdot\nabla^2\boldsymbol{a} = \nabla(\boldsymbol{a}\cdot\nabla\boldsymbol{a}) - (\nabla\boldsymbol{a})^2$ one finds that $\langle\boldsymbol{a}\cdot\nabla^2\boldsymbol{a}\rangle$ is of the order of $\langle a^2\rangle/R^2$, where R is the average grain radius. Spin structures of the type (4.27) were first investigated by Chudnovsky *et al* [64], although that work did not consider hysteretic $M(H)$

curves. On the other hand, both (4.27) and [64] imply smooth boundaries, ignoring for example the magnetization jumps discussed in section 4.5.

The effect of polycrystallinity on nanowires was investigated by Zheng *et al* [148]. The calculation yields an analytic expression for the magnetization as a function of the wires' structural and micromagnetic parameters. Since the magnetocrystalline anisotropy of the considered Ni nanowires is much smaller than the shape anisotropy of the wires, the linearization implied in (4.27) is a good approximation and the theoretical prediction agrees quite well with experiment. The only exception is the vicinity of the coercivity, where localization (section 4.7) and nonlinear effects (section 5.3) interfere.

In *isotropic* magnets, the absence of any net or 'coherent' anisotropy makes it impossible to use series expansions such as (4.27). The spin structure of isotropic magnets has first been studied in the context of the random-field problem, where individual atoms or particles (index i) are subjected to random fields H_i of magnitude H_0. The original paper by Imry and Ma [232] investigates random magnetic fields H_i characterized by $\langle H_i\rangle = 0$ and $\langle H_i H_j\rangle = H_0^2\delta_{ij}$. If the random field was the only consideration, the magnetization would follow the local field, but spatial variations of the magnetization are opposed by the interatomic exchange. This leads to magnetically correlated regions containing N atoms and characterized by the averages $\langle H\rangle = 0$ and $\langle H^2\rangle = H_0^2/N$. In other words, there remains a contribution of the order of $\pm H_0/\sqrt{N}$ reminiscent of the standard deviation in statistical data analysis. The number N of correlated spins depends on the competition between the random field (or random anisotropy) and exchange energies. To determine N, one must minimize the average energy density η. In the random anisotropy picture

$$\eta = \frac{A}{L^2} - K_1\frac{1}{\sqrt{N}} \tag{4.28}$$

where L is the magnetic correlation length. In d dimensions, the volume of the correlated regions is of the order of $L^d \approx NR^d$, where R is the grain radius. Minimizing the resulting expression:

$$\eta = \frac{A}{L^2} - K\frac{R^{d/2}}{L^{d/2}} \tag{4.29}$$

with respect to L yields the scaling relation

$$L \sim R(\delta_0/R)^{4/(4-d)} \tag{4.30}$$

where $\delta_0 = (A/K)^{1/2}$ is the wall-width parameter introduced in section 4.2. From (4.30) we see that $d = 4$ is a marginal dimension below which small grains ($R < \delta_0$) yield intergranular correlations ($L > R$ and $N > 1$). In nanowires, the existence of an additional length scale (wire diameter) leads to modifications of (4.30) and to crossover regimes [145].

Since $K_1/N^{1/2}$ can be considered as an effective anisotropy, the formation of correlated regions ($R < \delta_0$) reduces the coercivity. Using (4.30) to determine N and exploiting that $H_c \approx 2K_1/M_s$ yields

$$H_c \sim \frac{2K_1}{\mu_0 M_s}(R/\delta_0)^{2d/(4-d)}. \tag{4.31}$$

In three dimensions, this means that the coercivity scales as R^6 [13, 233]. As pointed out by Herzer [24, 25], this random anisotropy nanostructuring is a powerful tool to reduce the coercivity of soft magnetic materials. It is exploited, for example, in Fe–Si–B–Cu–Nb alloys [23]. For $R > \delta_0$, the coercivity reaches a maximum value of the order of the anisotropy field $H_a = 2K_1/\mu_0 M_s$. For randomly oriented and interaction-free Stoner–Wohlfarth particles $H_c = 0.479H_a$, but real-structure imperfections tend to reduce this value.

The coercivity reduction due to random anisotropy is undesired in permanent magnets. On the other hand, intergranular exchange improves the remanence by favouring parallel spin alignment in neighbouring grains [17, 155–157, 236, 276]. This is known as *remanence enhancement*. Note that isotropic structures are comparatively easy to produce, but the remanent magnetization M_r of randomly oriented grains with uniaxial anisotropy is only half the saturation magnetization M_s. Since energy product scales as M_r^2, this amounts to an energy-product reduction by a factor 4, and partial spin alignment (remanence enhancement) is a valuable tool to increase the energy product. In iron-type ($K_1 > 0$) and nickel-type ($K_1 < 0$) cubic magnets, the interaction-free M_r/M_s has values of 0.832 and 0.866, respectively, but the low anisotropy of cubic magnets (see the appendix) inhibits the use of single-phase cubic materials as permanent magnets. For soft regions sandwiched between hard planes with random in-plane anisotropies, a 'projective' remanence enhancement $M_r/M_s \leqslant 8/\pi^2$ is obtained [67, 277].

Experimentally, both single-phase and two-phase magnets have been investigated: examples of two-phase systems are nanocrystalline $Nd_2Fe_{14}B/Fe_3B$–Fe and $Sm_2Fe_{17}N_3$/Fe composites produced by melt-spinning [17] and mechanical alloying [156], respectively. It is important to note that traditional random anisotropy and random field theories [64, 151, 272] focus on the *ground-state behaviour* of isotropic magnets. In less than four dimensions, the ground state of random anisotropy magnets does not exhibit long-range ferromagnetic order [151]. However, the ground-state behaviour of random anisotropy magnets is of little consequence to the hysteresis [164] and, in spite of the absence of true ferromagnetism, some of these structures exhibit huge coercivities.

In some cases, magnetic grains are coupled through a nonmagnetic or weakly ferromagnetic matrix. Examples are the soft magnetic Fe–Si–B–Cu–Nb alloys discussed in section 2.5 [23, 24, 278] and Sm–Co–Cu–Ti permanent magnets for high-temperature applications [258]. In this case, the magnetization change is largely localized in the grain-boundary region. Using the results of section 4.5 yields the effective exchange stiffness $A_{eff} = A'R/D$, where D is the surface-to-surface distance of the grains. In the case of a matrix with a very small exchange coupling ($T < T_C$), A' is the exchange stiffness of the matrix, whereas in a paramagnetic matrix A' is an exponential function of D. The explicit dependence of A on R modifies the scaling behaviour to $L \sim R^{(2-d)/(4-d)}$ and $H_c \sim R^{d/(4-d)}$. Note that the exponent for L changes sign for $d \leqslant 2$. In this case, the exchange through the grain boundary is not able to overcompensate the reduction of grain size and there are no correlated grains with $L > R$.

4.7. Magnetic localization and cooperativity of magnetization reversal

A key feature of most magnetization processes in real nanostructures is the *localization* of the reversal mode. The coherent-rotation and curling modes discussed in section 4.3 are delocalized, that is, they extend throughout the magnet. Delocalized magnetization states are favourable from the point of view of interatomic exchange, because the magnetization gradient is small. However, exchange is not the only consideration, because local variations of the magnetization cost some exchange energy but may be favourable from the point of view of local anisotropy, $K_1(\boldsymbol{r})$. This competition leads not only to a reduction of the nucleation field but also to a localization of the nucleation mode. In a sense, localization explains the failure of the Stoner–Wohlfarth theory (section 4.3). In terms of the quantum-mechanical analogy, the micromagnetic localization problem is equivalent to the problem of electron localization [279] in disordered solids. From the localization behaviour of a one-dimensional electron gas [279] it follows that arbitrarily weak disorder causes the localization of all magnetic eigenmodes

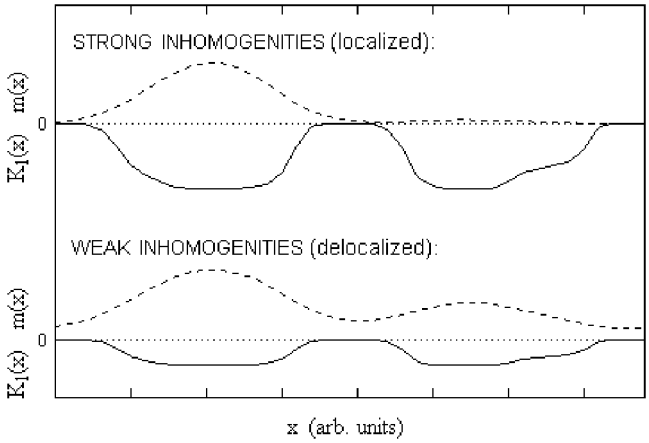

Figure 17. Localization in weakly and strongly disordered magnets.

in one dimension [66]. Alternatively, micromagnetic delocalization can be interpreted as a 'tunnelling' through hard magnetic regions.

In practice, localization is caused by structural, geometrical and chemical imperfections, which make it impossible to consider the magnets as perfect ellipsoids of revolution [8, 65, 254]. The degree of the localization and of the accompanying coercivity reduction depends on the competition between the exchange and anisotropy energies. For a soft inclusion in a very hard matrix, as considered in section 4.4, the localization is complete, that is, the magnetic localization length L is equal to the size of the inclusion. In general, the localization length depends on the structural correlation length (grain size), on the exchange stiffness, on the amplitude of the anisotropy inhomogeneity and on the dimensionality of the problem. Mathematically, the nucleation modes are the lowest-lying eigenfunctions of (4.16). Figure 17 shows two one-dimensional anisotropy profiles (full curves) and the corresponding nucleation modes (broken curves). The stronger the anisotropy inhomogeneity, the smaller the localization length.

An example is electrodeposited thin transition-metal nanowires (section 2.4). The leading anisotropy contribution in soft and semihard nanowires is shape anisotropy [38, 127, 144], but the Stoner–Wohlfarth predictions fail to describe the hysteresis of the wires [38, 133, 145, 146, 148, 280]. First, the coercivity measured along the wire axis ranges from about 0.2 to 0.3 T for Fe, from about 0.10 to 0.25 T for Co and from 0.04 to more than 0.09 T for Ni, whereas the respective Stoner–Wohlfarth predictions $H_c = M_s/2$ are 1.07, 0.88 and 0.31 T [38, 133, 135, 144, 148, 281]. Second, experimental activation volumes (section 5.3), which correspond to the localization length, are often much smaller than the wire volume [38, 77, 145, 280, 282]. For example, Wegrowe *et al* [282] found that their magnetization data could be fitted to the infinite-wire curling prediction only with the paradoxical assumption that the shape of the 'infinite cylinder' is like a rugby ball, with an aspect ratio of the order of 2:1.

In very thin wires, with radii down to less than 5 nm, it is possible to neglect the radial variation (section 4.4) of the magnetization [38, 145, 147, 148, 283]. Let us consider a single anisotropy inhomogeneity of the type $K_1(x) = K_0 - \Delta\delta K\delta(x)$, where δK is the magnitude of the anisotropy reduction and Δ is its extension along the z axis. Away from the perturbation,

the mode decays exponentially, $m(z) \sim \exp(-z/L)$ [145]. The localization length obeys

$$L = \frac{2A}{\Delta\delta K} \tag{4.32}$$

and the coercivity is

$$H_c = H_A - \frac{\delta K^2 \Delta^2}{2A\mu_0 M_s}. \tag{4.33}$$

For zero disorder, the localization length goes to infinity and the reversal degenerates into coherent rotation.

Equations (4.32) and (4.33) provide a qualitatively correct explanation of the observed mode localization and coercivity reduction but does not aim at specifying the real-structure origin of the localization. Typically, it reflects polycrystallinity, wire-thickness fluctuations, chemical inhomogeneities or geometrical features at the wire ends, or a combination of these factors. Note that the nanomagnetic localization discussed in this section is essentially a zero-temperature effect. Thermal activation may, in principle, create a localized nucleus but, due to the small Boltzmann factor $\exp(-E_B/k_BT)$, this is an extremely unlikely event (section 5.3).

An alternative way of interpreting the real-space character of magnetization processes is to consider the degree of *cooperativity* of magnetization processes [284]. Cooperative effects are of great importance in advanced technology. For example, in high-density magnetic recording media they lead to the formation of interaction domains, which may improve the thermal stability but reduce the storage density. In permanent magnets the vanishing of the two-phase shoulders in hysteresis loops can be considered as a cooperative effect [69, 284], as is the above-discussed low coercivity of soft magnetic random anisotropy magnets.

From an atomic point of view, all magnetization processes are cooperative, because the interatomic exchange suppresses the reversal of individual spins. In temperature units, the exchange energy J associated with the switching of a single atomic spin is of the order of 1000 K, whereas the anisotropy energy per atom rarely exceeds a few tenths of a K. Since $A \approx J/a$ and $A/K_1 = \delta_0^2$ (section 4.2), the range of atomic cooperativity extends over a few nanometres. On larger length scales, magnetization processes may or may not be cooperative.

By definition, the coherent-rotation and curling modes are cooperative. Weakly interacting particles and grains are cooperative from the point of view of intraparticle magnetization processes but noncooperative from the point of view of interparticle interactions. When the interactions exceed a certain threshold, then the behaviour of the magnet changes from noncooperative to cooperative. Examples are the difficult-to-realize curling limit in macroscopic ellipsoids of revolution (section 4.3) and the strong-interaction limit of random anisotropy magnets (section 4.6). Only a few problems involving cooperative effects have exact solutions. An example is magnetostatic interactions in corrals of small dots [113]. Figures 18(c), (d) show various nucleation modes whose cooperativity is caused by flux closure.

A simple approach to describe interacting between particles or grains is to map the interactions onto interaction fields. Examples are the micromagnetic mean-field model, the Preisach model [285, 286] and approaches based on Wohlfarth's remanence relation [287], such as Henkel [288], delta-M [289, 290] and delta-H [291] plots. In the mean-field approximation, the influence of neighbouring grains or particles is treated in terms of effective fields $\boldsymbol{H}_{eff} = \boldsymbol{H} + \lambda \boldsymbol{M}$, where the coupling parameter λ contains both magnetostatic and exchange contributions. However, for large λ the model yields an unphysical hysteresis-loop overskewing and unreasonably large coercivities [66]. In the context of the coercivity of random anisotropy magnets, the limited applicability of the mean-field approximation has been emphasized by Callen *et al* [276]. The reason is that cooperative phenomena cannot be mapped onto interaction fields [284]. One example is that two strongly interacting particles

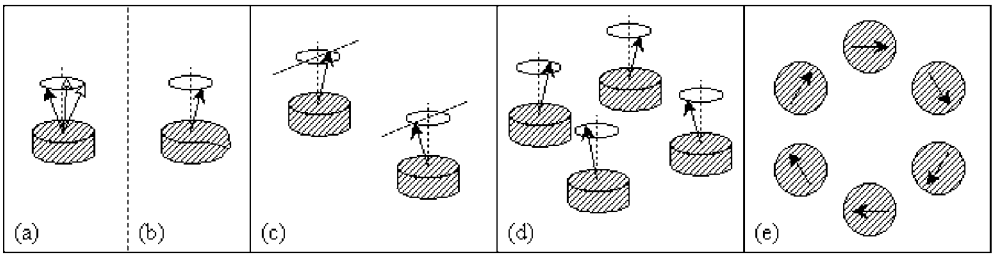

Figure 18. Cooperative effects in nanodot arrays: (a) degeneracy of the coherent-rotation mode in a small particle, (b) angular localization due to a defect, (c) two-particle cooperative mode, (d) cooperative mode involving more than two dots and (e) flux closure as one origin of cooperative behaviour.

behave like one particle and there is no point in adding the strong internal interaction field λM to any external-field expression. Another example is figures 18(c)–(e), where the flux closure contribution to the total energy is comparable to or even larger than the dot's interaction-field energy contribution.

A rough criterion for the applicability of interaction-field models is obtained from the slope of the hysteresis loop at coercivity, $\chi_c = \mathrm{d}M(H_c)/\mathrm{d}H$. When M_s/χ_c is smaller than the interaction field, then the behaviour of the magnet is governed by cooperative effects [67, 284]. Since M_s/χ_c can also be interpreted as a switching-field distribution, cooperative and noncooperative regimes of magnetization reversal correspond to narrow and broad switching-field distributions, respectively. In terms of figure 17, this is not surprising, because broad switching-field distributions correspond to pronounced inhomogeneities and therefore to strong localization.

5. Magnetization dynamics

An important aspect of nanomagnetism is the nonequilibrium character of the involved magnetization processes. In fact, most dynamic magnetization phenomena of interest in science and technology are of nanostructural origin. An exception is fast atomic-scale processes, whose study is a separate issue but which affect nanomagnetism by realizing intrinsic magnetism. For example, the change of the spontaneous magnetization of Fe on heating from 4.2 to 600 K reflects quantum-statistical processes realized on a scale of a few atoms and is not accompanied by hysteresis. Nanoscale processes are, in general, much slower, with times ranging from about 1 ns in some high-frequency experiments to many millions of years in magnetic rocks.

On an atomic scale, the magnetic structure is driven by intra- and interatomic exchange and by interatomic hopping, and typical energy differences between 0.1 and 1 eV lead to characteristic times $\hbar/E$ of about 10^{-14} s. The corresponding fast equilibration times make it possible to consider intrinsic properties as equilibrium properties described by the partition function $Z = \Sigma_i \exp(-E_i/k_BT)$. Due to the implicit involvement of the partition function, the energy functional (4.1) is also known as the micromagnetic *free* energy [8, 227]. Typical magnetostatic and anisotropy energies per atom, about 0.1 meV, correspond to times of the order of 10^{-10} s. This governs a variety of precession, resonance and damping phenomena of importance in nanomagnetics.

Aside from relatively fast processes, there are thermally activated jumps over free-energy barriers giving rise to a time dependence of extrinsic magnetic properties. For example,

freshly magnetized permanent magnets lose a small fraction of their magnetization during the first few hours (magnetic viscosity} and the coercivity depends on the sweep rate $\mathrm{d}H/\mathrm{d}t$ of the external magnetic field [8, 246, 292]. Since thermal activation involves the Boltzmann factor $\exp(-E_a/k_BT)$, extrinsic equilibration times vary over many orders of magnitudes, from nanoseconds or milliseconds in superparamagnetic particles to millions of years in magnetic rocks.

5.1. Fundamental equations

The time-dependent many-body Schrödinger equation $\mathrm{i}\hbar\partial|\Psi\rangle/\partial t = H|\Psi\rangle$ can, in principle, be used to predict the evolution of any physical system, but this method is not feasible in practice[5]. First, the deterministic character of the Schrödinger equation forbids irreversible processes. Second, the large number of involved degrees of freedom, such as lattice vibrations, complicates the description of real magnetic systems. To make meaningful predictions about relevant magnetic degrees of freedom, such as the position of a domain wall, one must treat the irrelevant degrees of freedom as a heat bath. A simple classical analogue of this 'coarse graining' [293–295] is a system of masses coupled by harmonic springs. The system has a recurrence time τ_{rec} scaling as $1/\Delta\omega$, where $\Delta\omega$ is the system's smallest eigenfrequency difference. For any finite system the recurrence time is finite, but for an infinite number of degrees of freedom, corresponding to a heat bath, $\Delta\omega = 0$ and $\tau_{rec} = \infty$.

The coarse-graining procedure provides the justification for various nonequilibrium approximations. One example is the Landau–Lifshitz equation:

$$\frac{\mathrm{d}\boldsymbol{M}}{\mathrm{d}t} = \gamma\boldsymbol{M}\times\boldsymbol{H}_{eff} - \frac{1}{M_s^2\tau_0}\boldsymbol{M}\times(\boldsymbol{M}\times\boldsymbol{H}_{eff}) \tag{5.1}$$

where γ is the gyromagnetic ratio, τ_0 is an inverse attempt frequency of the order of 10^{-11}–10^{-9} s [11, 292, 296] and $\mu_0\boldsymbol{H}_{eff} = -\partial E/\partial\boldsymbol{M}(\boldsymbol{r})$ is a local effective field [192, 297–299]. Equation (5.1), and similar relations such as the Gilbert and Bloch–Bloembergen equations, describe the precession of the magnetization around $\boldsymbol{H}_{eff}$ as well as its relaxation towards the local or global energy minima associated with $\boldsymbol{H}_{eff}$. However, they are not able to describe thermally activated jumps over energy barriers. An equation describing thermal activation is the *Langevin* equation:

$$\frac{\partial\underline{s}}{\partial t} = -\frac{\Gamma_0}{k_BT}\frac{\partial E}{\partial\underline{s}} + \sqrt{2\Gamma_0}\underline{\xi}(t). \tag{5.2}$$

Here $\underline{s}$ is a magnetic phase-space vector and the random forces $\underline{\xi}(t)$ obey $\langle\underline{\xi}(t)\rangle = 0$ and $\langle\underline{\xi}(t)\cdot\underline{\xi}(t')\rangle = \delta(t-t')$. The probability distribution belonging to (5.2) obeys the diffusion-type magnetic *Fokker-Planck* equation [295, 300, 301]:

$$\tau_0\frac{\partial p}{\partial t} = \frac{1}{k_BT}\frac{\partial}{\partial\underline{s}}\left(P\frac{\partial E}{\partial\underline{s}}\right) + \frac{\partial^2 P}{\partial\underline{s}^2}. \tag{5.3}$$

Both (5.2) and (5.3) can be derived from a phenomenological master or rate equation:

$$\frac{\partial P(\underline{s})}{\partial t} = \int[W(\underline{s},\underline{s}')P(\underline{s}') - W(\underline{s}',\underline{s})P(\underline{s})]\,\mathrm{d}\underline{s}' \tag{5.4}$$

where the $W(\underline{s},\underline{s}') = W(\underline{s}'\to\underline{s})$ are appropriately chosen transition rates. A simplified version of the master equation, valid for transitions between two energy minima, is $\partial P_1/\partial t = W_{12}P_2 - W_{21}P_1$ and $\partial P_2/\partial t = -W_{12}P_2 + W_{21}P_1$. *Kramers' escape-rate theory* [300, 302]

[5] An exception is quantum tunnelling, which dominates thermally activated magnetization processes at very low temperatures.

shows that the transition rates are proportional to the Boltzmann factor $\exp(-E_a/k_BT)$ so long as $E_a \gg k_BT$. The theory was originally used to describe chemical reaction kinetics but later applied to magnetism, where it is also known as the Arrhenius–Néel or Néel–Brown theory. In equilibrium, (5.2)–(5.4) all reproduce the Boltzmann distribution $P(\underline{s}) = (1/Z)\exp(-E(\underline{s})/k_BT)$, where $Z = \int \exp(-E(\underline{s})/k_BT)\,\mathrm{d}\underline{s}$ is the partition function, but there is no closed solution for nonequilibrium magnetization processes.

5.2. Spin waves

Since Bloch's 1930 article on the temperature dependence of spontaneous magnetization of ferromagnets [303], spin waves have attracted much attention in the solid-state and magnetism communities [204, 304, 305]. In particular, Bloch's spin-wave arguments indicate that there is no long-range isotropic ferromagnetism in two or less dimensions [8, 117, 151, 181, 184, 186, 303]. In Bloch's original approach, the long-wavelength magnetization reduction due to spin waves is proportional to the integral $\int k^{d-3}\,\mathrm{d}k$, which exhibits a long-wavelength divergence for $d \leqslant 2$. On the other hand, the behaviour of experimental wires is reminiscent of bulk ferromagnets, and the question arises how low-dimensional effects manifest themselves in magnetic nanostructures.

Ignoring damping effects, $\tau_0 = \infty$ in (5.1), the resonance is described by $\mathrm{d}\boldsymbol{M}/\mathrm{d}t = \gamma(\boldsymbol{M} \times \boldsymbol{H}_{eff})$. For homogeneously magnetized ellipsoids of revolution, the effective field is equal to the applied field $\boldsymbol{H} = H\boldsymbol{e}_z$ plus the anisotropy field $\boldsymbol{H}_a$ and the resonance problem is solved by the diagonalization of a 2×2 matrix. This uniform or ferromagnetic resonance (FMR) yields resonance frequencies determined by [165]

$$\omega^2 = \gamma^2(H + H_{ax} - H_{az})(H + H_{ay} - H_{az}) \tag{5.5}$$

where $\boldsymbol{e}_x$ and $\boldsymbol{e}_y$ correspond to the principal axes of the 2×2 matrix. In systems with rotational symmetry, such as perfect nanowires aligned parallel to the external magnetic field, this equation degenerates into

$$\omega = \gamma(H + 2K_{eff}/\mu_0 M_s) \tag{5.6}$$

where $K_{eff} = K_1 + \mu_0 M_s^2/4$. Note that the spin-wave problem is closely related to the nucleation problem, because the coherent-rotation mode is essentially a $\omega = 0$ spin-wave mode [192]. Nonuniform modes, that is, spin waves in a narrower sense, involve an exchange term similar to that in (4.16) [192, 298, 299]. The electron spin resonance (ESR) of these modes is known as spin-wave resonance (SWR), in contrast to the simpler FMR described by (5.5) [165].

Spin-wave type excitations in perfect nanodots and nanowires have recently been studied by a number of groups [306–312]. There are, for example, spin-wave quantization effects associated with the nanoscale dimensions of the magnet [308, 311, 312]. In addition, magnetization modes, such as nucleation modes, exhibit a pronounced *real-structure* dependence [8, 308]. Figure 19 shows various types of spin-wave modes in nanowires. In very thin nanowires, where $R < R_{coh}$, curling-type modes can be ignored [38, 145] and the perpendicular magnetization components obey $M_x = M_s m(z)\cos(\omega t)$ and $M_y = M_s m(z)\sin(\omega t)$. The function $m(z)$ is given by

$$-2A\frac{\mathrm{d}^2 m}{\mathrm{d}z^2} + \left(2K_{eff}(z) + \mu_0 M_s H - \frac{\omega}{\gamma}\right)m = 0. \tag{5.7}$$

For $\omega = 0$, this equation reduces to (4.16), whereas $\mathrm{d}m/\mathrm{d}z = 0$ reproduces (5.6). Mathematically, (5.7) is a well-known random potential eigenvalue problem, which can be solved numerically or by transfer-matrix methods. Figures 17 and 19(f) show some examples.

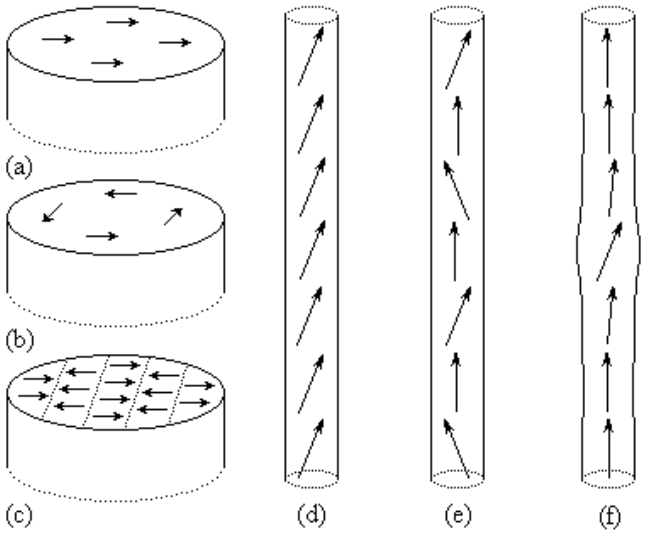

Figure 19. Spin-wave modes in nanowires: (a) and (d) coherent mode, (b) curling mode, (c) bulk mode with $k_\perp > 1/R$, (e) mode with $k\| > 0$ and (f) localized nucleation mode. The bulk modes are essentially superpositions of plane waves. Since the diameter of typical nanowires is much larger than the interatomic distance, there are many excited perpendicular modes and the finite-temperature magnetization $M_s(T)$ is reminiscent of bulk magnets.

An interesting point is that all modes are localized, as one can expect from the quantum-mechanical analogue of a one-dimensional electron gas in a random potential [279]. The localization length depends on ω and is largest for high frequencies. The real-space meaning of figure 17 is illustrated in figure 19(f)

As discussed, for example, in [204], the uniform FMR resonance mode (5.5) corresponds to the spatially uniform precession of magnetization, with a spin-wave (magnon) wavevector $k = 0$. In contrast, the modes predicted by (5.7) are generally *nonuniform*. To excite such a mode, the magnetic field must have a nonzero projection onto the mode, which is usually the case for modes of the type shown in figure 19(f). In traditional SWR, this projection is realized by surface anisotropies. Due to structural disorder, excitations of the type shown in figure 19(f) exhibit a resonance-line broadening, but this broadening is qualitatively different from the inhomogeneous linewidth broadening used, for example, to gauge the homogeneity of the applied magnetic field. The difference is the involvement of the exchange term, which is important due to the nanoscale nature of the problem [308].

Another aspect of spin waves in nanowires is their quantization. In the Bloch theory [303], each spin wave yields a magnetization reduction corresponding to the switching of a single spin, so that $M_s(T)$ is obtained by k-space integration over all excited spin waves. The finite radius of the wires, about 5 nm [38], leads to a radial spin wave quantization in terms of Bessel functions [308] and nonzero level spacings. This means that curling-type and higher-order excitations can be ignored at very low temperatures. In contrast, the large length of typical nanowires, about 1000 nm [38], means that spin waves travelling parallel to the wire form a quasi-continuum. Due to the finite wire radius, these waves occupy a comparatively large fraction of the spin-wave phase space, and even at low temperatures a large number of them are excited. The corresponding magnetization contribution scales as $M_0 - M_s(T) \sim (T/T_C)(\delta_{eff}/a)$, where a is the interatomic distance [308] and $\delta_{eff} = (A/K_{eff})^{1/2}$. For fictitious isotropic magnets, where $K_{eff} = 0$ and $\delta_{eff} = \infty$, the magnetization collapses, as

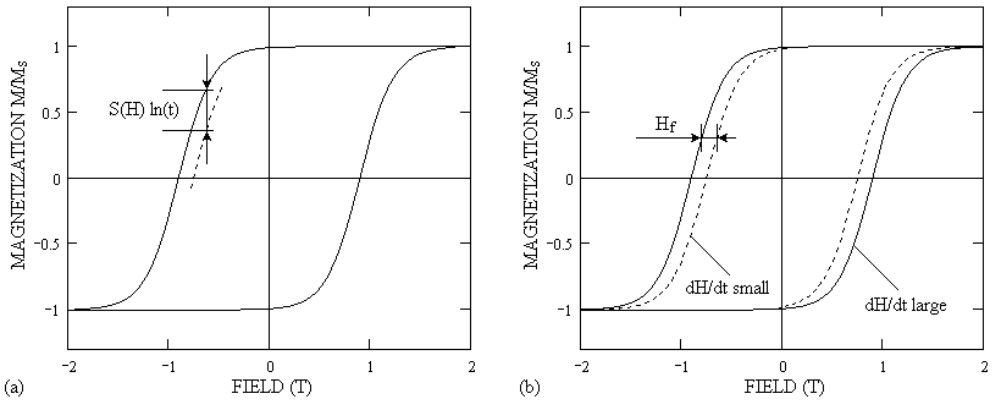

Figure 20. Dynamic hysteresis-loop effects: (a) magnetic viscosity and (b) sweep rate dependence.

expected from Bloch's original theory [303]. In fact, it can be shown that the wires do not exhibit true ferromagnetism but form correlated regions with macroscopically large correlation lengths scaling as $\exp(-4\pi K_{eff}\delta_w R^2/k_B T)$.

5.3. Magnetic viscosity and sweep rate dependence of coercivity

The temperature dependence of extrinsic properties reflects two mechanisms. First, the atomic-scale intrinsic temperature dependence of K_1, A and M_s translates into a static or 'intrinsic' temperature dependence of the free-energy barriers. Second, thermally activated jumps over metastable free-energy barriers yield a dynamic or 'extrinsic' contribution. Thermally activated jumps yield only small corrections, because typical energy barriers in ferromagnets are much larger than $k_B T$, but they affect the long-time stability of permanent magnets and recording media [32, 76, 313]. For a constant field, $\mathrm{d}H/\mathrm{d}t = 0$, the magnetization corrections are known as magnetic viscosity, whereas $\mathrm{d}H/\mathrm{d}t \neq 0$ yields a sweep rate dependence of the coercivity. Figure 20 illustrates the difference between sweep rate and magnetic viscosity experiments.

To describe magnetic viscosity it is convenient to consider generalized magnetization variables x, such as the domain-wall position in pinning-type magnets (figure 12) and the coherent-rotation angle θ of a fine particle. Another comparatively transparent case is two-particle magnets [284, 295, 314, 315]. In more complex systems, such as interacting particles and bulk magnets, x describes eigenmodes of the magnetization reversal [284, 316]. In general, the modes contain localization and cooperative effects (section 4.7) as well as the effect of magnetostatic self-interactions, which are important, for example, in thin films [317].

Using a two-level master equation and ignoring the typically very small probability of jumps *against* the external field, the equation of motion is $\tau \mathrm{d}x/\mathrm{d}t = x_0 - x$, where x_0 is the equilibrium value of x. The relaxation time is given by the Arrhenius (or Néel–Brown) law

$$\tau = \tau_0 \exp\left(\frac{E_a}{k_B T}\right) \tag{5.8}$$

where τ_0 is a microscopic attempt time of the order of 1 ns [11, 246, 292, 296, 301, 318]. In laboratory experiments, magnetization processes are often considered as frozen when $\tau \geqslant 100$ s. In addition to the leading energy dependence of τ, there is an effect due to the activation *entropy* [295]. Replacing E_a by $F_a = E_a - T S_a$ changes τ_0 to $\tau_0 \exp(-S_a/k_B)$. This means that a large activation entropy, corresponding to many available phase-space paths,

reduces the relaxation time. However, since $E_a \gg k_B T$, entropic contributions are often negligible.

For time-independent energy barriers, the equation of motion yields an exponential decay of the magnetization variable. Real-structure averaging over all relaxation times (5.8) leads to a logarithmic time dependence of the magnetization [8, 32, 246, 264, 318, 319]:

$$M(H,t) = M(H,t_0) - S\ln(t/t_0). \tag{5.9}$$

This is known as the logarithmic magnetic-viscosity law. It determines, for example, the stability of the information stored in magnetic and magneto-optical recording media [32] and yields small time-dependent magnetization corrections in permanent magnets [8]. For an ensemble of noninteracting particles, x can be interpreted as the magnetization $M = M_z$ of the individual particles, and the logarithmic law is obtained by averaging over

$$M(t) = -M_s + 2M_s \exp(-t/\tau). \tag{5.10}$$

Exploiting (5.8) and introducing an energy-barrier distribution $P(E_a)$ yields

$$M(t) = -M_s + 2M_s \int_{-\infty}^{\infty} P(E_a) \mathrm{e}^{-(t/\tau_0)\exp(-E_a/k_B T)}\,\mathrm{d}E_a. \tag{5.11}$$

Next we exploit that $\alpha\exp(\beta E) = \exp(\beta E + \ln\alpha)$ and $\exp(-\exp(-x/\varepsilon)) \approx \Theta(x)$, where $\varepsilon \ll 1$ and $\Theta(x)$ is the step function, defined by $\Theta(x<0)=0$ and $\Theta(x>0)=1$. The result of the calculation is (5.9) with the magnetic-viscosity constant

$$S = 2k_B T P(0) M_s. \tag{5.12}$$

The close relationship between the energy barrier distribution and the logarithmic magnetic-viscosity law has been known for many decades [246]. One explicit example is the assumption of a rectangular energy-barrier distribution of width W, where $P(0) = 1/W$ [246]. Note that (5.9) breaks down in the limits $t = 0$ and ∞; for some expressions with improved asymptotics see [192, 320, 321].

An important aspect of magnetic viscosity is its *field dependence*. For example, $S(H)$ tends to exhibit a maximum near the coercivity. To explain this finding one must consider the energy-barrier density P, the irreversible part χ_{irr} of the susceptibility and the field derivative of the energy barriers. Since $\mathrm{d}M/M_s = 2P\,\mathrm{d}E$, $\chi_{irr} = \partial M/\partial H$ and $\mathrm{d}E_a = (\partial E_a/\partial H)\,\mathrm{d}H$, the logarithmic law can also be written as [296]

$$M(t) = M(t_{ref}) - k_B T \frac{\chi_{irr}}{(\partial E_a/\partial H)} \ln(t/t_{ref}) \tag{5.13}$$

where t_{ref} is a reference time. This equation is frequently used to rationalize energy-barrier effects [32, 249, 264, 296]. A phenomenological energy-barrier expression is

$$E_a(H) = K_0 V_0 \left(1 - \frac{H}{H_0}\right)^m \tag{5.14}$$

where K_0, V_0 and m are micromagnetic parameters. V_0 is closely related to the switching or Barkhausen volumes of the magnet (see below). In some cases it is possible to derive (5.14) from the magnet's real structure. For example, aligned spherical Stoner–Wohlfarth particles are characterized by $K_0 = K_1$, $V_0 = 3\pi R^3/4$, $m = 2$ and $H_0 = 2K_1/\mu_0 M_s$. Note that typical anisotropy constants of 1 MJ m^{-3} and activation volumes of $10 \times 10 \times 10$ nm^3 correspond to a temperature equivalent of $K_0 V_0 \approx 100\,000$ K. This is the reason for the thermal stability of magnetization of most nanostructures.

Very small particles, where $K_0 V_0$ is comparable to $k_B T$, exhibit a rapid decay of the magnetization, which is known as *superparamagnetism* [14, 322, 323]. Defining

superparamagnetism by a waiting time of $\tau = 100$ s yields, with (5.8) and (5.14), the zero-field stability condition $K_0V_0/k_BT \geqslant 25$, where $K_0V_0/k_BT \equiv \xi$ is referred to as the stability parameter. Thermal stability for 10 y corresponds to $\xi = 40$.

Since $t = \tau$ is the time necessary to jump over the energy barrier, equation (5.8) can be used to estimate the coercivity. Writing it as

$$E_a(H_c) = k_BT \ln(\tau/\tau_0) \tag{5.15}$$

and substituting (5.14) yields [8, 32, 292, 295, 324]

$$H_c = H_0\left(1 - \left(\frac{k_BT}{K_0V_0}\ln(\tau/\tau_0)\right)^{1/m}\right). \tag{5.16}$$

Improving on (5.16) by a master-equation approach yields a relatively unimportant factor of $\ln 2 = 0.693$ [292], which is usually incorporated into τ_0. A characteristic feature of this equation is the involvement of a term $T^{1/m}$ in addition to the intrinsic temperature dependence $K_0(T)$.

Going beyond the waiting-time expression (5.15) and explicitly considering the effect of the sweep rate $\eta = \mathrm{d}H/\mathrm{d}t$ reveals that $\ln(\tau/\tau_0) \approx 25$ must be replaced by a complicated m-dependent expression smaller than $\ln(\tau/\tau_0)$ by about 20% [325]. The sweep rate dependence of the coercivity can be rationalized in terms of a *fluctuation field* H_f [252, 326], as illustrated in figure 20(b). The corresponding coercivity expression is

$$H_c(\eta) = H(\eta_{ref}) + H_f \ln(\eta/\eta_{ref}) \tag{5.17}$$

where η_{ref} is a reference sweep rate. In the case of nonlinear energy barriers, where $m \neq 1$, this equation can be derived, for example, by taking into account that $\eta \sim 1/\tau$ and linearizing (5.16) with respect to $\ln(\tau/\tau_{ref})$ [295].

Equation (5.14) shows that thermally activated magnetization processes involve a Barkhausen-type switching volume V_0. For noninteracting particles, this volume is equal to the particle or grain volume, but cooperative and localization effects tend to increase and decrease the volume, respectively [32, 283, 284]. Experimentally, the switching volume manifests itself as an *activation volume* V^*. Both sweep rate and magnetic-viscosity measurements can be used to determine the activation volume. Assuming a linear law ($m = 1$) of the type $E_a(H) = \mu_0M_sV^*(H_0 - H_c)$ and using experimental fluctuation fields determined using (5.17) yields $V^* = k_BT/\mu_0M_sH_f$. A method to derive V^* is to exploit the relation $\mu_0M_sV^* = -\partial E_a/\partial H$ [32, 296, 327–329], where the derivative is taken at coercivity. For arbitrary m, this yields a $T^{1/m}$ temperature dependence of the activation volume [8, 283, 295]. In the case of magnetic-viscosity measurements, equation (5.13) yields $V^* = k_BT\chi_{irr}/M_sS$ [32, 249, 296, 327, 329]. Typical orders of magnitude of room-temperature activation volumes are 500 nm^3 in permanent magnets [249] and 2000 nm^3 in transition-metal nanowires [283], but the extrinsic character of V^* leads to a strong real-structure dependence.

The question remains how the energy barriers (5.14) relate to the real structure of the magnet. A simple approach, based on ideas developed in catastrophe theory [330], is to use an expansion of the micromagnetic energy. Including linear, quadratic and cubic terms, the energy can be written as

$$E(x) = a_0 + a_1x + \frac{a_1}{2}x^2 + \frac{a_3}{3}x^3 - b_0Hx. \tag{5.18}$$

Here x is the generalized magnetization variable of the reversal mode. The phenomenological parameters a_0, a_1, a_2, a_3 and b_0 describe the real structure of the magnet; they depend on $K_1(\boldsymbol{r}, T)$, $A(\boldsymbol{r}, T)$ and $M_s(\boldsymbol{r}, T)$ and must be determined separately.

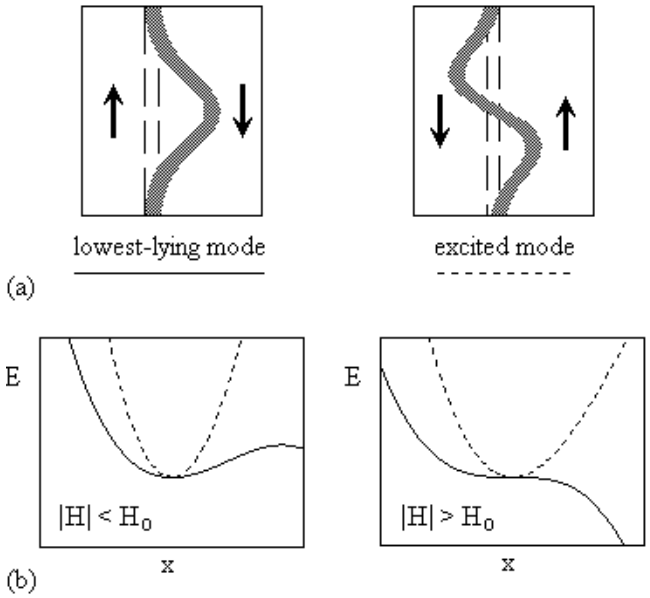

Figure 21. Multidimensionality of the coercivity problem: only the trajectory corresponding to the lowest-lying mode contributes to the switching.

Figure 21 illustrates the meaning of (5.17) for two exemplary normal modes and elucidates their role in magnetization reversal. For reverse fields $|H| < H_0$, the energy exhibits one maximum and one metastable minimum, both obeying $\partial E/\partial x = 0$. The static switching field H_0 corresponds to the vanishing of the metastable minimum when $\partial E/\partial x = 0$ and $\partial^2 E/\partial x^2 = 0$. Using these relations and (5.18) yields, after a short calculation, an equation of the type (5.14) with $m = 3/2$. This exponent, first derived by Néel [331], is quite common and describes a variety of coherent and incoherent magnetization processes. Examples are strong domain-wall pinning, misaligned Stoner–Wohlfarth particles and nucleation in polycrystalline nanowires [8, 264, 283, 295, 316, 319, 326]. An exponent $m = 2$ is obtained for energy landscapes where $a_3 = 0$ by symmetry. It is then necessary to include fourth-order terms and the power-law exponent changes to $m = 2$. A typical example is the Stoner–Wohlfarth expression (4.8), whose expansion does not contain odd-order terms. Experimental values of m tend to vary between 1.5 and 2 [283, 318].

Linear laws, where $m = 1$, are often used as simple phenomenological models but have no sound physical basis [8, 325, 326, 332]. Nonanalytic energy landscapes $E(x)$ could, in principle, establish a linear law [319, 326], but so far it has not been possible to derive it from realistic energy landscapes [147, 325, 326, 332]. Sharp interfaces and other atomic-scale imperfections [243] can be considered as nonanalytic features, but atomic-scale structural features are convoluted with the domain-wall profile, as exemplified by (4.13). A good example is the pinning of a domain wall by a small 'needle-shaped' $\delta(x)$ anisotropy inhomogeneity, where the smooth domain-wall fine structure destroys the nonanalyticity of the energy landscape and re-establishes $m = 3/2$. Other approaches to derive $m = 1$ start from unrealistic [333, 334] or ill-defined [335] energy landscapes.

It is important to note that thermally activated switching processes involve paths close to the lowest-lying reversal mode [8, 38, 192, 246, 316]. In figure 21(b), this mode is drawn as a full curve. Other reversal modes are not forbidden by the Boltzmann term $\exp(-E_a/k_BT)$,

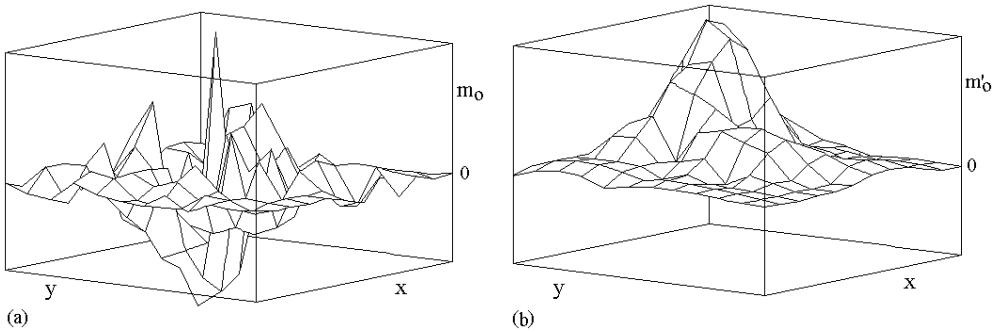

Figure 22. High-temperature modes in spin glasses: (a) original magnetization $m = M_z/M_s$ and (b) gauge-transformed mode m'.

but they are extremely unlikely because they involve unreasonably large energy differences $E_a \gg k_B T$. One example is the broken curve in figure 21(b). As a consequence, 'giant fluctuations' associated with arbitrary energy barriers can safely be ignored [8, 38, 192]. In particular, modes with higher nucleation fields, such as those proposed in [336], are irrelevant to the problem of ferromagnetic hysteresis [192]. Simplifying somewhat, the reverse magnetic field $\boldsymbol{H} = -H\boldsymbol{e}_z$ field pushes the magnet close to the vanishing of the metastable local energy minimum and reduces the energy barrier until thermally activated jumps become effective.

5.4. Freezing behaviour

Magnetic hysteresis is a nonequilibrium phenomenon related to glass-like freezing. Well-known examples of magnetic freezing processes are the superparamagnetic freezing of small particles and ferrofluids [15, 72, 163] and spin glasses [13, 151, 160]. The magnetization dynamics of ferrofluids is characterized by the distinction between Brownian and Néel relaxations. Brownian relaxation refers to the mechanical rotation of the particles in a magnetic field, whereas Néel relaxation involves jumps over magnetic energy barriers (section 5.3); the latter dominates in small nanoparticles.

In spin glasses, random interatomic exchange yields very complicated ground-state configurations, but since coercivity is a nonequilibrium problem, the spin-glass character of the ground state is of little consequence to the coercivity [164]. To assimilate the spin-glass problem to the problem of the magnetism of disordered ferromagnets, one can use a Mattis-type gauge transformation of the spin-glass Hamiltonian $-\Sigma_{ik} J_{ik} s_i s_k$. Introducing gauge-transformed spins $s_i' = \tau_i s_i$, where $\tau_i = \pm 1$ [161], it is straightforward to make the majority of all bonds ferromagnetic, $\langle J_{ik}' \rangle = \langle \tau_i J_{ik} \tau_k \rangle > 0$, although the remaining nonferromagnetic bonds give rise to some frustration [337]. Approaching the spin-glass freezing from high temperatures, the problem can be solved by diagonalizing the interaction matrix. Figures 22(a) and (b) show the corresponding excited modes $m_i = \langle s_i \rangle$ and $\langle s_i' \rangle$, respectively, for a two-dimensional Ising spin glass. In general, the modes are localized, but on further cooling less localized modes freeze and the modes start to interact in a complicated way reminiscent of what is known as Griffiths singularities [338] and spin-glass droplets [339].

The appearance of 'frozen' modes below $T_0 = J_0/k_B T$, where J_0 is the largest eigenvalue of J_{ik} (or, alternatively, J_{ik}') affects the dynamics of the system. From figure 22(b) we see that the modes can be considered as quasi-ferromagnetic regions containing N spins. In ideal ferromagnets, $N = \infty$ below $T_C \approx T_0$ corresponds to nonergodic behaviour [151]. In spin

glasses, $N(T)$ remains finite on crossing T_0, but due to the involvement of a finite number N of spins there are cooperative blocking effects. For simplicity, let us consider N coupled spins characterized by one rotational degree of freedom ϕ_i per spin ($i = 1 \ldots N$). The dynamics of the system is then described by the Langevin equation

$$\frac{\partial \phi_i}{\partial t} = -\frac{\Gamma_0}{k_B T}\frac{\partial E_{tot}}{\partial \phi_i} + \sqrt{2\Gamma_0}\,\xi_i(t). \tag{5.19}$$

In this set of N equations, $\Gamma_0 = 1/\tau_0$ is a microscopic attempt frequency and $\xi_i(t)$ is a delta-correlated random force obeying $\langle \xi_i(t) \rangle = 0$ and $\langle \xi_i(t)\xi_j(t') \rangle = \delta_{ij}\delta(t - t')$. The total energy E_{tot} contains both on-site anisotropy and interactions J_{ij}. In general, the interactions lead to very complicated scenarios, but there are two exceptions. In the absence of interactions, $J_{ij} = 0$, the spins are independent and (5.19) can be replaced by

$$\frac{\partial \phi}{\partial t} = -\frac{\Gamma_0}{k_B T}\frac{\partial E}{\partial \phi} + \sqrt{2\Gamma_0}\,\xi(t) \tag{5.20}$$

where $E(\phi)$ is the single-spin energy. In the limit of strong ferromagnetic exchange interactions, all spins are parallel and therefore $\phi_i = \phi$. Adding all contributions $\partial\phi_i/\partial t$ in (5.19) yields

$$N\frac{\partial \phi}{\partial t} = -N\frac{\Gamma_0}{k_B T}\frac{\partial E}{\partial \phi} + \sqrt{2\Gamma_0 N}\,\xi(t). \tag{5.21}$$

In this equation, N enters the random-force term in a square-root form, because $\Sigma_i \Sigma_j \langle \xi_i(t)\xi_j(t') \rangle = N\delta(t - t')$. Physically, the thermal forces acting on the coupled spin system average to zero, except for a comparatively small fluctuation contribution. Equation (5.21) can be derived from (5.20) using the substitutions $\Gamma_0 \to \Gamma_0/N$ and $E \to EN$. In other words, exchange coupling enhances the energy barriers and reduces the attempt frequency. Both effects lead to reduction of the relaxation rate.

Since the number of coupled spins strongly increases with decreasing temperature (from a very few spins above T_0 to many spins below T_0), the slowing down of the relaxation is very pronounced. As analysed for the one-dimensional case, the temperature dependence of the relaxation rate is stronger than exponential, reminiscent of the Vogel–Fulcher–Tamman (VFT) law $\Gamma = \Gamma_0 \exp(-E_a/k_B(T - T_g))$ [337]. The energy barrier appearing in the present theory is proportional to the anisotropy constant $0 < K < \infty$. By contrast, typically considered Heisenberg and Ising spin glasses correspond to the rather unrealistic limits $K = 0$ and ∞, ignoring and misinterpreting the roles of the anisotropy, respectively. Note, finally, that the present theory does not require order parameters quadratic [151, 160] in the magnetization. This shows that spin glasses can essentially be considered as partially frustrated ferromagnets, although the ground state is not necessarily ordered.

5.5. Conduction phenomena and spin electronics

The mean free path of conduction electrons is often of the order of a few or several nanometres, so that magnetic nanostructures are of interest as magnetic sensors and in spin electronics [28, 29, 40, 41, 51, 114, 282, 340]. In sensors, various magnetoresistive effects are exploited. Anisotropic magnetoresistance (AMR) reflects the distortion of electron clouds due to spin–orbit coupling, similar to that illustrated in figure 7. Giant magnetoresistance (GMR) is caused by nanoscale magnetization inhomogeneities $\nabla \cdot \boldsymbol{M}$ (section 4.5) and observed in multilayers (spin valves), granular materials and nanowires [28, 29, 40, 51, 142, 143, 282]. Similar magnetization inhomogeneities occur in magnetic nanojunctions (tunnel junctions and contact junctions) [43, 51, 116, 341, 342]. In multilayers, the spin structure is determined

by RKKY-type interactions through nonmagnetic metallic layers [48, 50]. From section 4.5, especially from figures 15 and 16, we see that only a part of the magnetization gradient is realized in the boundary or junction region. This puts an upper limit to the scattering ability. For example, an interface with zero thickness has the same spin structure as a bulk magnet and a quite low domain-wall scattering.

A class of sensor materials with particularly interesting and versatile properties is transition-metal oxides. Powder magnetoresistance (PMR) is an interface effect (section 4.5) observed, for example, in compacted CrO_2 particles [52], whereas colossal magnetoresistance (CMR) exploits temperature-dependent electronic-structure changes realized in nanoscale regions [41, 53–55]. A variety of oxides, such as CrO_2 and $(La_{0.7}Sr_{0.3})MnO_3$, and some intermetallics, such as the semi-Heusler alloy NiMnSb, are half-metallic ferromagnets, that is, the density of states at the Fermi level is zero for one spin channel [40, 41, 269]. Ideally, this amounts to an infinite magnetoresistance ratio, but in reality this ratio is greatly reduced by mechanisms such as finite-temperature spin mixing in the bulk, probably reflecting magnon–phonon coupling [340], and at nanojunctions [342].

Phenomena of interest in the field of magnetoresistive sensors are exchange biasing unidirectional anisotropy. The field has its origin in the discovery of exchange-biased hysteresis by Meiklejohn and Bean [343], who investigated Co nanoparticles surrounded by CoO. By definition, there are only even-order anisotropy terms, but unidirectional anisotropies—which are observed as an asymmetry (shift) of the hysteresis loop, as in figure 9(d)—may occur due to antiferromagnetic phases, such as NiO and CoO, relativistic Moriya–Dzialoshinskii interactions [13, 151] and particular micromagnetic regimes [344]. Recently, exchange biasing has attracted much attention in magnetic recording and thin-film technology, because it can be used to tune the behaviour of magnetic recording heads [345–350]. These phenomena are also known as exchange anisotropy, but it should be kept in mind that exchange is essentially an isotropic phenomenon: like ordinary magnetocrystalline anisotropy, anisotropic exchange is a small correction caused by spin–orbit coupling.

6. Summary and conclusions

In this review, we have discussed the properties of a broad range of magnetic nanostructures. Varying size, geometry and chemical composition of the structures makes it possible to realize properties not achievable in single-phase bulk and thin-film materials. Some examples are the energy-product enhancement in suitably nanostructured two-phase magnets, where adding a soft magnetic phase improves the hard magnetic performance, multilayered and granular spin-value structures, nanostructured soft magnets, and advanced magnetic-recording media. Due to the very limited range of naturally occurring compounds, the importance of nanostructures in technology and materials science is likely to increase in the future, and many research groups are or will be involved in this development.

From a scientific point of view, the magnetism of nanostructures is intermediate between atomic-scale magnetism and macroscopic magnetism. Both intrinsic properties, such as magnetization and anisotropy, and extrinsic properties, such as coercivity and energy product, are affected by nanostructuring, but the length scale on which this happens depends on the phenomenon considered. Intrinsic properties, such as spontaneous magnetization, Curie temperature and magnetocrystalline anisotropy, reflect comparatively strong quantum-mechanical and spin–orbit interactions. They are realized on atomic length scales and therefore well defined for nanostructures. Extrinsic properties, such as coercivity, involve rather weak but long-range magnetostatic interactions. They are realized on larger length scales and exhibit pronounced real-structure dependence. The competition of the energy contributions is

realized on a scale of the order of $a_0/\alpha = 7.52$ nm and it is therefore not possible to reduce nanomagnetism to atomic phenomena, nor can one consider nanoscale phenomena as a special case of macroscopic magnetism.

The atomic-scale origin of intrinsic properties does not mean that surface and finite-size effects are unimportant. A particularly subtle property is the Curie temperature, which describes the onset of ferromagnetism and involves long-range thermodynamic fluctuations. In a strict sense, the Curie temperature of finite bodies is zero, but the nonequilibrium character of practically encountered magnetic phenomena and the low energy differences associated with long-range thermodynamic fluctuations mean that particles or grains larger than about 1 nm are quasi-indistinguishable from true ferromagnets. For this reason, nanostructuring cannot be used for nanoscale Curie temperature improvements.

An important micromagnetic aspect of nanostructures is that structural length scales and those of spatial magnetization changes are generally different. Only in very small and noninteracting particles, where the Stoner–Wohlfarth theory applies, can the two length scales agree. General magnetization modes may be localized (confined to a small region of the structural unit) or cooperative (involving several structural units). An example of localization is the nucleation of reverse domains in nearly perfect ellipsoids of revolution, whereas cooperative behaviour is encountered, for example, in random anisotropy magnets of interest in soft magnetism. Localization and cooperativity are caused by structural imperfections and magnetic interactions, respectively, and the localization length is determined by the competition between interactions and disorder. A lower bound, realized in strongly inhomogeneous magnets with high anisotropy, is about 5 nm. The concept of localization equally well applies to excited magnetization modes (spin waves). For infinite wires, the analogy to the Anderson localization in less than two dimensions means that not only the nucleation mode but also all excited modes are localized.

While considering extrinsic properties it important to distinguish between equilibrium and nonequilibrium properties. The equilibrium behaviour of magnetic nanostructures, as epitomized by the critical single-domain radius, is of little relevance when hysteretic effects are important. For example, in highly anisotropic rare-earth transition-metal permanent magnets, the critical single-domain size is of the order of 1 μm, but this does not mean that the reversal in a particle having a diameter of 500 nm is Stoner–Wohlfarth-like. In fact, nature finds its way by exploiting minor imperfections, realizing reversal by nucleation on a length scale closer to the above-mentioned 5 nm. In fact, even in *perfect* particles of this size the reversal is realized by curling rather than by coherent rotation.

From a structural point of view, surfaces, interfaces and bottlenecks (contact junctions) have a strong impact on nanomagnetism. One issue is that exchange at grain boundaries affects the coupling between nanograins and, indirectly, the extrinsic properties of the structures. In the case of misaligned grains, or of grains subjected to external forces of different directions, reduced grain-boundary exchange leads to a quasi-discontinuity of the magnetization. In contrast, anisotropy changes in the grain-boundary region have no major effect on the spin structure, because the effect of anisotropy inhomogeneities averages over at least a few nanometres. Only a part of the magnetization gradient is realized in the grain-boundary region or at the junction, which puts an upper limit to the usable spin-dependent scattering ability.

A particularly interesting dynamic aspect of magnetic nanostructures is the effect of finite-temperature excitations. Intrinsic properties correspond to a very fast equilibrium, whereas the equilibration times of extrinsic properties cover a broad range, from about one nanosecond in soft magnetic resonance experiments to millions of years in magnetic rocks. In a sense, nanomagnetic equilibration times are intermediate between atomic-scale equilibration times and equilibration times of perfect bulk magnets, and widely encountered 'bulk' phenomena

such as magnetic viscosity have their origin in nanoscale real-structure features. The underlying mechanism is thermally activated jumps over nanomagnetic energy barriers. To some extent, the dynamic behaviour depends on whether sweep rate or magnetic-viscosity experiments are performed, but the Boltzmann factor determining the timescale of extrinsic dynamics is essentially given by the involved (free) activation energy. This results in small magnetic-viscosity corrections to the leading intrinsic contribution. In terms of the external magnetic field, the energy barriers obey a power law with a symmetry-dependent exponent of $3/2$ or 2. Since the phase-space trajectories responsible for thermally activated magnetization reversal are very close to static trajectories, 'giant' thermodynamic fluctuations involving arbitrary modes can safely be ignored. Similar counterarguments apply to power laws with other exponents, including linear laws.

In conclusion, magnetic nanostructures exhibit various scientifically interesting and technologically important deviations from bulk and thin-film magnets. The search for materials with improved intrinsic properties continues to be of scientific and technological interest, but a main thrust of research is the creation, understanding and exploitation of artificial nanostructures. This materials-by-design strategy makes it possible to produce materials and functional components not found in nature. An end to the search for new geometries and microchemistries is not yet in sight, and fully realizing the range of magnetic nanostructures and their potential for exploring new applications remains a challenge for future research. The technological progress is accompanied and stimulated by an ever-improving understanding of the magnetic properties of nanostructures. For example, we now understand the crucial effect of imperfections, which largely determine the hysteresis loop and the real-space realization of magnetization processes. In addition to model calculations, full-scale simulations of real structures are now on the horizon, and sophisticated experimental investigation and processing techniques will ensure far-reaching qualitative and quantitative developments. In one sentence, the future of the science and technology of magnetic nanostructures looks promising.

Acknowledgments

This work has benefited from discussions with P A Dowben, A Kashyap, R D Kirby, D Leslie-Pelecky, S-H Liou, J-P Liu, K Sorge, Y C Sui, M L Yan and D J Sellmyer. Thanks are due to V Skomski for help during the preparation of the manuscript, and the support of this research by AFOSR, DARPA/ARO, DOE, ONR, NSF MRSEC, the Keck Foundation and CMRA is gratefully acknowledged.

Appendix. Magnetic materials

Traditionally, magnetic materials are classified by their magnetic coercivity or hardness. The term is historical and refers to iron, where the addition of carbon increases not only the mechanical hardness (steel) but also the coercivity. In descending order, the hardness gives rise to a classification into hard magnets (permanent magnets), recording media and soft magnets. Tables A.1–A.4 show typical intrinsic and extrinsic parameters compiled from different sources [8, 89, 165, 206].

A.1. Permanent magnets

These have a wide range of applications, for example in electromotors, loudspeakers, windshield wipers, locks, microphones and hard-disk drives, and as toys and refrigerator magnets [8, 206]. Until the first half of the 20th century, most permanent magnets were made from steel. Steel magnets are now obsolete, because their low coercivities and energy

Table A.1. Intrinsic properties of some rare-earth free alloys and oxides. M_s and K_1 are room-temperature values.

Substance	$\mu_0 M_s$ (T)	T_C (K)	K_1 (MJ m^{-3})		Structure
Fe	2.15	1043	0.048	Cubic	bcc
Co	1.76	1388	0.53	Hex.	hcp
Ni	0.62	631	−0.0048	Cubic	fcc
PtCo	1.00	840	4.9	Tetr.	CuAu (I)
PtFe	1.43	750	6.6	Tetr.	CuAu (I)
PdFe	1.37	760	1.8	Tetr.	CuAu (I)
MnAl	0.62	650	1.7	Tetr.	CuAu (I)
MnBi	0.78	630	1.2	Hex.	NiAs
Fe_3O_4	0.60	858	−0.011	Cubic	$MgAl_2O_4$
$MnFe_2O_4$	0.52	573	−0.0028	Cubic	$MgAl_2O_4$
$CoFe_2O_4$	0.50	793	0.270	Cubic	$MgAl_2O_4$
$NiFe_2O_4$	0.34	858	−0.0069	Cubic	$MgAl_2O_4$
$CuFe_2O_4$	0.17	728	−0.0060	Cubic	$MgAl_2O_4$
$MgFe_2O_4$	0.14	713	−0.0039	Cubic	$MgAl_2O_4$
$BaFe_{12}O_{19}$	0.48	723	0.330	Hex.	M ferrite
$SrFe_{12}O_{19}$	0.46	733	0.35	Hex.	M ferrite
$PbFe_{12}O_{19}$	0.40	724	0.22	Hex.	M ferrite
$BaZnFe_{17}O_{27}$	0.48	703	0.021	Hex.	W ferrite
CrO_2	0.56	390	0.025	Tetr.	TiO_2
$NiMnO_3$	0.13	437	−0.26	Hex.	$FeTiO_3$
γ-Fe_2O_3	0.47	863	−0.0046	Cubic	disordered spinel

products made it necessary to resort to cumbersome horseshoe shapes, but the high saturation magnetization of $Fe_{65}Co_{35}$ (2.43 T) and its pronounced temperature stability continue to be exploited in alnico-type magnets. The moderate coercivity of those magnets originates from the shape anisotropy of elongated $Fe_{65}Co_{35}$ particles embedded in a Ni–Al matrix. Magnetocrystalline anisotropy is also exploited in hexagonal ferrites such as $BaFe_{12}O_{19}$, which are widely used to produce cheap ceramic magnets with coercivities of up to about 0.3 T (3 kOe), and in tetragonal $L1_0$ magnets such as PtCo. However, most high performance magnets are now made from rare-earth transition-metal intermetallics such as $Nd_2Fe_{14}B$ [229–231, 351] and $SmCo_5$ [26], where the rare-earth sublattice provides sufficient anisotropy to realize broad hysteresis loops with coercivities of the order of 1 T (0.8 MA m^{-1}). These magnets consist of 3d atoms, ensuring a high magnetization and a high Curie temperature, and rare-earth atoms, ensuring a high uniaxial anisotropy.

A.2. Magnetic recording media

These are used in computer and audio-visual technology, for example in magnetic tapes and for data storage in hard disk drives [32, 33, 35, 352]. Semihard materials used in storage media exhibit rectangular hysteresis loops having coercivities of the order of 0.1 T (80 kA m^{-1}). The moderate coercivity and the rectangular loop shape ensure the stability of the stored information without requiring bulky writing facilities. Traditional storage media are made using materials such as granular Fe_2O_3 and CrO_2. Advanced high-density recording media, characterized by more than 10 Gb in^{-2}(1.55 Gb cm^{-2}), are based on materials such as Co–Cr–Pt–B, where the Pt improves the anisotropy. Other classes of materials, such as rare-earth transition-metal nanocomposite films [39, 352], are also being considered. Some limitations in magnetic recording are the present use of longitudinal or in-plane recording media, with spin configurations similar to figure 10(f), and thermal instabilities at ultrahigh

Table A.2. Intrinsic properties of some magnetic materials containing rare earths or yttrium. M_s and K_1 are room-temperature values.

Substance	$\mu_0 M_s$ (T)	T_C (K)	K_1 (MJ m^{-3})	Structure	
$NdCo_5$	1.23	910	0.7	Hex.	$CaCu_5$
$SmCo_5$	1.07	1003	17.0	Hex.	$CaCu_5$
YCo_5	1.06	987	5.2	Hex.	$CaCu_5$
$Pr_2Fe_{14}B$	1.41	565	5.6	Tetr.	$Nd_2Fe_{14}B$
$Nd_2Fe_{14}B$	1.61	585	5.0	Tetr.	$Nd_2Fe_{14}B$
$Sm_2Fe_{14}B$	1.49	618	−12.0	Tetr.	$Nd_2Fe_{14}B$
$Dy_2Fe_{14}B$	0.67	593	4.5	Tetr.	$Nd_2Fe_{14}B$
$Er_2Fe_{14}B$	0.95	557	−0.03	Tetr.	$Nd_2Fe_{14}B$
$Y_2Fe_{14}B$	1.36	571	1.06	Tetr.	$Nd_2Fe_{14}B$
$Sm(Fe_{11}Ti)$	1.14	584	4.9	Tetr.	$ThMn_{12}$
$Y(Fe_{11}Ti)$	1.12	524	0.89	Tetr.	$ThMn_{12}$
$Y(Co_{11}Ti)$	0.93	940	−0.47	Tetr.	$ThMn_{12}$
Nd_2Co_{17}	1.39	1150	−1.1	Rhomb.	Th_2Zn_{17}
Sm_2Co_{17}	1.20	1190	3.3	Rhomb.	Th_2Zn_{17}
Dy_2Co_{17}	0.68	1152	−2.6	Rhomb. or hex.	
Er_2Co_{17}	0.91	1186	0.72	hex.	Th_2Ni_{17}
Y_2Co_{17}	1.25	1167	−0.34	Rhomb. or hex.	
Sm_2Fe_{17}	1.17	389	−0.8	Rhomb.	Th_2Zn_{17}
$Sm_2Fe_{17}N_3$	1.54	749	8.9	Rhomb.	Th_2Zn_{17}
Y_2Fe_{17}	0.84	320	−0.4	Hex.	Th_2Ni_{17}
$Y_2Fe_{17}N_3$	1.46	694	−1.1	Hex.	Th_2Ni_{17}
$Y_3Fe_5O_{12}$	0.16	560	−0.00067	Cubic	(garnet)
$Sm_3Fe_5O_{12}$	0.17	578	−0.0025	Cubic	(garnet)
$Dy_3Fe_5O_{12}$	0.05	563	−0.0005	Cubic	(garnet)

Table A.3. Micromagnetic parameters at room temperature. (The values for Fe and Ni are uniaxial estimates.)

Material	$\mu_0 M_s$ (T)	A (pJ m^{-1})	K_1 (MJ m^{-3})	δ (nm)	γ (mJ m^{-2})	l_{ex} (nm)	κ	R_{sd} (nm)	H_a (T)
Fe	2.15	8.3	0.05	40	2.6	1.5	0.12	6	0.06
Co	1.76	10.3	0.53	14	9.3	2.0	0.46	34	0.76
Ni	0.61	3.4	−0.005	82	0.5	3.4	0.13	16	0.03
$BaFe_{12}O_{19}$	0.47	6.1	0.33	14	5.7	5.9	1.37	290	1.8
$SmCo_5$	1.07	22.0	17	3.6	77	4.9	4.35	764	40
$Nd_2Fe_{14}B$	1.61	7.7	4.9	3.9	25	1.9	1.54	107	7.6

Table A.4. Extrinsic properties of some typical magnets.

Material	$\mu_0 M_r$ (T)	$\mu_0 Hc$ (T)	$(BH)_{max}$ (kJ m^{-3})
Cobalt steel (hard magnetic)	1.0	0.025	8
Annealed iron (soft magnetic)	1.0	0.0001	0.04
Sintered hexagonal ferrite	0.39	0.30	28
Anisotropic alnico	1.30	0.07	50
Metal-bonded $SmCo_5$	0.92	1.88	175
Polymer-bonded $SmCo_5$	0.58	1.00	60
Sintered $Sm_2Co_{17}/SmCo_5$	1.08	1.0	225
Sintered Nd–Fe–B	1.33	1.6	400
Polymer-bonded Nd–Fe–B	0.55	0.75	48

recording densities (up to about 100 Gb in^{-2}). These problems can be tackled by suitable nanostructuring, using perpendicular recording [37] and highly anisotropic media [35] to avoid thermal demagnetization.

A related field is *magneto-optical* recording using thin-film materials such as amorphous $Tb_{22}Fe_{66}Co_{12}$ [33]. The materials are ferrimagnetic, with nearly equal transition-metal and rare-earth sublattice magnetizations M_R and M_T, respectively. The materials' magnetoelastic anisotropy is comparatively small, but due to $H_c \approx 2K_1/\mu_0 M_s$ the nearly compensated magnetization, $M_s = |M_R - M_T| \approx 0$, ensures a sufficiently high coercivity. Note that the low net magnetization has no negative impact on the magneto-optical reading of the information, because the two sublattices have different Kerr-response characteristics. The magnetic and magneto-optical properties of the films can be tuned by choosing suitable rare-earth and transition-metal stoichiometries, and the information can be stored by thermomagnetic and Curie temperature writing involving T_k and T_C, respectively [33, 353].

A.3. Soft magnetic materials

These are widely used for flux guidance in permanent-magnet and other systems, in transformer cores, for high-frequency and microwave applications, and in recording heads. Typical requirements are a low coercivity, a high initial permeability $\mathrm{d}M/\mathrm{d}H$ and low high-frequency losses [89, 159, 354]. Iron-based metallic magnets have long been used as soft magnetic materials. Examples are pure iron, Fe–Si $Fe_{50}Co_{50}$ and permalloy ($Ni_{80}Fe_{20}$). For example, permalloy has an anisotropy of about 0.15 kJ m^{-3}, an anisotropy field of about 0.4 mT and a typical coercivity of about 0.04 mT 0.4 Oe. More recently, amorphous and nanostructured metals have attracted much attention as soft magnetic materials. Essentially, they have the composition $T_{100-x}Z_x$(T = Fe, Co, Ni and Z = B, C, P, Zr, ...) where $x \approx 10$–20. Oxides, such as simple ferrites (TFe_2O_4, where T = Mn, Fe, Ni, Zn), and garnets ($R_3Fe_5O_{12}$, R = Y, Gd, ...) have a ferrimagnetic spin structure and, therefore, a rather low magnetization. However, their comparatively large resistivity suppresses eddy-current losses and makes them suitable for high-frequency applications, for example in antennas and microwave devices [33, 89].

Another important application of soft materials is inductive and magnetoresistive recording heads [33]. The function of inductive head materials is to realize flux closure for reading and writing on recording media. Typical materials are $Ni_{80}Fe_{20}$ (permalloy, $H_c = 0.01$–0.05 mT), hot-pressed Ni–Zn and Mn–Zn ferrites ($H_c = 0.02$ mT); Fe–Si–Al (sendust, $H_c = 0.025$ mT), as well as Fe–Ti–N and Fe–Rh–N alloys [33]. Magnetoresistive read heads exploit the AMR due to the spin-dependent scattering of conduction electrons by magnetic atoms or, more recently, the GMR effect exploiting the different Fermi-level spin-up and spin densities of the involved components. Almost all metallic ferromagnets exhibit GMR, but soft magnetic materials—such as permalloy—are easier to switch.

Tables A.1–A.3 show the magnetic moment m, the spontaneous magnetization M_s, the Curie temperature T_C and first uniaxial anisotropy constant K_1 for some magnetic materials [8, 354]. Not included are antiferromagnets, such as NiO, $GdFeO_3$ and Ti_2O_3. The metastable compound γ-Fe_2O_3 has a moment of 2.5 μ_B per formula unit and a Curie temperature of 950 K, but above about 400 °C it transforms into α-Fe_2O_3 [89].

References

[1] Heisenberg W 1928 *Z. Phys.* **49** 619
[2] Bloch F 1929 *Z. Phys.* **57** 545
[3] Slater J C 1936 *Phys. Rev.* **49** 537
[4] Stoner E C 1938 *Proc. R. Soc.* A **165** 372

[5] Bethe H 1929 *Ann. Phys., Lpz.* **3** 133
[6] Bloch F and Gentile G 1931 *Z. Phys.* **70** 395
[7] Brooks H 1940 *Phys. Rev.* **58** 909
[8] Skomski R and Coey J M D 1999 *Permanent Magnetism* (Bristol: Institute of Physics Publishing)
[9] Craik D 1995 *Magnetism: Principles and Applications* (New York: Wiley)
[10] Dunlop D J 1990 *Rep. Prog. Phys.* **53** 707
[11] Néel L 1949 *Ann. Géophys.* **5** 99
[12] Aitken M J 1999 *Rep. Prog. Phys.* **62** 1333
[13] Moorjani K and Coey J M D 1984 *Magnetic Glasses* (Amsterdam: Elsevier)
[14] Bean C P and Livingston J D 1959 *J. Appl. Phys.* **30** 120S
[15] Charles S W 1992 *Studies of Magnetic Properties of Fine Particles and their Relevance to Materials Science* ed J L Dormann and D Fiorani (Amsterdam: Elsevier) p 267
[16] Coey J M D, Venkatesan M, Fitzgerald C B, Douvalis A P and Sanders I S 2002 *Nature* **420** 156
[17] Coehoorn R, de Mooij D B, Duchateau J P W B and Buschow K H J 1988 *J. Physique Coll.* **49** C8 669
[18] Kneller E F and Hawig R 1991 *IEEE Trans. Magn.* **27** 3588
[19] Skomski R and Coey J M D 1993 *Phys. Rev.* B **48** 15812
[20] Al-Omari I A and Sellmyer D J 1995 *Phys. Rev.* B **52** 3441
[21] Liu J P, Luo C P, Liu Y and Sellmyer D J 1998 *Appl. Phys. Lett.* **72** 483
[22] Fullerton E E, Jiang J S, Sowers C H, Pearson J E and Bader S D 1998 *Appl. Phys. Lett.* **72** 380
[23] Yoshizawa Y, Oguma S and Yamauchi K 1988 *J. Appl. Phys.* **64** 6044
[24] Herzer G 1992 *J. Magn. Magn. Mater.* **112** 258
[25] Herzer G 1995 *Scr. Metall.* **33** 1741
[26] Kumar K 1988 *J. Appl. Phys.* **63** R13
[27] Zeng H, Li J, Liu J P, Wang Zh L and Sun Sh-H 2002 *Nature* **420** 395
[28] Berkowitz A E, Mitchell J R, Carey M J, Young A P, Zhang S, Spada F E, Parker F T, Hutten A and Thomas G 1992 *Phys. Rev. Lett.* **68** 3745
[29] Xiao J Q, Jiang J S and Chien C L 1992 *Phys. Rev. Lett.* **68** 3749
[30] New R M H, Pease R F W and White R L 1996 *J. Magn. Magn. Mater.* **155** 140
[31] Hayashi T, Hirono Sh, Tomita M and Umemura Sh 1996 *Nature* **382** 772
[32] Sellmyer D J, Yu M, Thomas R A, Liu Y and Kirby R D 1998 *Phys. Low-Dim. Struct.* **1/2** 155
[33] Comstock R L 1999 *Introduction to Magnetism and Magnetic Recording* (New York: Wiley)
[34] Terris B D, Folks L, Weller D, Baglin J E E, Kellock A J, Rothuizen H and Vettiger P 1999 *Appl. Phys. Lett.* **75** 403
[35] Weller D, Moser A, Folks L, Best M E, Lee W, Toney M F, Schwickert M, Thiele J-U and Doerner M F 2000 *IEEE Trans. Magn.* **36** 10
[36] Kirk K J 2000 *Contemp. Phys.* **41** 61
[37] Wood R 2000 *IEEE Trans. Magn.* **36** 36
[38] Sellmyer D J, Zheng M and Skomski R 2001 *J. Phys.: Condens. Matter* **13** 433
[39] Sellmyer D J, Luo C P, Qiang Y and Liu J P 2002 Nanomaterials and magnetic thin films *Handbook of Thin Film Materials* vol 5, ed H S Nalwa (San Diego, CA: Academic) p 337
[40] Ziese M and Thornton M J (ed) 2001 *Spin Electronics* (Berlin: Springer)
[41] Coey J M D, Viret M and von Molnár S 1999 *Adv. Phys.* **48** 167
[42] Parker J S, Watts S M, Ivanow P G and Xiong P 2002 *Phys. Rev. Lett.* **88** 196601
[43] Oleinik I I, Tsymbal E Y and Pettifor D G 2000 *Phys. Rev.* B **62** 3952
[44] Hunziker M and Landolt M 2000 *Phys. Rev. Lett.* **84** 4713
[45] Schulthess T C and Butler W H 2001 *J. Appl. Phys.* **89** 7021
[46] Cowburn R P and Welland M E 2000 *Science* **287** 1466
[47] Lagmago Kamta G and Starace A F 2002 *Phys. Rev. Lett.* **88** 107901
[48] Grünberg P, Schreiber R, Pang Y, Brodsky M B and Sowers H 1986 *Phys. Rev. Lett.* **57** 2442
[49] Baibich M N, Broto J M, Fert A, Nguyen Van Dau F, Petroff F, Etienne P, Creuzet G, Friederich A and Chazelas J 1988 *Phys. Rev. Lett.* **61** 2472
[50] Parkin S S P 1991 *Phys. Rev. Lett.* **67** 3598
[51] Himpsel F J, Ortega J E, Mankey G J and Willis R F 1998 *Adv. Phys.* **47** 511
[52] Coey J M D, Berkowitz A E, Balcells L, Putris F F and Barry A 1998 *Phys. Rev. Lett.* **80** 2815
[53] Singh R R P, Pickett W E, Hone D W and Scalapino D J 2000 *Comments Condens. Matter Phys.* B **2** 1
[54] Salamon M B and Jaime M 2001 *Rev. Mod. Phys.* **73** 583
[55] Coey J M D and Venkatesan M 2002 *J. Appl. Phys.* **91** 8345
[56] Craik D J and Tebble R S 1961 *Rep. Prog. Phys.* **24** 116

[57] Liou S-H and Yao Y D 1998 *J. Magn. Magn. Mater.* **190** 130
[58] Folks L, Best M E, Rice P M, Terris B D, Weller D and Chapman J N 2000 *Appl. Phys. Lett.* **76** 909
[59] Skomski R, Oepen H-P and Kirschner J 1998 *Phys. Rev.* B **58** 3223
[60] Skomski R and Sellmyer D J 2000 *J. Appl. Phys.* **87** 4756
[61] Bloch F 1932 *Z. Phys.* **74** 295
[62] Landau L and Lifshitz E 1935 *Phys. Z. Sowjetunion* **8** 153
[63] Kersten M 1943 *Z. Phys.* **44** 63
[64] Chudnovsky E M, Saslow W M and Serota R A 1986 *Phys. Rev.* B **33** 251
[65] Skomski R 1998 *J. Appl. Phys.* **83** 6503
[66] Skomski R, Liu J P and Sellmyer D J 1999 *Phys. Rev.* B **60** 7359
[67] Skomski R, Liu J P, Meldrim J M and Sellmyer D J 1998 *Magnetic Anisotropy and Coercivity in Rare-Earth Transition Metal Alloys* ed L Schultz and K-H Müller (Frankfurt/M: Werkstoffinformationsgesellschaft) p 277
[68] Hadjipanayis G C 1999 *J. Magn. Magn. Mater.* **200** 373
[69] Liu J P, Skomski R, Liu Y and Sellmyer D J 2000 *J. Appl. Phys.* **87** 6740
[70] Dormann J L, Bessais L and Fiorani D 1988 *J. Phys. C: Solid State Phys.* **21** 2015
[71] Dormann J L, Fiorani D and Tronc E 1994 *Nanophase Materials* ed G C Hadjipanayis and R W Sigel (Dordrecht: Kluwer) p 365
[72] Luo W-L, Nagel S R, Rosenbaum T F and Rosenzweig R E 1991 *Phys. Rev. Lett.* **67** 2721
[73] Jamet M, Wernsdorfer W, Thirion C, Mailly D, Dupuis V, Mélinon P and Pérez A 2001 *Phys. Rev. Lett.* **86** 4676
[74] Apsel S E, Emmert J W, Deng J and Bloomfield L A 1996 *Phys. Rev. Lett.* **76** 1441
[75] Wirth S, Anane A and von Molnár S 2000 *Phys. Rev.* B **63** 0124021
[76] Schrefl T, Fidler J, Kirk K J and Chapman J N 1997 *J. Magn. Magn. Mater.* **175** 193
[77] Ross C A, Chantrell R, Hwang M, Farhoud M, Savas T A, Hao Y, Smith H I, Ross F M, Redjdal M and Humphrey F B 2000 *Phys. Rev.* B **62** 14252
[78] Yu J, Rüdiger U, Kent A D, Thomas L and Parkin S S P 1999 *J. Appl. Phys.* **85** 5501
[79] Ledermann M, Schultz S and Ozaki M 1994 *Phys. Rev. Lett.* **73** 1986
[80] Wernsdorfer W, Bonet Orozco E, Hasselbach K, Benoit A, Barbara B, Demoncy N, Loiseau A, Pascard H and Mailly D 1997 *Phys. Rev. Lett.* **78** 1791
[81] Novosad V, Guslienko K Yu, Shima H, Otani Y, Kim S G, Fukamichi K, Kikuchi N, Kitakami O and Shimada Y 2002 *Phys. Rev.* B **65** 060402(R)
[82] Oepen H P and Kirschner J 1989 *Phys. Rev. Lett.* **62** 819
[83] Heinrich B, Cochran J F, Kowalewski M, Kirschner J, Celinski Z, Arrott A S and Myrtle K 1991 *Phys. Rev.* B **44** 9348
[84] Gradmann U 1993 *Handbook of Magnetic materials* vol 7, ed K H J Buschow (Amsterdam: Elsevier) p 1
[85] Heinrich B and Cochran J F 1993 *Adv. Phys.* **42** 523
[86] Sander D, Skomski R, Schmidthals C, Enders A and Kirschner J 1996 *Phys. Rev. Lett.* **77** 2566
[87] Sander D 1999 *Rep. Prog. Phys.* **62** 809
[88] Parhofer S M, Wecker J, Kuhrt Ch, Gieres G and Schultz L 1996 *IEEE Trans. Magn.* **32** 4437
[89] McCurrie R A 1994 *Ferromagnetic Materials—Structure and Properties* (London: Academic)
[90] Néel L 1954 *J. Phys. Rad.* **15** 376
[91] Millev Y, Skomski R and Kirschner J 1998 *Phys. Rev.* B **58** 6305
[92] Bland J A C and Heinrich B (ed) 1994 *Ultrathin Magnetic Structures* vol 1 (Berlin: Springer)
[93] Blügel S 1995 *Phys. Rev.* B **51** 2025
[94] Ferré J, Jamet J P and Meyer P 1999 *Phys. Status Solidi* a **175** 213
[95] Bander M and Mills D L 1988 *Phys. Rev.* B **38** 12015
[96] Nieber S and Kronmüller H 1989 *Phys. Status Solidi* b **153** 367
[97] Bowden G J, Beaujour J M L, Gordeev S, de Groot P A J, Rainford B D and Sawicki M 2000 *J. Phys.: Condens. Matter* **12** 9335
[98] Sawicki M, Bowden G J, de Groot P A J, Rainford B D, Beaujour J M L, Ward R C C and Wells M R 2000 *Phys. Rev.* B **62** 5817
[99] Fullerton E E, Jiang S J and Bader S D 1999 *J. Magn. Magn. Mater.* **200** 392
[100] Kleinefeld T, Valentin J and Weller D 1995 *J. Magn. Magn. Mater.* **148** 249
[101] Welitipiya D, Borca C N, Dowben P A, Jiang H, Gobulukoglu I, Robertson B W and Zhang J 1997 *Mater. Res. Soc. Symp. Proc.* **475** 257
[102] Haginoya Ch, Heike S, Ishibashi M, Nakamura K, Koike K, Yoshimura T, Yamamoto J and Hiriyama Y 1999 *J. Appl. Phys.* **85** 8327

[103] Zheng M, Yu M, Liu Y, Skomski R, Liou S-H, Sellmyer D J, Petryakov V N, Verevkin Y K, Polushkin N I and Salashchenko N N 2001 *Appl. Phys. Lett.* **79** 2606
[104] Chantrell R W, Weller D, Klemmer T J, Sun S and Fullerton E E 2002 *J. Appl. Phys.* **91** 6866
[105] Hu X-D and Das Sarma S 2000 *Phys. Rev.* A **61** 062301-1
[106] Nielsch K, Wehrspohn R B, Barthel J, Kirschner J, Gösele U, Fischer S F and Kronmüller H 2001 *Appl. Phys. Lett.* **79** 1360
[107] Chou S Y, Wei M, Krauss P R and Fisher P B 1994 *J. Vac. Sci. Technol* B **12** 3695
[108] Hehn M, Ounadjela K, Bucher J-P, Rousseaux F, Decanini D, Bartenlian B and Chappert C 1996 *Science* **272** 1782
[109] Yu Ch-T, Li D-Q, Pearson J and Bader S D 2001 *Appl. Phys. Lett.* **78** 1228
[110] Kent A D, von Molnár S, Gider S and Awschalom D D 1994 *J. Appl. Phys.* **76** 6656
[111] Warin P, Hyndman R, Glerak J, Chapman J N, Ferré J, Jamet J P, Mathet V and Chappert C 2001 *J. Appl. Phys.* **90** 3850
[112] Mathieu C, Hartmann C, Bauer M, Buettner O, Riedling S, Roos B, Demokritov S O, Hillebrands B, Bartenlian B, Chappert C, Decanini D, Rousseaux F, Cambril E, Müller A, Hoffmann B and Hartmann U 1997 *Appl. Phys. Lett.* **70** 2912
[113] Skomski R 2002 *J. Appl. Phys.* **91** 7053
[114] Tornow M, Weiss D, v Klitzing K, Eberl K, Bergman D J and Strelniker Y M 1996 *Phys. Rev. Lett.* **77** 147
[115] Cowburn R P, Adeyeye A O and Bland J A C 1997 *Appl. Phys. Lett.* **70** 2309
[116] Tsymbal E Y, Mryasov O N and LeClair P R 2003 *J. Phys.: Condens. Matter* **15** R109
[117] Shen J, Skomski R, Klaua M, Jenniches H, Manoharan S S and Kirschner J 1997 *Phys. Rev.* B **56** 2340
[118] Wirth S, Field M, Awschalom D D and von Molnár S 1998 *Phys. Rev.* B **57** R14028
[119] Masuda H and Satoh M 1996 *Japan. J. Appl. Phys.* 2 **35** L126
[120] Wernsdorfer W, Doudin B, Mailly D, Hasselbach K, Benoit A, Meier J, Ansermet J-Ph and Barbara B 1996 *Phys. Rev. Lett.* **77** 1873
[121] Li F-Y and Metzger R M 1997 *J. Appl. Phys.* **81** 3806
[122] Roxlo B, Deckman H W, Gland J, Cameron S D and Cianelli R 1987 *Science* **235** 1629
[123] Masuda H and Fukuda K 1995 *Science* **268** 1466
[124] Sugawara A, Streblechenko D, McCartney M and Scheinfein M R 1998 *IEEE Trans. Magn.* **34** 1081
[125] Ozin G A 1992 *Adv. Mater.* **4** 612
[126] Martin C R 1994 *Science* **266** 1961
[127] Fert A and Piraux L 1999 *J. Magn. Magn. Mater.* **200** 338
[128] Sun L, Searson P C and Chien C L 2000 *Phys. Rev.* B **61** R6463
[129] Keller F, Hunter M S and Robinson D L 1953 *J. Electrochem. Soc.* **100** 411
[130] Routkevitch D, Tager A A, Haruyama J, Almawlawi D, Moskovits M and Xu J M 1996 *IEEE Trans. Magn.* **43** 1646
[131] Jessensky O, Müller F and Gösele U 1998 *J. Electrochem. Soc.* **145** 3735
[132] Kawai S and Ueda R 1975 *J. Electrochem. Soc.* **122** 32
[133] Zangari G and Lambeth D N 1997 *IEEE Trans. Magn.* **33** 3010
[134] Menon L, Zheng M, Zeng H, Bandyopadhyay S and Sellmyer D J 2000 *J. Electron. Mater.* **29** 510
[135] Zeng H, Zheng M, Skomski R, Sellmyer D J, Liu Y, Menon L and Bandyopadhyay S 2000 *J. Appl. Phys.* **87** 4718
[136] Shiraki M, Wakui Y, Tokushima T and Tsuya N 1985 *IEEE Trans. Magn.* **21** 1465
[137] Saito M, Kirihara M, Taniguchi T and Miyagi M 1989 *Appl. Phys. Lett.* **55** 607
[138] Li A-P, Müller F, Birner A, Nielsch K and Gösele U 1999 *Adv. Mater.* **11** 483
[139] Mizuki I, Yamamoto Y, Yoshino T and Baba N 1987 *J Met. Surf. Finish. Soc. Japan* **38** 561
[140] Wang J B, Liu Q F, Xue D S, Peng Y, Cao X Z and Li F S 2001 *J. Phys. D: Appl. Phys.* **34** 3442
[141] Huang Y H, Okumura H, Hadjipanayis G C and Weller D 2002 *J. Appl. Phys.* **91** 6869
[142] Blythe H J, Fedosyuk V M, Kasyutich O I and Schwarzacher W 2000 *J. Magn. Magn. Mater.* **208** 251
[143] Evans P R, Yi G and Schwarzacher W 2000 *Appl. Phys. Lett.* **76** 481
[144] Huysmans G T A and Lodder J C 1988 *J. Appl. Phys.* **64** 2016
[145] Skomski R, Zeng H, Zheng M and Sellmyer D J 2000 *Phys. Rev.* B **62** 3900
[146] Paulus P M, Luis F, Kröll M, Schmid G and de Jongh L J 2001 *J. Magn. Magn. Mater.* **224** 180
[147] Skomski R, Zeng H and Sellmyer D J 2002 *J. Magn. Magn. Mater.* **249** 175
[148] Zheng M, Skomski R, Liu Y and Sellmyer D J 2000 *J. Phys.: Condens. Matter* **12** L497
[149] Wegrowe J-E, Kelly D, Jaccard Y, Guittienne Ph and Ansermet J-Ph 1999 *Europhys. Lett.* **45** 626
[150] Michels A, Weissmüller J, Erb U and Barker J G 2002 *Phys. Status Solidi* a **189** 509
[151] Fischer K-H and Hertz A J 1991 *Spin Glasses* (Cambridge: Cambridge University Press)

[152] McCormick P G, Miao W F, Smith P A I, Ding J and Street R 1998 *J. Appl. Phys.* **83** 6256
[153] Sellmyer D J 2002 *Nature* **420** 374
[154] Coehoorn R, de Mooij D B and de Waard C 1989 *J. Magn. Magn. Mater.* **80** 101
[155] Müller K-H, Schneider J, Handstein A, Eckert D, Nothnagel P and Kirchmayr H R 1991 *Mater. Sci. Eng.* A **133** 151
[156] Ding J, McCormick P G and Street R 1993 *J. Magn. Magn. Mater.* **124** L1
[157] Manaf A, Buckley P A and Davies H A 1993 *J. Magn. Magn. Mater.* **128** 302
[158] Leslie-Pelecky D and Schalek R L 1999 *Phys. Rev.* B **59** 457
[159] Jiles D 1998 *Introduction to Magnetism and Magnetic Materials* (London: Chapman and Hall)
[160] Edwards S F and Anderson P W 1975 *J. Phys. F: Met. Phys.* **5** 965
[161] Mattis D C 1976 *Phys. Lett.* A **56** 421
[162] Sellmyer D J and Nafis S 1986 *Phys. Rev. Lett.* **57** 1173
[163] Wohlfarth E P 1984 *J. Phys. F: Met. Phys.* **14** L155
[164] Skomski R 1996 *J. Magn. Magn. Mater.* **157/158** 713
[165] Kittel C 1986 *Introduction to Solid-State Physics* (New York: Wiley)
[166] Thole B T, Carra P, Sette F and van der Laan G 1992 *Phys. Rev. Lett.* **68** 1943
[167] Coehoorn R 1989 *Phys. Rev.* B **39** 13072
[168] Sandratskii L M 1998 *Adv. Phys.* **47** 91
[169] Sabiryanov R F and Jaswal S S 1998 *J. Magn. Magn. Mater.* **177–181** 989
[170] MacLaren J M, Schulthess T C, Butler W H, Sutton R and McHenry M 1999 *J. Appl. Phys.* **85** 4833
[171] Dowben P A, Hürsch W and Landolt M 1993 *J. Magn. Magn. Mater.* **125** 120
[172] Jones W and March N H 1973 *Theoretical Solid State Physics* vol 1 (London: Wiley)
[173] Skomski R, Waldfried C and Dowben P A 1998 *J. Phys.: Condens. Matter* **10** 5833
[174] Dowben P A 2000 *Surf. Sci. Rep.* **40** 151
[175] Cyrot-Lackmann F 1968 *J. Phys. Chem. Solids* **29** 1235
[176] Heine V 1980 *Solid State Phys.* **35** 1
[177] Sutton A P 1993 *Electronic Structure of Materials* (Oxford: Oxford University Press)
[178] Desjonquères M C and Spanjaard D 1993 *Concepts in Surface Physics* (Berlin: Springer)
[179] Sandratskii L M 2001 *Phys. Rev.* B **64** 134402
[180] Duc N H, Hien T D, Givord D, Franse J J M and de Boer F R 1993 *J. Magn. Magn. Mater.* **124** 305
[181] Ashcroft N W and Mermin N D 1976 *Solid State Physics* (Philadelphia, PA: Saunders)
[182] Skomski R 1999 *Europhys. Lett.* **48** 455
[183] De Toro J A, López de la Torre M A, Riveiro J M, Bland J, Goff J P and Thomas M F 2001 *Phys. Rev.* B **64** 224421
[184] Yeomans J M 1992 *Statistical Mechanics of Phase Transitions* (Oxford: Oxford University Press)
[185] Smart J S 1966 *Effective Field Theories of Magnetism* (Philadephia, PA: Saunders)
[186] Ising E 1925 *Z. Phys.* **31** 253
[187] Brush S G 1967 *Rev. Mod. Phys.* **39** 883
[188] Fisher M E 1974 *Rev. Mod. Phys.* **46** 579
[189] de Jongh L J and Miedema A R 1975 *Adv. Phys.* **23** 1
[190] Fisher M E and Barber M N 1972 *Phys. Rev. Lett.* **28** 1516
[191] Maciejewski W and Duda A 1987 *Solid State Commun.* **64** 557
[192] Aharoni A 1996 *Introduction to the Theory of Ferromagnetism* (Oxford: Oxford University Press)
[193] Zhang D-J, Klabunde K J, Sorensen C M and Hadjipanayis G C 1998 *Phys. Rev.* B **58** 14167
[194] Mills D L 1971 *Phys. Rev.* B **3** 3887
[195] Binder K and Hohenberg P C 1972 *Phys. Rev.* B **6** 3461
[196] Ma H-R and Tsai C-H 1985 *Solid State Commun.* **55** 499
[197] Sy H K 1987 *Phys. Lett.* A **120** 203
[198] Maciejewski W 1990 *IEEE Trans. Magn.* **26** 213
[199] Wang R W and Mills D L 1992 *Phys. Rev.* B **46** 11681
[200] Bovensiepen U, Wilhelm F, Srivastava P, Poulopoulos P, Farle M, Ney A and Baberschke K 1998 *Phys. Rev. Lett.* **81** 2368
[201] Hernando A and Kulik T 1994 *Phys. Rev.* B **49** 7064
[202] Hernando A, Navarro I, Prados C, García D, Vásquez M and Alonso J 1996 *Phys. Rev.* B **53** 8223
[203] Coey J M D (ed) 1996 *Rare-Earth Iron Permanent Magnets* (Oxford: Oxford University Press)
[204] Farle M 1998 *Rep. Prog. Phys.* **61** 755
[205] Osborn J A 1945 *Phys. Rev.* **67** 351
[206] Bozorth R M 1951 *Ferromagnetism* (Princeton, NJ: van Nostrand-Reinhold)

[207] Ballhausen C J 1962 *Ligand Field Theory* (New York: McGraw-Hill)
[208] Hutchings M T 1964 *Solid State Phys.* **16** 227
[209] Herbst J F 1991 *Rev. Mod. Phys.* **63** 819
[210] Steinbeck L, Richter M, Nitzsche U and Eschrig H 1996 *Phys. Rev.* B **53** 7111
[211] Kuhrt C, O'Donnell K, Katter M, Wecker J, Schnitzke K and Schultz L 1992 *Appl. Phys. Lett.* **60** 3316
[212] Sato Turtelli R, Sinnecker J P, Grössinger R and Vázquez M 1995 *J. Appl. Phys.* **78** 2590
[213] Johnson M T, Bloemen P J H, den Broeder F J A and de Vries J J 1996 *Rep. Prog. Phys.* **59** 1409
[214] Victora R H and McLaren J M 1993 *Phys. Rev.* B **47** 11583
[215] Chuang D S, Ballentine C A and O'Handley R C 1994 *Phys. Rev.* B **49** 15084
[216] Gay J G and Richter R 1986 *Phys. Rev. Lett.* **56** 2728
[217] Bruno P 1989 *Phys. Rev.* B **39** 865
[218] Daalderop G H O, Kelly P J and Schuurmans M F H 1990 *Phys. Rev.* B **42** 7270
[219] Wang D-S, Wu R-Q and Freeman A J 1993 *Phys. Rev.* B **47** 14932
[220] Eisenbach M, Györffy B L, Stocks G M and Újfalussy B 2002 *Phys. Rev.* B **65** 144424-1
[221] Komelj M, Ederer C, Davenport J W and Fähnle M 2002 *Phys. Rev.* B **66** 140407-1
[222] Cadogan J M, Gavigan J P, Givord D and Li H S 1988 *J. Phys. F: Met. Phys.* **18** 779
[223] Hu J-F, Kleinschroth I, Reisser R, Kronmüller H and Zhou Sh 1993 *Phys. Status Solidi* a **138** 257
[224] Lectard E, Allibert C H and Ballou R 1994 *J. Appl. Phys.* **75** 6277
[225] Skomski R 1998 *J. Appl. Phys.* **83** 6724
[226] Liu J F, Chui T, Dimitrov D and Hadjipanayis G C 1998 *Appl. Phys. Lett.* **85** 3007
[227] Brown W F 1963 *Micromagnetics* (New York: Wiley)
[228] Skomski R, Liu J P and Sellmyer D J 1999 *Mater. Res. Soc. Symp. Proc.* **562** 309
[229] Sagawa M, Fujimura S, Yamamoto H and Matsuura Y 1984 *IEEE Trans. Magn.* **20** 1584
[230] Sagawa M, Hirosawa S, Yamamoto H, Fujimura S and Matsuura Y 1987 *Japan. J. Appl. Phys.* **26** 785
[231] Rodewald W, Wall B, Katter M, Üstüner K and Steinmetz S 2002 *Rare-Earth Magnets and their Applications (Proc. 17th REM)* ed G C Hadjipanayis and M J Bonder (Princeton, NJ: Rinton Press) p 25
[232] Imry Y and Ma S-K 1975 *Phys. Rev. Lett.* **35** 1399
[233] Alben R, Becker J J and Chi M C 1978 *J. Appl. Phys.* **49** 1653
[234] Skomski R 1992 *Phys. Status Solidi* b **174** K77
[235] Astalos R J and Camley R E 1998 *Phys. Rev.* B **58** 8646
[236] Zhang H-W, Li B-H, Wang J, Zhang J, Zhang Sh-Y and Shen B-G 2000 *J. Phys. D: Appl. Phys.* **33** 3022
[237] Skomski R 2001 *Spin Electronics* ed M Ziese and M J Thornton (Berlin: Springer) p 204
[238] Kronmüller H and Schrefl T 1994 *J. Magn. Magn. Mater.* **129** 66
[239] Fischer R and Kronmüller H 1998 *J. Magn. Magn. Mater.* **184** 166
[240] Schrefl T and Fidler J 1998 *J. Magn. Magn. Mater.* **177–181** 970
[241] Lyberatos A 2000 *J. Phys. D: Appl. Phys.* **33** R117
[242] Belashchenko K D and Antropov V P 2002 *Phys. Rev.* B **66** 144402-1
[243] Hilzinger H R and Kronmüller H 1975 *Phys. Lett.* A **51** 59
[244] Skomski R, Zeng H and Sellmyer D J 2001 *IEEE Trans. Magn.* **37** 2549
[245] Kittel C 1949 *Rev. Mod. Phys.* **21** 541
[246] Becker R and Döring W 1939 *Ferromagnetismus* (Berlin: Springer)
[247] Chikazumi S 1964 *Physics of Magnetism* (New York: Wiley)
[248] Hubert A and Schäfer R 1998 *Magnetic Domains* (Berlin: Springer)
[249] Givord D and Rossignol M F 1996 *Rare-Earth Iron Permanent Magnets* ed J M D Coey (Oxford: Oxford University Press) p 218
[250] Kronmüller H 1987 *Phys. Status Solidi* b **144** 385
[251] Kronmüller H, Durst K-D and Sagawa M 1988 *J. Magn. Magn. Mater.* **74** 291
[252] Néel L 1951 *J. Phys. Rad.* **12** 339
[253] Stoner E C and Wohlfarth E P 1948 *Phil. Trans. R. Soc.* A **240** 599
[254] Aharoni A 1962 *Rev. Mod. Phys.* **34** 227
[255] Aharoni A 1997 *J. Appl. Phys.* **82** 1281
[256] Livingston J D and Martin L D 1977 *J. Appl. Phys.* **48** 1350
[257] Fidler J 1982 *J. Magn. Magn. Mater.* **30** 58
[258] Zhou J, Skomski R, Chen C, Hadjipanayis G C and Sellmyer D J 2000 *Appl. Phys. Lett.* **77** 1514
Zhou J, Skomski R and Sellmyer D J 2001 *IEEE Trans. Magn.* **37** 2518
[259] Chen C H, Walmer M S, Walmer M H, Liu S, Kuhl E and Simonet G 1998 *J. Appl. Phys.* **83** 6706
[260] Huang M Q, Wallace W E, McHenry M, Chen Q and Ma B M 1998 *J. Appl. Phys.* **83** 6718
[261] Jiang C, Venkatesan M, Gallagher K and Coey J M D 2001 *J. Magn. Magn. Mater.* **236** 49

[262] Al-Omari I A, Skomski R, Thomas R A, Leslie-Pelecky D and Sellmyer D J 2001 *IEEE Trans. Magn.* **37** 2534
[263] Chen Z, Meng-Burany X, Okumura H and Hadjipanayis G C 2000 *J. Appl. Phys.* **87** 3409
[264] Gaunt P 1986 *J. Appl. Phys.* **59** 4129
[265] Brown W F 1945 *Rev. Mod. Phys.* **17** 15
[266] Liu J P, Liu Y, Skomski R and Sellmyer D J 1999 *J. Appl. Phys.* **85** 4812
[267] Fukunaga H and Inoue H 1992 *Japan. J. Appl. Phys.* **31** 1347
[268] Bruno P 1999 *Phys. Rev. Lett.* **83** 2425
[269] Versluijs J J, Bari M A and Coey J M D 2001 *Phys. Rev. Lett.* **87** 026601
[270] Goto E, Hayashi N, Miyashita T and Nakagawa K 1965 *J. Appl. Phys.* **36** 2951
[271] Richter J and Skomski R 1989 *Phys. Status Solidi* b **153** 711
[272] Harris R, Plischke M and Zuckermann M J 1973 *Phys. Rev. Lett.* **31** 160
[273] Löffler J F, Braun H B and Wagner W 1999 *J. Appl. Phys.* **85** 5187
[274] Suzuki K and Cadogan J M 1999 *J. Appl. Phys.* **85** 4400
[275] Chi M C and Alben R 1977 *J. Appl. Phys.* **48** 2987
[276] Callen E, Liu Y J and Cullen J R 1977 *Phys. Rev.* B **16** 263
[277] Zhao G-P, Lim H-S, Ong C-K and Feng Y-P 1999 *J. Phys.: Condens. Matter* **11** 3323
[278] Ślawska-Waniewska A, Gutowski M, Nowicki P, Lachowicz H K, Kulik T and Matyja A 1993 *Phys. Rev.* B **46** 14594
[279] Anderson P W 1958 *Phys. Rev.* B **109** 1492
[280] O'Barr R and Schultz S 1997 *J. Appl. Phys.* **81** 5448
Lederman M, O'Barr R and Schultz S 1995 *IEEE Trans. Magn.* **31** 3793
Lederman M, O'Barr R and Schultz S 1993 *J. Appl. Phys.* **73** 6961
[281] AlMawlawi D, Coombs N and Moskovits M 1991 *J. Appl. Phys.* **70** 4421
[282] Wegrowe J-E, Kelly D, Franck A, Gilbert S E and Ansermet J-Ph 1999 *Phys. Rev. Lett.* **82** 3681
[283] Zeng H, Skomski R, Menon L, Liu Y, Bandyopadhyay S and Sellmyer D J 2002 *Phys. Rev.* B **65** 134426
[284] Skomski R and Sellmyer D J 2001 *J. Appl. Phys.* **89** 7263
[285] Preisach F 1935 *Z. Phys.* **94** 277
[286] Bertotti G and Basso V 1993 *J. Appl. Phys.* **73** 5827
[287] Wohlfarth P 1958 *J. Appl. Phys.* **29** 595
[288] Henkel D 1964 *Phys. Status Solidi* **7** 919
[289] Che X-D and Bertram H N 1992 *J. Magn. Magn. Mater.* **116** 121
[290] Basso V, LoBue M and Bertotti G 1994 *J. Appl. Phys.* **75** 5677
[291] Veitch R J 1990 *IEEE Trans. Magn.* **26** 1876
[292] Kneller E 1966 *Handbuch der Physik XIII/2: Ferromagnetismus* ed H P J Wijn (Berlin: Springer) p 438
[293] Zwanzig R 1961 *Phys. Rev.* **124** 983
[294] Mori H 1965 *Prog. Theor. Phys.* **33** 423
[295] Skomski R, Kirby R D and Sellmyer D J 1999 *J. Appl. Phys.* **85** 5069
[296] Street R and Wooley J C 1949 *Proc. Phys. Soc.* A **62** 562
[297] Brown W F 1959 *J. Appl. Phys.* **30** 625
[298] Vonsovskii S V 1966 *Ferromagnetic Resonance* (Oxford: Pergamon)
[299] Vonsovskii S V 1974 *Magnetism* (New York: Wiley)
[300] Kramers H A 1940 *Physica* **7** 284
[301] Brown W F 1963 *Phys. Rev.* **130** 1677
[302] Hänggi P, Talkner P and Borkovec M 1990 *Rev. Mod. Phys.* **62** 251
[303] Bloch F 1930 *Z. Phys.* **61** 206
[304] Eshbach J R and Damon R W 1960 *Phys. Rev.* **118** 1208
[305] Dyson F J 1956 *Phys. Rev.* **102** 1217
[306] Encinas-Oropesa A, Demand M, Piraux L, Huynen I and Ebels U 2001 *Phys. Rev.* B **63** 104415
[307] Arias R and Mills D L 2001 *Phys. Rev.* B **63** 134439
[308] Chipara M I, Skomski R and Sellmyer D J 2002 *J. Magn. Magn. Mater.* **249** 246
[309] Ebels U, Duvail J-L, Wigen P E, Piraux L, Buda L D and Ounadjela K 2001 *Phys. Rev.* B **64** 144421
[310] Guslienko K Y, Ivanov B A, Novosad V, Otani Y, Shima H and Fukamichi K 2002 *J. Appl. Phys.* **91** 8037
[311] Jorzick J, Demokritov S O, Hillebrands B, Bailleul M, Fermon C, Guslienko K Y, Slavin A N, Berkov D V and Gorn N L 2002 *Phys. Rev. Lett.* **88** 047204
[312] Wang Z K, Kuok M H, Ng S C, Lockwood D J, Cottam M G, Nielsch K, Wehrspohn R B and Gösele U 2002 *Phys. Rev. Lett.* **89** 027201-1
[313] Miles J, Middleton B, Olson T and Wood R 2002 *J. Appl. Phys.* **91** 7083
[314] Lyberatos A and Chantrell R W 1993 *J. Appl. Phys.* **73** 6501

[315] Berkov D V 1998 *J. Appl. Phys.* **83** 7390
[316] Victora R H 1989 *Phys. Rev. Lett.* **63** 457
[317] Lottis D K, White R M and Dahlberg E D 1991 *Phys. Rev. Lett.* **67** 2362
[318] Kneller E 1962 *Ferromagnetismus* (Berlin: Springer)
[319] Gaunt P 1983 *Phil. Mag.* B **48** 261
[320] Skomski R and Christoph V 1989 *Phys. Status Solidi* b **156** K149
[321] Berkov D V 1992 *J. Magn. Magn. Mater.* **111** 327
[322] Livingston J D and Bean C P 1959 *J. Appl. Phys.* **30** 118S
[323] Kneller E F and Luborsky F E 1959 *J. Appl. Phys.* **34** 656
[324] Sharrock M P 1994 *J. Appl. Phys.* **76** 6413
[325] Skomski R, Kirby R D and Sellmyer D J 2003 *J. Appl. Phys.* **93** at press
[326] Skomski R 1990 *PhD Thesis* TU Dresden
[327] Sellmyer D J, Yu M and Kirby R D 1999 *Nanostruct. Mater.* **12** 1021
[328] Givord D, Lienard A, Tenaud P and Viadieu T 1987 *J. Magn. Magn. Mater.* **67** L281
[329] Givord D, Lu Q, Rossignol M F, Tenaud P and Viadieu T 1990 *J. Magn. Magn. Mater.* **83** 183
[330] Pinto M A 1987 *Phys. Rev. Lett.* **59** 2798
[331] Néel L 1950 *J. Phys. Rad.* **11** 49
[332] Sellmyer D J and Skomski R 2002 *Scr. Mater.* **47** 531
[333] Egami T 1973 *Phys. Status Solidi* a **19** 747
[334] Liu S, Yang J, Doyle G, Potts G and Kuhl G E 2000 *J. Appl. Phys.* **87** 6728
[335] Walton D 1990 *Phys. Rev. Lett.* **65** 1170
[336] Braun H-B and Bertram N H 1994 *J. Appl. Phys.* **75** 4609
[337] Skomski R and Leslie-Pelecky D 2001 *J. Appl. Phys.* **89** 7036
[338] Griffiths R B 1969 *Phys. Rev. Lett.* **23** 17
[339] Fisher D S and Huse D A 1986 *Phys. Rev. Lett.* **56** 1601
[340] Skomski R and Dowben P A 2002 *Europhys. Lett.* **58** 544
[341] Tanaka C T, Nowak J and Moodera J S 1997 *J. Appl. Phys.* **81** 5515
[342] MacDonald A H, Jungwirth T and Kasner M 1998 *Phys. Rev. Lett.* **81** 705
[343] Meiklejohn W H and Bean C P 1956 *Phys. Rev.* **102** 1413
[344] Skomski R, Oepen H-P and Kirschner J 1998 *Phys. Rev.* B **58** 11138
[345] Malozemoff A P 1987 *Phys. Rev.* B **35** 3679
[346] Miller B H and Dan Dahlberg E 1996 *Appl. Phys. Lett.* **69** 3932
[347] Koon N C 1997 *Phys. Rev. Lett.* **78** 4865
[348] Takano K, Kodama R H, Berkowitz A E, Cao W and Thomas G 1997 *Phys. Rev. Lett.* **79** 1130
[349] Schulthess T C and Butler W H 1998 *Phys. Rev. Lett.* **81** 4516
[350] Leighton C, Nogués J, Suhl H and Schuller Ivan K 1999 *Phys. Rev.* B **60** 12837
[351] Hertel R 2001 *J. Appl. Phys.* **90** 5752
[352] Velu E M T and Lambeth D N 1991 *J. Appl. Phys.* **69** 5175
[353] Keys R W 1973 *Comments Solid State Phys.* **5** 97
[354] Evetts J E (ed) 1992 *Concise Encyclopedia of Magnetic and Superconducting Materials* (Oxford: Pergamon)